

Finite Element Modeling of  
Tow-Placed Variable-Stiffness Composite Laminates

Patrick Tyler Langley

Thesis submitted to the Faculty of the  
Virginia Polytechnic Institute and State University  
in partial fulfillment of the requirements for the degree of

Master of Science  
In  
ENGINEERING MECHANICS

Committee Members:

Zafer Gürdal, Chair

Romesh Batra

Robert Jones

Keywords: Curvilinear-Fiber, Variable-Stiffness, Tow-  
Placed, Composite Lamina, Finite Element

# Finite Element Modeling of Tow-Placed Variable-Stiffness Composite Laminates

Tyler Langley

(Abstract)

Tow-placement machines have made it possible to manufacture curved-fiber composite tow paths. A composite structure with curved-fiber tow paths can be formed in a manner similar to filament winding. The result is a laminate with spatially varying stiffness and response. This manufacturing method can also result in overlap regions between adjacent tow paths. In previous research, a closed-form solution was developed to determine the response of these variable-stiffness laminates, but the overlap regions were not included in this model. Additionally, the fiber-orientation angle throughout the panel was based on individual fiber path definitions and not tow path definitions. In this thesis, a method of creating a finite element model of tow-placed variable-stiffness composite panels is presented. This method provides a representation of the overlap regions and an accurate model of the fiber-orientation angle change throughout the laminate. The GENESIS finite element analysis and design package is used to solve for the static response of the models created. The results of these analyses compare favorably with the results of the previous research and give some insight into the interaction of the thickness and fiber-orientation variation. Additionally, some of the advanced design capabilities of the finite element modeling method, and some results of those designs are demonstrated.

## **Acknowledgments**

I would like to thank my advisor Dr. Zafer Gürdal for answering my questions and making sure I was asking the right questions. I would also like to thank Dr. Robert Jones and Dr. Romesh Batra for being on my advisory committee. I would especially like to thank Loretta Tickle and the other staff in the office for answering the questions no one else could. Finally, I would like to thank Virginia Tech and the Engineering Science and Mechanics Department for providing funding for my graduate education through teaching assistantships.

## Table of Contents

<b>Chapter 1 Introduction</b> .....	1
1.1 Variable-Stiffness Composite Laminates.....	1
1.1.1 Methods of Creating Variable-Stiffness Laminates .....	2
1.1.2 Manufacturing of Curvilinear-Fiber Variable-Stiffness Laminates.....	6
1.1.1 Curvilinear-Fiber Variable-Stiffness Laminate Research.....	10
1.2 The Finite Element Method .....	13
1.2.1 System of Equations .....	14
1.2.2 Boundary Conditions .....	14
1.2.3 Finite Element Results .....	15
1.3 Methods of Optimization.....	15
1.1.2 Optimization .....	15
1.3.1 Optimization of Composite Laminates.....	17
1.3.2 Previous Research on Variable-Stiffness Laminate Optimization ....	18
1.4 Focus of this Research.....	20
<b>Chapter 2 Curvilinear-Fiber Variable -Stiffness Laminate Design</b> .....	21
2.1 Tow-Path Geometry .....	21
2.2 Definition of a Curvilinear-Fiber Reference-Path Centerline.....	24
2.2.1 Coordinate Definitions .....	24
2.2.2 Reference-Path Orientation-Angle Definition .....	26
2.2.3 Path Position Definition .....	30
2.3 Shifted Fiber Paths.....	31
2.4 Variable-Stiffness-Lamina Nomenclature .....	36

<b>Chapter 3 Finite Element Modeling of Variable-Stiffness Laminates</b> .....	39
3.1 Global Finite Element Model .....	39
3.2 GENESIS .....	43
3.2.1 Element Geometry .....	43
3.2.2 Material Properties .....	45
3.2.3 Failure Criteria.....	45
3.3 Creation of Variable Stiffness Finite Element Model .....	49
3.3.1 Finite Element Modeling of a Reference Path.....	49
3.3.2 Shifting of the Reference Path .....	53
3.4 Evaluation of Results.....	57
3.4.1 Force Results .....	57
3.4.2 Stiffness Calculation.....	58
3.5 Mesh Size Convergence .....	60
3.5.1 Static Response .....	60
3.5.2 Thickness Resolution .....	61
<b>Chapter 4 Results of Finite Element Analysis</b> .....	67
4.1 In-plane Results for $[\pm\langle 0 45 \rangle]_s$ Variable Stiffness Laminate .....	67
4.1.1 Finite Element Model Definition.....	67
4.1.2 Displacement Results.....	69
4.1.3 Force Resultants .....	70
4.1.4 Failure Results .....	76
4.1.5 Stresses in Tow Paths.....	80
4.2 Comparison to Previous Research.....	82
4.2.1 Comparison of $N_x$ Results for $[90\pm\langle 45 75 \rangle]_s$ Model .....	83
4.2.2 $N_y$ and $N_{xy}$ Comparison Results for $[90\pm\langle 45 75 \rangle]_s$ .....	86
4.2.3 Comparison of $N_x$ Results for $[0\pm\langle 45 75 \rangle]_s$ Model .....	86
4.2.4 Comparison of $N_y$ Results for $[0\pm\langle 45 75 \rangle]_s$ Model .....	89
4.2.5 Comparison of $N_{xy}$ Results for $[0\pm\langle 45 75 \rangle]_s$ Model .....	91

<b>Chapter 5 Advanced Design Capabilities .....</b>	<b>93</b>
5.1 $T_0$ and $T_1$ Variation .....	93
5.2 Shift Variation .....	95
5.3 Mixed Lay-up Analysis.....	97
5.4 Parallel-Fiber Methods and Shifted-Fiber Methods .....	98
<b>Chapter 6 Concluding Remarks.....</b>	<b>104</b>
<b>Bibliography .....</b>	<b>104</b>
<b>Appendix A: Layer_Def.txt</b>	
<b>Appendix B: RT15.f90</b>	
<b>Vita</b>	

## List of Figures

Figure 1.1	Lamina with varying volume fraction .....	3
Figure 1.2	Laminate with internally dropped plies .....	4
Figure 1.3	Example of 18 element quarter panel with central hole.....	5
Figure 1.4	Schematic of Hercules Inc. tow placement machine.....	7
Figure 1.5	Bridged Material caused by high-tension filament winding.....	10
Figure 1.6	Shifted path lamina based on linearly varying reference path.....	12
Figure 1.7	Parallel-path lamina based on linearly varying reference path.....	13
Figure 2.1	Single tow path and tow-placement head .....	22
Figure 2.2	Point on tow-path centerline.....	23
Figure 2.3	Panel (xy) and tow-path (x'y') coordinate systems .....	24
Figure 2.4	Linearly varying centerline .....	25
Figure 2.5	Geometry for defining a variable-stiffness reference path.....	26
Figure 2.6	Curvilinear-fiber reference path centerline for $T_0=0^\circ$ and $T_1=45^\circ$ .....	27
Figure 2.7	Linear variation of fiber-orientation angle for $T_0=0^\circ$ and $T_1=45^\circ$ .....	28
Figure 2.8	A reference-path centerline for $\phi = 0^\circ$ , $T_0=0^\circ$ and $T_1=45^\circ$ .....	29
Figure 2.9	A reference-path centerline for $\phi=90^\circ$ , $T_0=0^\circ$ and $T_1=45^\circ$ .....	30
Figure 2.10	A single shifted-path centerline .....	32
Figure 2.11	Path centerlines for a variable-stiffness lamina.....	32
Figure 2.12	Change in projected tow path height for lamina .....	33
Figure 2.13	Laminates with single thickness at center .....	35
Figure 2.14	Laminates with single thickness at edge .....	36
Figure 3.1	Case I: Uniform end shortening .....	40
Figure 3.2	Case II: Uniform end shortening .....	41
Figure 3.3	Case I: Quarter panel model.....	42
Figure 3.4	Case II: Quarter panel model.....	42

Figure 3.5	Generalized quadrilateral element .....	44
Figure 3.6	Through-the-thickness view of composite element .....	45
Figure 3.7	Discretized single $\langle 0/45 \rangle$ reference tow path .....	50
Figure 3.8	Variation of orientation angle across reference path .....	52
Figure 3.9	Variation of orientation angle for a single $\langle 0/45 \rangle$ discretized path... ..	53
Figure 3.10	Thickness plot of $\pm\langle 0/45 \rangle_s$ laminate .....	54
Figure 3.11	Two variable stiffness layers with one flat side .....	55
Figure 3.12	Two-layer midplane-symmetric variable-stiffness laminate .....	55
Figure 3.13	Edge of discretized two layer laminate.....	56
Figure 3.14	$N_x$ distribution along displaced edge .....	59
Figure 3.15	Thickness plot for 2,500 elements.....	63
Figure 3.16	Thickness plot for 3,600 elements.....	64
Figure 3.17	Thickness plot for 4,900 elements.....	65
Figure 3.18	Thickness plot for 10,000 elements.....	66
Figure 4.1	Thickness plot of $[\pm\langle 0/45 \rangle]_s$ .....	68
Figure 4.2	Displacement of $[\pm\langle 0/45 \rangle]_s$ for $u_0 = -0.5"$ .....	70
Figure 4.3	$N_x$ distribution across $[\pm\langle 0/45 \rangle]_s$ panel .....	71
Figure 4.4	$N_y$ distribution for $[\pm\langle 0/45 \rangle]_s$ panel.....	72
Figure 4.5	$N_{xy}$ distribution across $[\pm\langle 0/45 \rangle]_s$ panel .....	73
Figure 4.6	Shearing of an axially compressed $-45^\circ$ element.....	74
Figure 4.7	Positive shear force per unit length.....	74
Figure 4.8	Failure indices in second layer of $[\pm\langle 0/45 \rangle]_s$ panel.....	77
Figure 4.9	Failure indices in central layer of $[\pm\langle 0/45 \rangle]_s$ panel.....	78
Figure 4.10	Stresses in fiber direction, $\sigma_1$ , of the middle layer .....	79
Figure 4.11	Stresses transverse to fiber direction, $\sigma_2$ , in middle layer.....	79
Figure 4.12	Shear stresses, $\tau_{12}$ , in middle layer .....	80
Figure 4.13	Variation of $\sigma_1$ for a single $\langle 0/45 \rangle$ path.....	81
Figure 4.14	Thickness plot of $[90\pm\langle 45/75 \rangle]_s$ panel.....	84
Figure 4.15	$N_x$ distribution for $[90\pm\langle 45/75 \rangle]_s$ panel.....	85
Figure 4.16	Closed-form $N_x$ solution for $[90\pm\langle 45/75 \rangle]_{9s}$ , from Waldhart [11] .....	85



Figure 4.17	Thickness plot of for $[0\pm\langle 45/75 \rangle]_s$ panel.....	87
Figure 4.18	$N_x$ distribution for $[0\pm\langle 45/75 \rangle]_s$ quarter panel .....	88
Figure 4.19	Closed-form $N_x$ solution for $[0\pm\langle 45/75 \rangle]_{9s}$ .....	88
Figure 4.20	$N_y$ distribution for $[0\pm\langle 45/75 \rangle]_s$ quarter panel .....	90
Figure 4.21	Closed-form $N_y$ distribution for $[0\pm\langle 45/75 \rangle]_{9s}$ panel.....	90
Figure 4.22	$N_{xy}$ distribution for $[0\pm\langle 45/75 \rangle]_s$ panel .....	92
Figure 4.23	Closed-form $N_{xy}$ distribution for $[0\pm\langle 45/75 \rangle]_{9s}$ .....	92
Figure 5.1	Orientation angle of $\langle +25 -45 \rangle$ tow path.....	94
Figure 5.2	Thickness distribution of $[\langle \pm 25 \mp 45 \rangle]_s$ panel .....	95
Figure 5.3	Thickness plot of $[\pm 45]_s$ panel with 2" shift .....	96
Figure 5.4	$N_x$ distribution for $[\pm 45]_s$ panel with 2" shift.....	97
Figure 5.5	Thickness of $[[90 \langle 0 \pm 25 \rangle] / [0 \langle 0 \pm 45 \rangle]]_s$ Laminate.....	98
Figure 5.6	Orientation angle variation in layer of parallel tow paths .....	100
Figure 5.7	Orientation angle variation in layer of flat-shifted paths.....	100
Figure 5.8	$N_x$ distribution for parallel $[\pm\langle 0 45 \rangle]_s$ laminate .....	102
Figure 5.9	$N_x$ distribution for flat-shifted $[\pm\langle 0 45 \rangle]_s$ laminate .....	102

## List of Tables

Table 3-1	Convergence data for various mesh sizes. ....	61
Table 4-1	Case I total force and weight ratio results for selected laminates ...	75
Table 4-2	Case II total force and weight ratio results for selected laminates .	76

# Chapter 1

## Introduction

Many modern engineering applications demand high-performance materials that combine high stiffness, high strength and low weight. Composite materials often provide the best combination of these properties. Lamina consisting of high-stiffness high-strength fibers can be combined in different orientations and thicknesses to create a composite material tailored to specific loading conditions. The ability to customize the mechanical properties and structural response of a composite material allows for the most efficient structure to be determined and economically produced. The challenge to the engineer is to determine an effective means of achieving the most efficient structure. While many techniques for optimizing traditional composite materials have been developed, modern processing methods allow for more complex composite structures to be conceived and created.

### 1.1 Variable-Stiffness Composite Laminates

Traditional composite laminates consist of multiple plies of composite lamina. Each composite ply has specific material properties, thickness and orientation angles that remain constant throughout the ply. Traditional composite laminates have a specific loading response that remains constant throughout each ply. Composite plies with different material properties, thicknesses and/or orientation angles can be stacked together to tailor the response to a specific loading condition resulting in a very efficient structure. In some cases, however, it is advantageous to have a higher level of tailorability in order to reduce overall manufacturing costs or weight.

Variable-stiffness laminates differ from traditional straight-fiber composite laminates by varying material properties, thickness and/or fiber orientation spatially throughout the laminate. Variations in layer material properties, thickness and/or fiber orientation results in a spatially varying response. Variable-stiffness designs allow for the composite to be tailored to a wider range of potential applications than straight-fiber laminates.

### *1.1.1 Methods of Creating Variable-Stiffness Laminates*

There are three primary methods for varying the material properties, thickness and orientation angle of a laminate spatially. The primary methods include varying volume fraction of fibers, dropping or adding of plies to the laminate and varying the orientation angle through a ply. A brief overview of previous research on each of these methods will now be given.

One method of changing the response properties of a composite laminate is to vary the volume fraction of fibers within the laminate. Leissa and Martin [1] have investigated the vibration and buckling responses of single-layer composite plates with variably spaced parallel fibers. Variation of the fiber spacing along the x direction changed the engineering properties spatially. Thus, the response properties of the plate became functions of position along the x-axis. An example of such a lamina is shown in Figure 1.1. The variation in properties complicated the elasticity problem and solutions making it difficult to obtain an exact solution. The Ritz method was used to determine the initial stress distribution of the planar elasticity problem. The Ritz method was used to solve the vibration and buckling problems. Three different types of composite with various levels of orthotropy were investigated. Leissa and Martin showed that by varying the fiber spacing it was possible to raise the buckling load by as much as 38% and the fundamental frequency by as much as 21%. Additionally, it was shown that both the buckling load and vibration frequency could be decreased in some cases.

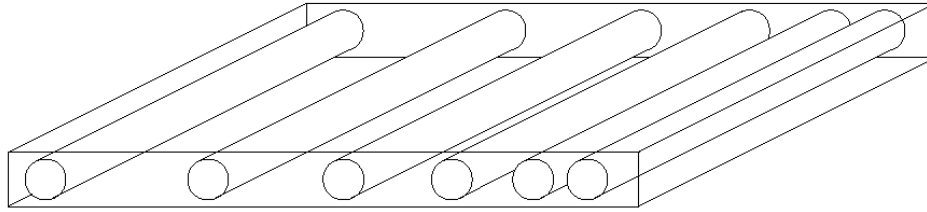


Figure 1.1 Lamina with varying volume fraction, from Waldhart [11]

A second method of creating a variable-stiffness laminate is to change the thickness within the laminate structure. DiNardo and Lagace [2] have investigated the buckling and post-buckling response of laminates with ply drop-offs. Ply drop-off laminates are created by terminating placement of a lamina before the layer has filled the entire laminate area. Figure 1.2 is a simple example of how dropping composite plies leads to a thickness change of the laminate. The response of graphite/epoxy composite plates with internal ply drop-offs was evaluated both experimentally and analytically. Three different types of plates were considered: normal flat plates, plates with one or more internal plies dropped along the centerline and plates where one or more layers abruptly changes fiber angle along the centerline. As with the Leissa and Martin research, the dropping of internal plies resulted in complex buckling behavior. A superelement method was used to predict the buckling loads, and the buckling behavior was found to depend on several effects. One of the effects was the difference in bending stiffness between the thick region with the internal plies and the region without the internal plies. Another potential effect studied was the geometric eccentricity caused by the thickness change at the edge of the internally dropped plies. It was determined that the change in bending stiffness from the normal region to the non-drop-off region had a larger effect on the buckling behavior than the local eccentricities due to thickness change.

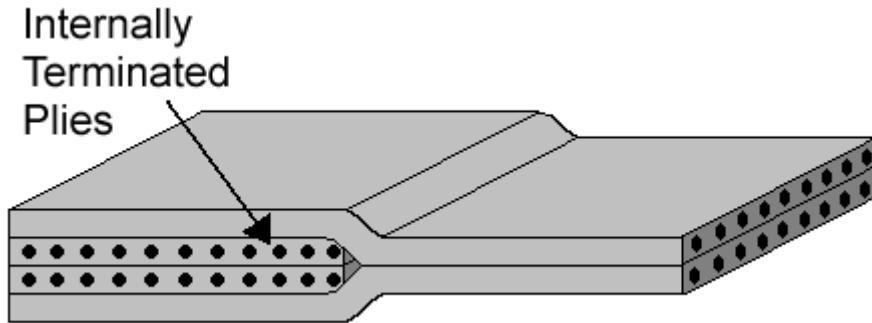


Figure 1.2 Laminate with internally dropped plies

The final method of creating a variable-stiffness laminate is to vary the fiber orientations throughout each lamina, also known as a "curvilinear-fiber lamina". Hyer and Lee [3] investigated using curvilinear fibers to increase the buckling resistance of a plate with a centrally located hole. A finite element model of 18 elements was used to model a quarter panel with a hole. The composite laminate consisted of 12 curvilinear lamina sandwiched between layers of  $\pm 45^\circ$  straight fiber lamina. Each element has a unique fiber-orientation angle. An example of such a quarter panel is shown in Figure 1.3. Sensitivity analyses and gradient searches were used to determine fiber-orientation angles that optimized the buckling resistance of the plate. Additionally, the research evaluated the tensile strength of the plates. The buckling load was increased by up to 2.96 times the buckling load of the baseline designs. This optimal design resulted in orientation-angle changes that varied by as much as  $75^\circ$  between adjacent elements. Such designs would be impossible to manufacture with even the most advanced current technology. Variations of less than  $15^\circ$ - $20^\circ$  between adjacent elements would be more practical.

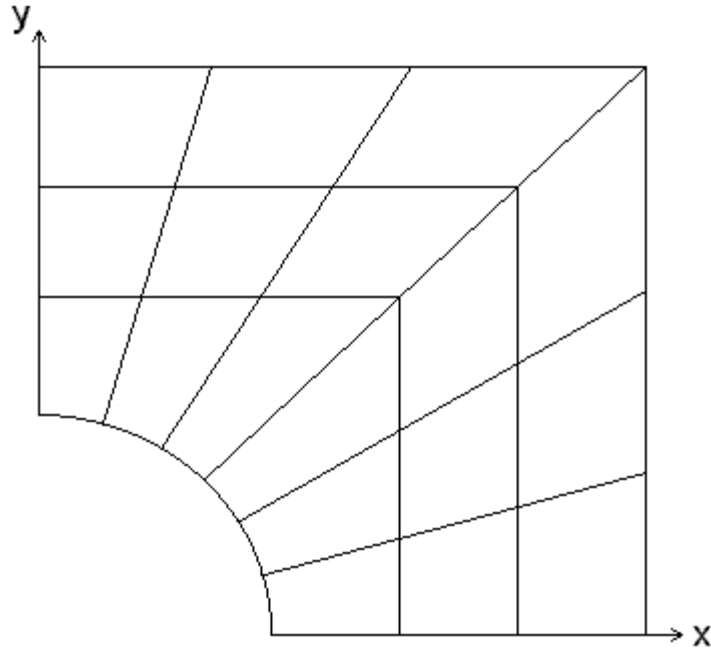


Figure 1.3 Example of 18 element quarter panel with central hole

A second approach was used to produce results that were more feasible from a manufacturing standpoint. The number of independent fiber-angle regions was decreased from 18 to six radially oriented regions. While a decrease in the number of independent regions might be expected to increase the likelihood of discontinuities between regions, it actually served to average out orientation-angle changes, caused by stresses near the hole, between the radially oriented regions. The decrease of independent regions resulted in a panel that had a more gradual change in fiber angle. The manufacturability came at the cost of some of the increase in buckling load. The increase in buckling load was still 1.85 times that of the baseline design.

Hyer and Lee then examined the effect of the optimal fiber angles on the tensile properties of the panel. The tensile strength was decreased 38%. A final design provided an increase in the buckling load of 30% and an increase of 35% of the tensile load. In all designs, the selective orientation of the fibers made it possible to redistribute the load from the region near the hole to the edge region.

The Hyer and Lee research illustrates just one of the many beneficial possibilities of curvilinear-fiber composite laminates.

### *1.1.2 Manufacturing of Curvilinear-Fiber Variable-Stiffness Laminates*

As noted before, the ability to design an efficient but complex composite structure is useless if it cannot be economically manufactured. Modern manufacturing techniques make it economically feasible to produce composite structures in a wide variety of shapes and forms. While manual lay-up is still in wide practice, automation of the composite manufacturing process reduces costs and results in more consistent final products. Automated techniques such as filament winding, tape lay-up and pultrusion have made mass production of composite laminates and composite structures a financially viable alternative to traditional materials. In order to manufacture variable-stiffness structures composed of curvilinear lamina, it is necessary to harness some of the most advanced composite manufacturing methods.

The processing of complex composite structures is currently possible with automated tow-placement machines. This emerging technology is characterized by a using a computer-controlled multi-axis delivery head to place numerous flat narrow strips of composite material known as "tows". This process allows design and production of parts that would be extremely difficult or impossible with other methods such as tape lay-up or filament winding. Two examples of tow-placement machines have been reviewed and will now be presented to familiarize the reader with the tow-placement method.

Evans, Vanigila and Hopkins [4] reviewed the capabilities of Cincinnati Milacron's FPX tow-fiber-placement machine. Two tow-placement machines, made by Hercules, were reviewed by Barth [5]. While these machines are, by no means, identical they share some traits common amongst tow-placement machines. These common traits are a wide range of motion, computer control, automation of the entire process, low-tension placement of multiple prepreg fiber tows that can be individually cut or restarted and differential tow-payout speeds.



The ability to produce complicated shapes depends on a full range of motion. Tow-placement machines have seven degrees of freedom that allow them the requisite wide range of motion. The first degree of freedom is the rotation of the mandrel. Three degrees of freedom allow for the entire machine to be translated on a carriage in the x, y and z directions. The final three degrees of freedom allow for the tow-placement head to be rotated about the x, y and z axes. A basic schematic of a Hercules tow placement machine and the seven axes of motion are seen in Figure 1.4, taken from Barth [5]. The rotation of the mandrel is denoted as "Axis 1." The translation axes are denoted as "Axis 2", "Axis 3" and "Axis 4". The three rotational axes in the magnification of the tow-placement head are denoted "R1", "R2" and "R3." The Cincinnati Milacron machine shares a similar configuration with seven axes.

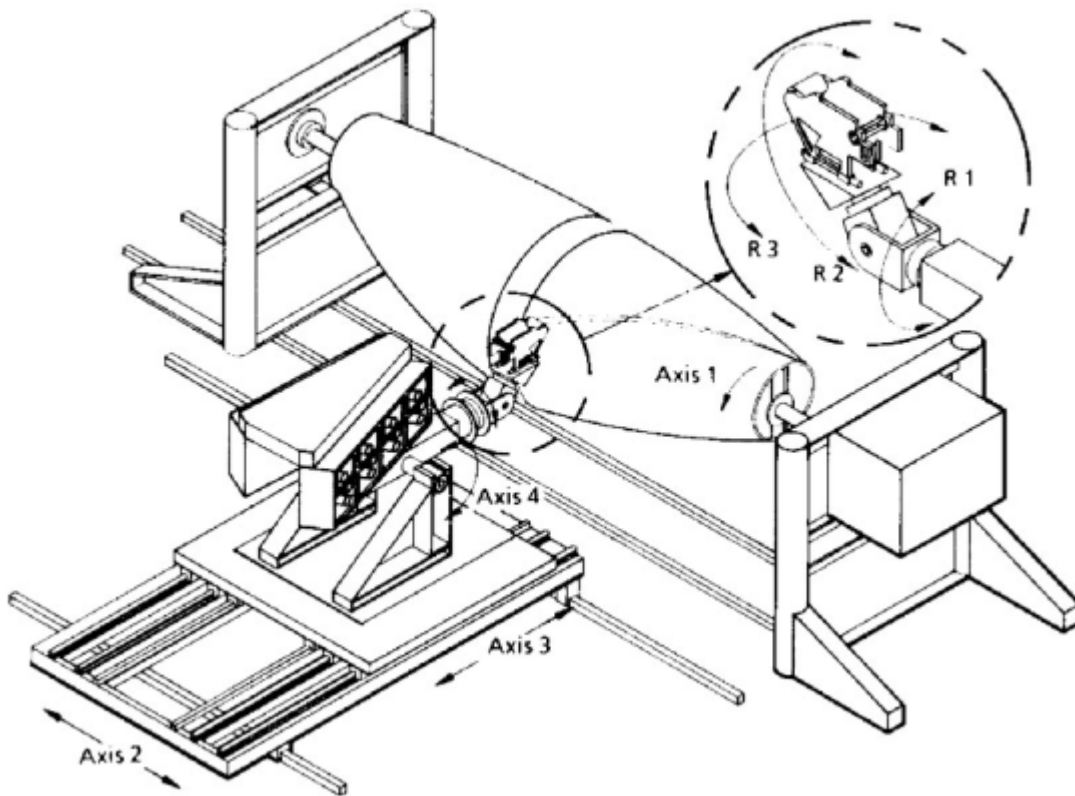


Figure 1.4 Schematic of Hercules Inc. tow placement machine, from Barth [5].

The carriage and mandrel of the largest Hercules Inc. machine allow fabrication of parts over 30 feet in length. Finally, the full range of motion afforded to the tow head with its three-axes of rotation allows for tows to be

aligned in any direction. This task is impossible for filament-winding methods, which limit the fibers to follow near-geodesic paths.

The wide range of motion is useless if it cannot be precisely controlled. Both the Hercules Inc. and the Cincinnati Milacron machines use computer control and automation extensively. Bullock, Kowalski and Young [6] give a detailed overview of the various computer resources and procedures used to program the robotic systems of the Hercules Inc. machine. Enders and Hopkins [7] provide a similar overview for the Cincinnati Milacron machine. Offline programming and simulation are used to determine the feasibility of the design. For both machines, 3-D simulations confirm that the machine can make the required movements. Once the design has been confirmed, the information is translated into machine motions and verified in a "dry" run. Not only is computer control harnessed to automate the task, but it also monitors the many different subsystems to control tow tension and prevent tow breakage.

The composite tows come in a variety of materials including, but not limited to, graphite, fiberglass and Kevlar. Tows are approximately  $\frac{1}{8}$ " in width with a rectangular cross section. They are preimpregnated with thermoset epoxies commonly used in composite manufacturing. The tow material is therefore "tacky" and will stay in position once placed. Enders and Hopkins [6] acknowledge that the variety and quality of the tow material is not comparable to the base materials used in other processes but that is expected to change as tow placement comes into more widespread use.

The heart of the tow-placement machine is the tow-placement head. The tows are fed off spools through a tensioning system to the tow-placement head. The tow-placement head of the Cincinnati Milacron machine can accommodate up to 24 individual tows while the Hercules Inc machines have 2 different tow head configurations; 12 and 32 tows. The result is path widths of up to 3 inches in the Cincinnati Milacron machine and up to 4 inches for the Hercules Inc. machines. The tow-placement heads also house cutting mechanisms, which can cut individual tows. A second mechanism allows cut tows to be restarted. The path width is controlled by increasing or decreasing the number of individual

tows. For instance, if a design requires a constant thickness for each layer the band width can be adjusted by adding or dropping the appropriate number of tows. Adjustable tow width also results in more efficient use of materials by stopping tows that are not necessary and reducing the amount of post-cure machining required for a finished product.

In order to drop and add individual tows in the tow-path band, it is necessary to have a differential payout system. Differential tow payout allows different tows to be fed through the head at different rates. In the case of a dropped tow, the head stops the payout altogether. Differential tow payout has an important additional benefit. The tow head can be steered along the mold surface to create curved paths that are non-geodesic. Filament winding and tape laying are confined to near-geodesic paths because they rely on the friction and the tension of the material to hold individual fiber paths in place. Tow placement uses controlled compaction of the tow head against the part surface and low tension of the tow material to allow fibers to be placed in a curved fashion. Enders and Hopkins [6] report that it is possible to form curves with a radius of curvature of five inches. Nagendra, Kodiyalam, Davis and Parthasarathy [8] indicate that such extreme curvatures show some local fiber buckling and suggest 25 inches as the minimum radius of curvature. Additionally, the ability to lay path in any direction allows for paths to be laid axially which is impossible to do with tape laying or filament winding.

As mentioned in the previous paragraph, low-tension positioning is used in the tow-placement method, because tension is not necessary to hold the tows in place. Low-tension positioning also allows for parts with concave surfaces to be formed. The high tension necessary to hold fibers and tapes in place for tape-laying and filament-winding processes causes material to "bridge over" concave surfaces (i.e., the tow material forms a bridge over the concave surface), as shown in Figure 1.5. To form a concave surface with tape laying or filament winding, some degree of hand layup is necessary which usually results in discontinuous fibers.

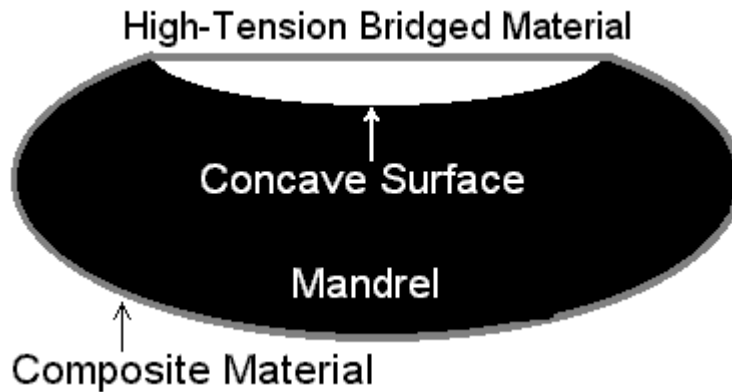


Figure 1.5 Bridged Material caused by high-tension filament winding

Bullock, Kowalski and Young [6] estimate the speed of tow placement to be as much as seven times faster than hand layup, which is the only method capable of producing such a wide range of parts. Barth [5] provides a limited comparison of tow-placement parts as compared to hand layup and shows that tow-placement parts have similar strength in compression-after-impact tests. Tow-placement machines combine a wide range of motion, automated computer control and low-tension placement of multiple prepreg fiber tows producing a very practical method with seemingly unlimited potential. Tow-placement machines provide a combination of the best features of tape laying and filament winding, fast production rate and repeatability, with the numerous shape possibilities previously only possible with hand layup.

### *1.1.1 Curvilinear-Fiber Variable-Stiffness Laminate Research*

The potential of curvilinear-fiber variable-stiffness laminates has fostered a new area of research in laminated composite materials. The increased freedom of design also increases the complexity and requires novel approaches to many common problems in composite laminates engineering. Many different approaches have been used to attempt to adequately model and predict the response of variable-stiffness laminates.

Hyer and Lee [3] approached this problem by modeling the laminate as a group of finite elements with piecewise continuous fiber directions. While a

substantial increase of buckling resistance was produced, the optimal designs had a tendency to result in fiber configurations that would be difficult or impossible to construct. Hyer and Lee constrained the fiber orientations such that small variations in orientation angle occurred in adjacent elements, it was possible to increase buckling resistance while producing designs that could be more easily fabricated. More recent research has addressed the specific advantages of the tow-placement process and has provided two different methods of modeling tow-path laminates.

Nagendra, Kodiyalam, Davis and Parthasarathy [8] looked specifically at the Cincinnati Milacron tow-placement machine and proposed a method for modeling the fiber orientations. The goal of their research was to develop a method of optimizing tow paths. The paths were defined by passing a single curve through a set of control points based on a single cubic NURBS (Non-Uniform Rational B-Splines) curve. This curve defined the path center of the tow head across the part surface. The width of the tow head was taken into account and the entire procedure was repeated to cover the entire surface. This information was then mapped on to a finite element mesh in order to calculate the fiber-orientation angles. From this information the desired analyses could be performed. One example was problem of maximizing buckling load addressed by Hyer and Lee [3]. After five design iterations, the buckling load was increased 85% over the initial straight-fiber design.

A second method of defining the tow paths was presented by Gürdal and Olmedo [9,10]. The fiber-orientation angles varied linearly along the length of the composite laminate. A reference path was defined that passed through the center of a flat rectangular plate. The path was then shifted a uniform distance to define fiber paths for the entire plate. A square panel composed of shifted-path centerlines is shown in Figure 1.6. The shift distance and shift direction is shown by the equal-length arrows. It is important to note that the shifted-path centerlines create an optical illusion which causes the arrows appear to be different lengths. Analysis of such configurations showed that increases in the

axial stiffness of up to 50% and favorable buckling response due to redistribution of the load to high-stiffness regions were possible [10].

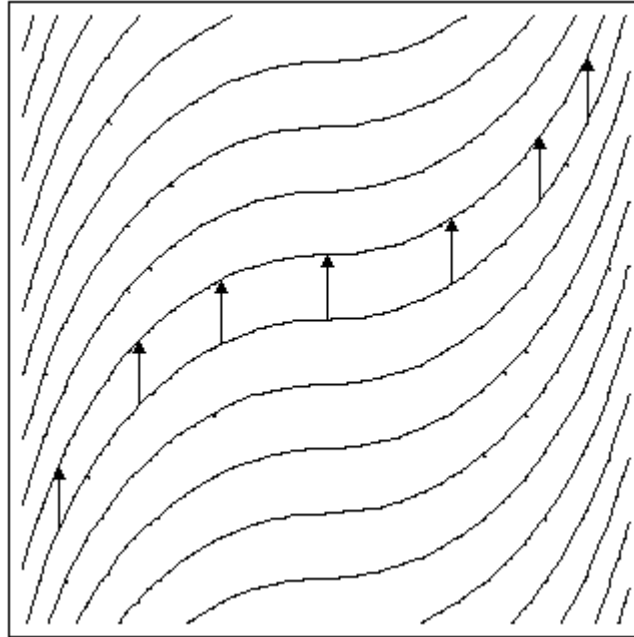


Figure 1.6 Shifted path lamina based on linearly varying reference path

In an extension of the research, Waldhart examined two different possible methods of using the formulation proposed by Gürdal and Olmedo [11]. A reference path based on a linearly varying curve is created at the origin. Then two different methods are used to form the remainder of the plate. The first method was the same shifted method used by Gürdal and Olmedo, where the reference fiber was repeatedly shifted a prescribed distance to form the remainder of the fiber paths. The second method is to create new paths that are parallel to the reference fiber. An interval-search method was used to determine the distance of adjacent paths from the reference path. This process is repeated until the entire plate was defined, as shown in Figure 1.7. It was shown that a 44% increase of buckling load and an increase in the axial stiffness of 124% over straight-fiber laminates was possible using the shifted-path method. The parallel-fiber laminates also resulted in increases of stiffness over straight fiber laminates, but less than the shifted-fiber laminates.

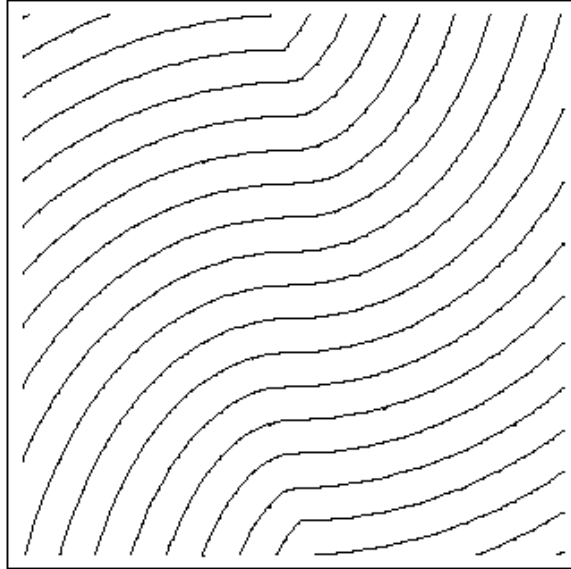


Figure 1.7 Parallel-path lamina based on linearly varying reference path

Parallel-path methods also can lead to kinking of the tow paths. The method used to create parallel-path laminates means that changes in curvature will be exaggerated in subsequent paths. This effect is seen near the middle of the top and bottom edges of the parallel-path lamina in Figure 1.7. In order to correct this problem, constraints on the curvature of the reference path were used.

The methods presented represent three possible methods for defining variable-stiffness laminates based on variation of the fiber angles throughout the laminate. In all three methods, it was shown that the buckling load and axial stiffness could be improved by selectively designing the fiber orientations throughout the laminate. While all three methods were based on theoretically flat laminates with no overlap, in practice overlap can occur and will have an effect on the response of the laminate.

## 1.2 The Finite Element Method

The finite element method (FEM) is an approximation technique that provides solutions for differential and integral equations, which may otherwise be impossible to solve in a closed-form. The finite element method is particularly useful in problems with complex geometry, loading and stiffness variations, such

as variable-stiffness composite plates. For structures, the general approach is to divide a single complex geometry into a defined group of smaller, simpler shapes known as "finite elements". A system of equations composed of a known stiffness matrix a set of unknown displacements and a set of known forces. The displacements can be determined by solving the set of linear equations such that the equilibrium conditions are satisfied and the boundary conditions are satisfied.

### *1.2.1 System of Equations*

The interactions between the finite elements are related through a set of linear equations.

$$[K]\{u\} = \{F\}$$

In this equation,  $K$  represents the global stiffness matrix, which is created from the stiffness matrix of each element. The variables  $u$  and  $F$  represent the displacement vector and load vector, respectively. These two vectors describe the response at each degree of freedom throughout the model. This set of equations coupled with a set of known boundary conditions allows for the static response of the entire system to be determined.

### *1.2.2 Boundary Conditions*

In order to solve the linear set of equations, it is necessary to specify a set of boundary conditions. The boundary conditions are comprised of known displacements or known forces at different locations. At the very least, for static analysis, there must be sufficient boundary conditions to ensure there will be no translation or rotation of the model. For 2-dimensional analysis, the model must be fixed in the x and y directions, and there must be no rotation about the z axis. For uniform end shortening of a plate, the minimum boundary condition requirements are fulfilled by specifying the x displacement along two edges and fixing one point in the y direction.

The boundary conditions are also used to reduce the number of degrees of freedom by reducing the stiffness matrix and load vector. The degrees of



freedom are reduced by eliminating those degrees of freedom that correspond to zero displacement quantities. If the degrees of freedom at the boundary nodes are not removed, then the system is indeterminate and cannot be solved. By removing these terms, the system can be solved. After the analysis, it is possible to recover the forces required to produce the prescribed displacements.

### *1.2.3 Finite Element Results*

The system of linear equations and the boundary conditions can be used to determine the values of all the displacement and rotation degrees of freedom. Once the displacements are known, it is possible to calculate the force resultants, stresses and strains for each element. The force resultants along the displaced edge can be used to characterize the relative stiffness of the entire panel. The stresses and strains can be used in conjunction with failure criteria to determine whether the element will fail under the prescribed displacement.

## 1.3 Methods of Optimization

Since the first structures were built in ancient times, people have desired to know how strong, how light or how tall they could be built. Often the most convenient method was trial and error. Today engineers possess many mathematical methods to determine optimal designs. Modern computational facilities have also made it feasible to design and evaluate systems in virtual environments. The fundamentals of optimization and composite optimization will be covered in this section. Previous research in the optimization of composite laminates will also be discussed.

### *1.1.2 Optimization*

Optimization is the process of finding the best design within predetermined restrictions. An example of a simple design problem would be to minimize the weight of a statically indeterminate truss under a given load. The first step in optimization is the design problem formulation. The system must be characterized as an objective function dependent on a set of design variables.

The goal is to minimize or maximize the objective function, i.e., minimize weight or maximize buckling load. The design variables are the parameters that can be changed to attempt to find the best design. For the simple truss problem, the design variables might be the areas of each member of the truss.

Usually a set of constraints that dictate the bounds of other relationships also exists. In the truss example, a constraint would be necessary to prevent the stress of any component from exceeding the yield stress of the material. Finally, there must also be upper and lower bounds on all design variables. These upper and lower bounds can be used to reflect manufacturing constraints. A lower bound could be used to prevent the cross-sectional area of lightly loaded members from approaching zero, and thus becoming impractical for joining to other members. An upper bound might be used to prevent diameters of highly stressed members from becoming so large that they would violate the initial dimensional constraints of the design (e.g., the distance between two adjacent members is 2 inches, but the cross-sectional area of a single cylindrical member results in a radius of 3 inches).

Most optimization problems can be expressed in a simple generalized form. The general optimization formulation is:

$$\text{Min / Max : } f(\mathbf{x}) = f(x_1, x_2, \dots, x_m)$$

$$\text{such that : } g_j(\mathbf{x}) \geq 0, \quad j = 1, \dots, n$$

$$h_k(\mathbf{x}) = 0, \quad k = 1, \dots, p$$

$$\mathbf{x}_{lb} \leq \mathbf{x}_i \leq \mathbf{x}_{ub} \quad i = 1, \dots, m$$

The mathematical problem is to minimize or maximize the objective function,  $f(\mathbf{x})$ , subject to  $n$  inequality constraints and  $p$  equality constraints, where  $g_j(\mathbf{x})$  are the inequality constraints and  $h_k(\mathbf{x})$  are the equality constraints. The objective function and constraints are all function of  $m$  design variables,  $x_i$  that have upper and lower bounds  $x_{ub}$  and  $x_{lb}$ , respectively. This general form can be used for both linear and nonlinear problems. Once the problem is formulated,

the goal is to find an accurate and efficient method of determining the optimal design.

If the problem can be formulated as a linear problem, where the objective function and constraints can be formulated as linear functions of the design variables, then simple methods such as linear programming can be used. Often the problem contains some nonlinear terms and must be handled by more advanced techniques.

### *1.3.1 Optimization of Composite Laminates*

In almost all respects, composite laminates provide us with a more complex problem than isotropic materials. Increased complexity certainly is the case for optimization of composite laminates. The most noticeable difference is the number of design variables. For an isotropic material, possible design variables include thickness, width, height, cross-sectional area or type of material. For composite materials, not only are those variables applicable but also the number of plies and the ply orientations. Laminates normally consist of multiple plies, thus the number of design variables increases very dramatically over isotropic materials.

Another complexity of optimizing composite materials is predicting the response. While the response of isotropic materials depend on two material properties, composite laminates are governed by a 6x6 matrix of 18 independent stiffness constants, which are functions of both material properties and laminate geometry. If the composite laminate is not designed carefully, unexpected couplings between bending, shearing and stretching can occur. For these reasons, composite materials are often restricted in a number of ways.

Composite materials usually come in fixed thicknesses which reduces the thickness from a continuous variable to a discrete variable. When optimizing a composite laminate, designers typically limit themselves to certain ply common ply angles such as  $0^\circ$ ,  $\pm 45^\circ$ ,  $90^\circ$  or  $0^\circ$ ,  $30^\circ$ ,  $60^\circ$ ,  $90^\circ$ . The use of specific ply orientations results in transformation of ply angle from a continuous variable to a discrete variable. While using specific ply orientations reduces the design space

from a continuous field of infinite possible solutions to a discrete field of limited possibilities, it also places more constraints on the optimum design and can make the problem more difficult to solve.

Haftka and Gürdal [12] presented numerous methods of approaching the composite laminate design problem. Typically, the goal of these problems is to determine the stacking sequence that maximizes or minimizes one of the stretching or bending stiffness constants. Conversion of the composite material properties to stress invariant representation results in a simpler, more intuitive, formulation. This formulation consists of five stress invariants, which are functions of only ply orientation. Many examples are shown which include graphical techniques.

### *1.3.2 Previous Research on Variable-Stiffness Laminate Optimization*

Variable-stiffness laminates present a more complex system than traditional straight-fiber laminates, thus further complicating the optimization process. In straight-fiber composite laminates, the ply angle remains constant throughout each layer, but in variable-stiffness laminates, the fiber-orientation angle varies spatially in the plane of the laminate. Manufacturing constraints usually require the fiber orientation to be a gradually changing, continuous function. In order to simplify the optimization, it is necessary to develop a consistent method to design the fiber paths. Even with a consistent method, countless fiber-orientation possibilities exist.

As mentioned earlier, some of the first research on optimizing curvilinear-fiber variable-stiffness laminates was performed by Hyer and Lee [3]. The first goal was to maximize buckling load with no constraints on fiber orientations. The buckling load was maximized by using finite element model of a quarter panel with a centrally located hole along with a sensitivity study approach. A finite element mesh of 18 elements was first created. Throughout each element, the fiber orientation was constant. The orientation angles of the fibers in each element became the design variables. The orientation of the  $0^\circ$  layers in a  $(\pm 45, 0_6)_s$  laminate was allowed to change. The buckling load sensitivity of each

element to changes in the fiber orientation of the 18 elements was then determined. For each element there existed an angle, that will maximize the buckling load.

To pick the 18 angles from the sensitivity analysis would be a very simple task, if not for the fact that the response in each element depends on the orientation in every other element. The solution to this problem was to use a gradient search that simultaneously treated each of the element fiber orientations as a variable. It is important to note that this method does not necessarily give the global maximum. The gradient search will find the local maximum nearest the initial values given.

As was explained earlier, with no constraints on the angles in each element, the initial results led to a design that would be impossible to fabricate. By reformulating the problem such that the fiber-orientation angles in adjacent elements would be more continuous, it was possible to achieve a more feasible design. Additionally, the response of the designs to tensile loads was also examined producing a final design with a 30% improvement in buckling load and a 35% improvement of maximum tensile load.

Nagendra, Kodyalam, Davis and Parthasarathy [8] conducted additional research in the area of optimization of curvilinear-fiber variable-stiffness laminates. This research was based on the capabilities and limitations of the Cincinnati Milacron tow-placement machine. As was mentioned earlier, the fiber-path orientation was described by a NURBS curve designed by passing the curve through a set of defining points, known as "control points". The optimization method used was based on a shape function approach. This approach forms a final fiber path based on a linear combination of predefined basis curves. The design variables In this case, are a set of coefficients that are multiplied into the basis shape functions. When the coefficients are multiplied by the shape functions, a new set of control points is created which defines the reference tow path. From this path, additional parallel tow paths were constructed such that there was no overlap between adjacent paths. The optimization was constrained using the Tsai-Wu failure criterion with a modified

Hashin criterion. This failure formulation allowed the mode of failure to also be examined. The formulation resulted in a 72% increase in the buckling load for a panel with a central hole. These results are similar to the results Hyer and Lee achieved on a similar problem.

#### 1.4 Focus of this Research

Previous research has shown that variable-stiffness laminates have a great deal of potential in composite structures design. The curvilinear-fiber concept in particular, along with tow-placement machines, allow for a wide range of possibilities. Waldhart [11] showed that substantial gains in buckling load and in-plane stiffness can be realized using either the parallel-path method or the shifted-path method. Of these two methods, the shifted-path method produced the best results. The shifted-path method produces an unexpected secondary effect, which was not addressed in the previous research. Adjacent shifted paths will overlap each other causing variations in thickness. This secondary effect results in a complex geometry that cannot be accurately modeled and solved in closed-form.

The goal of this research is to develop a tool that can be used to accurately model and design variable-stiffness composite laminates. First, a review of the computational methods used to create a finite element model based on the conventions established by Gürdal and Olmedo [9] will be reviewed. These finite element models will be used with the GENESIS finite element analysis and design package to solve for the static response of various variable-stiffness configurations. The static response and failure results of these analyses will be presented. Additionally, techniques for evaluating the stiffness as an objective function and evaluating the constraint conditions will be presented. Finally, additional capabilities of the program will be demonstrated.

## Chapter 2

### Curvilinear-Fiber Variable-Stiffness Laminate Design

The increased design possibilities of variable-stiffness lamina, as compared to straight-fiber lamina, require a more complex design formulation than is used for traditional composite lamina. In this section, the method used to design curvilinear-fiber variable-stiffness laminates will be described. First, the definition of a tow path will be given. Next, a curvilinear-fiber reference path will be defined. A description of how this path is shifted to create additional paths to create a single lamina will then be presented. The lamina definitions will be followed by some geometric implications of the shifted-path variable-stiffness lamina design process. Finally, a description of how laminates are formed from the individual lamina, and the nomenclature used to describe curvilinear-fiber variable-stiffness laminates will be addressed.

#### 2.1 Tow-Path Geometry

The tow path consists of a band of multiple composite tows. The tows are laid down side-by-side by a tow-placement head. As mentioned earlier, the tow-placement head can be translated and rotated freely in all directions. To create a composite laminate structure multiple passes are made along predefined paths. The tow-placement head rotations at each point in the placement process must also be defined in addition to the path of the tow-placement head. A single planar tow path consisting of six individual tows is shown in Figure 2.1. The direction of travel is denoted by the large arrow on the tow-placement head.

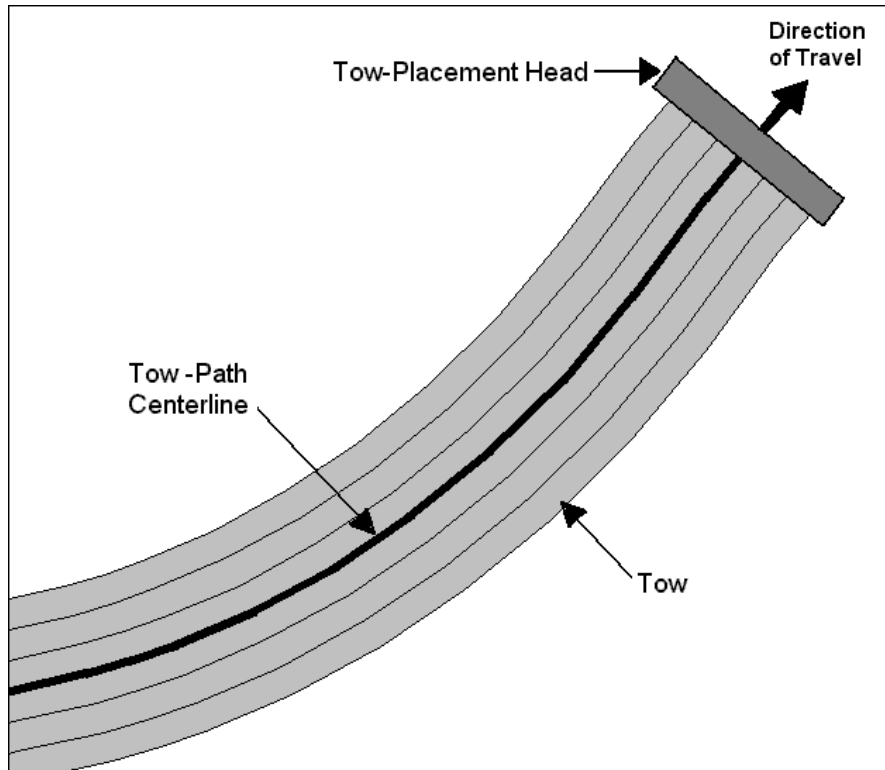


Figure 2.1 Single tow path and tow-placement head

The centerline of the tow path is also shown in Figure 2.1. The tow-path centerline is important because it is used to define the path of the tow-placement head. Additionally, the tow-placement head rotation about an axis perpendicular to the lamina plane is defined such that all of the tows are oriented parallel to the centerline. In order to design a tow-placed curvilinear-fiber variable-stiffness lamina, it is necessary to determine both the coordinates and the fiber orientation of each point of the tow-path centerline as a function of position. Once these functions are known, it is possible to determine the fiber-orientation angle at any other point in the tow path, as shown in Figure 2.2.



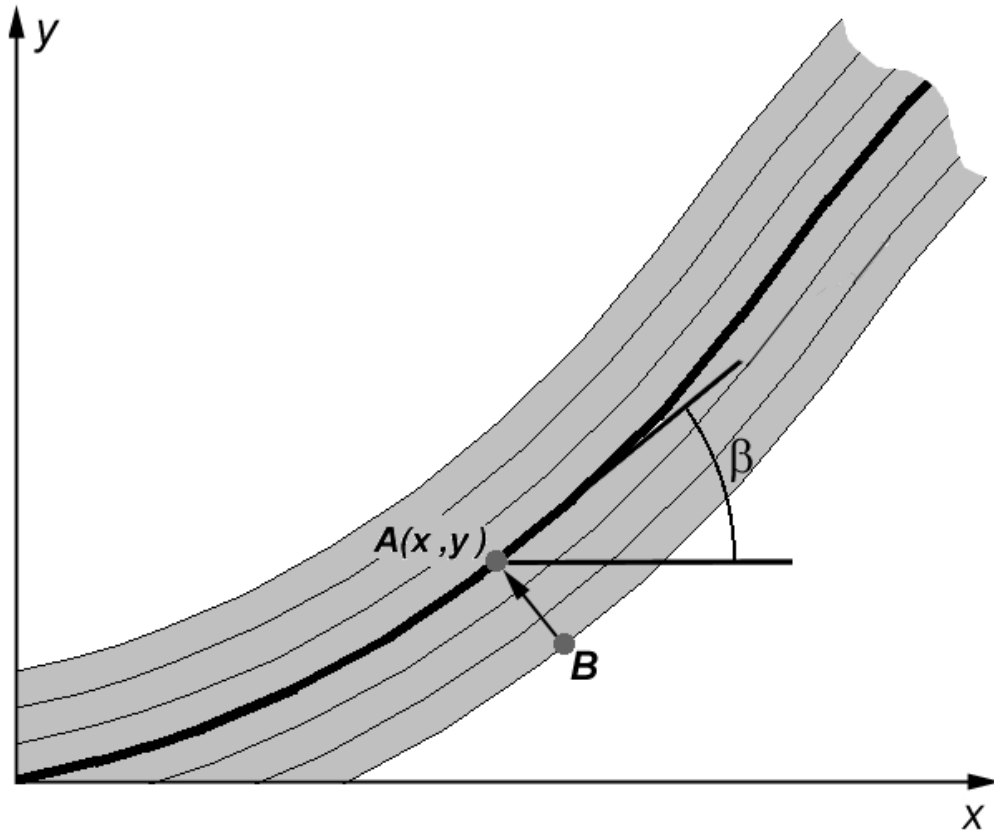


Figure 2.2 Point on tow-path centerline with xy-coordinates and fiber-orientation angle,  $\beta$

In Figure 2.2, point A is a point on the tow-path centerline, which is defined by a set of xy-coordinates. Additionally, the tow-placement-head angle at point A, is defined as  $\beta$ . Point B in Figure 2.2 is a point within the width of the tow path. The orientation angle at point B is defined by the fiber-orientation angle at the closest point on the reference path. In this case, Point A is the closest point, thus the fiber-orientation angle at B is also equal to  $\beta$ . Thus, if a tow-path centerline can be defined, it is possible to define the geometry of the entire tow path. It is also important to note that, the tow path is a collection of parallel tows. If the fiber-orientation angle is changing too rapidly, it is possible that the tow path will kink or fold due to high compressive forces on one edge and stretching on the opposite edge of the tow. This phenomenon also can limit the rotation of the tow-placement head.

## 2.2 Definition of a Curvilinear-Fiber Reference-Path Centerline

Straight-fiber composite lamina can be adequately described by a set of basic material properties, a thickness and a single orientation angle. Curvilinear-fiber variable-stiffness lamina require information not only regarding the material and thickness but also a convenient method of describing the different fiber orientations at any point in a single lamina. The method used in this research, will be that established by Gürdal and Olmedo [9]. The first step is to define the path that passes through the origin, known as the "reference path."

### 2.2.1 Coordinate Definitions

The  $xy$ -coordinate system, shown in Figure 2.2, will be used to define the dimensions of a single layer of a square panel. The curvilinear path is defined in a coordinate system defined by orthogonal axes  $x'$  and  $y'$ . The  $x'y'$ -coordinate system are rotated counter-clockwise from the panel  $xy$ -coordinate system by a tow-path rotation angle,  $\phi$ , as shown in Figure 2.3.

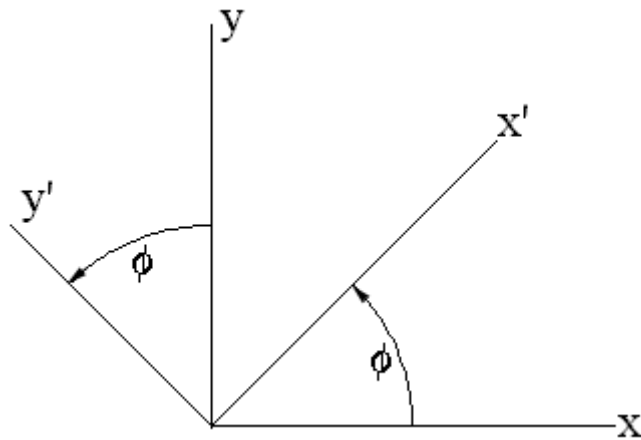


Figure 2.3 Panel ( $xy$ ) and tow-path ( $x'y'$ ) coordinate systems

Changing from one set of coordinates to the other can be accomplished using a simple transformation, recalling that the rotation angle,  $\phi$ , is positive in the counter-clockwise direction.

$$x' = x \cos \phi + y \sin \phi$$

$$y' = -x \sin \phi + y \cos \phi$$

*or*

$$x = x' \cos \phi - y' \sin \phi$$

$$y = x' \sin \phi + y' \cos \phi$$

In this research, the tow-path-rotation angle,  $\phi$ , will be either  $0^\circ$  or  $90^\circ$ . The method also uses a fiber-orientation angle,  $\theta$ , along the tow-path centerline which is defined as a linear function of position along the  $x'$  axis. An example of a linearly varying tow-path centerline is shown in Figure 2.4.

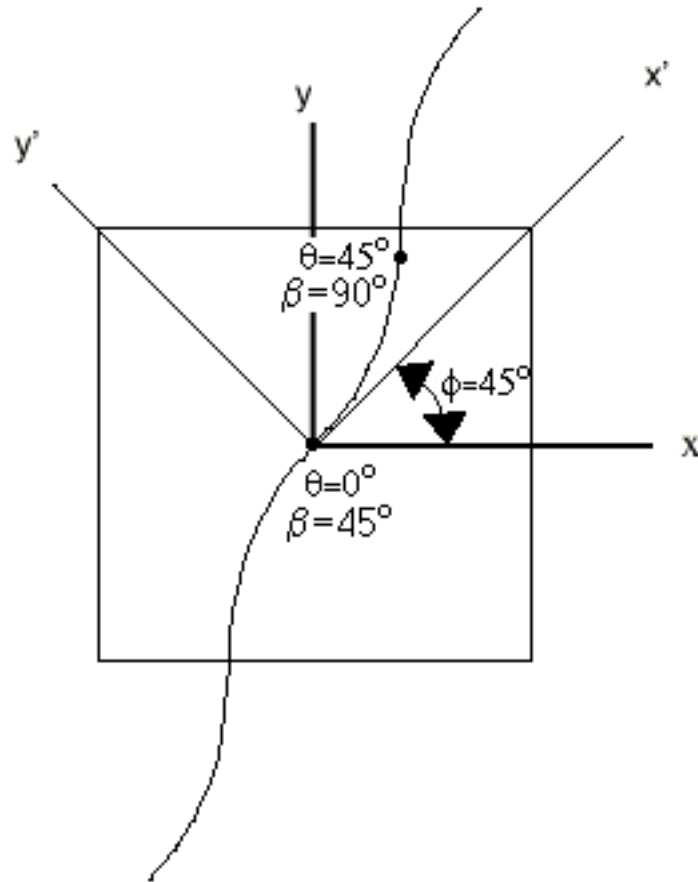


Figure 2.4 Linearly varying centerline

The tow-placement-head angle,  $\beta$ , is then defined as a function of the constant tow-path rotation angle,  $\phi$ , and the varying fiber-orientation angle,  $\theta(x')$ .

$$\beta = \phi + \theta(x')$$

### 2.2.2 Reference-Path Orientation-Angle Definition

In this research, the fiber-orientation angle,  $\theta$ , is defined as a linear function of  $x'$ . The fiber-orientation angle varies linearly between two angles along the  $x'$  axis. The first of the two angles,  $T_0$ , is the fiber-orientation angle at the center of the panel. The second angle,  $T_1$ , is the fiber-orientation angle at a characteristic distance  $a/2$  from the center of the plate, where  $a$  represents the width of the panel. This convention simplifies the tow-path definition process and also allows for a large degree of design flexibility. Figure 2.5 is a schematic of where  $T_0$  and  $T_1$  are defined along the  $x'$  axis. The general plate dimensions are also shown in Figure 2.5.

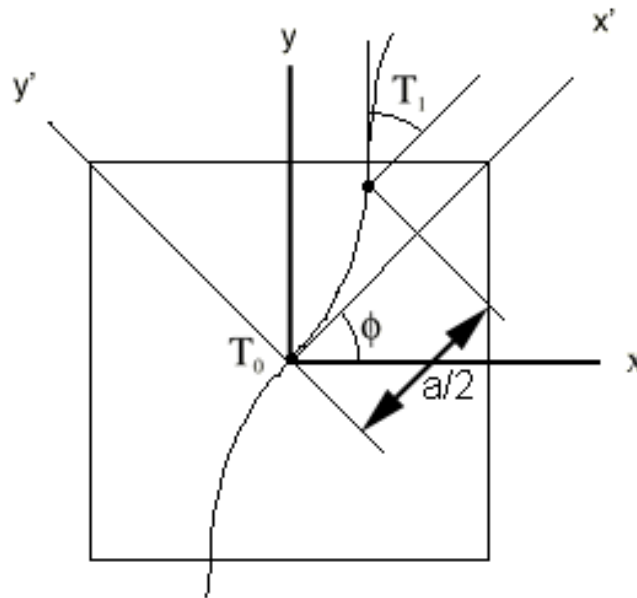


Figure 2.5 Geometry for defining a variable-stiffness reference path

The result of a linearly varying tow path is a smooth, continuous reference-path centerline, as shown in Figure 2.6. Figure 2.6 is a simple curvilinear-fiber-path centerline where  $T_0=0^\circ$ ,  $T_1=45^\circ$  and  $\phi=0^\circ$ . The fiber-orientation angles  $T_0$  and  $T_1$  are labeled at the appropriate positions along the path.

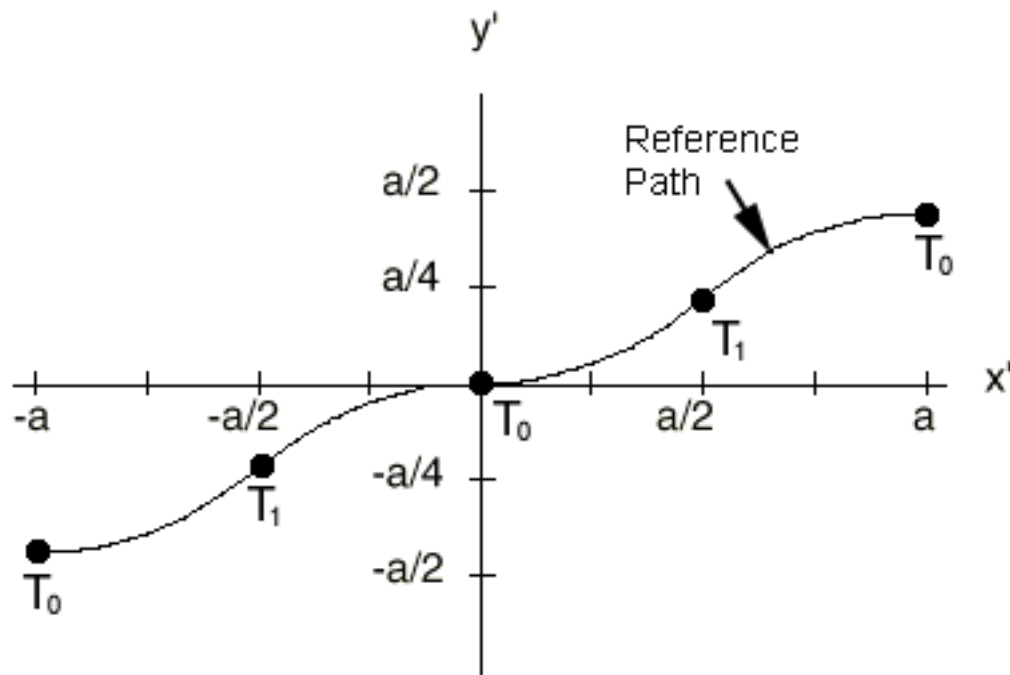


Figure 2.6 Curvilinear-fiber reference path centerline for  $T_0=0^\circ$  and  $T_1=45^\circ$ , from Waldhart [11]

The linear variation of fiber angle produces a reference-path centerline with continuous change in fiber orientation. This path can be plotted in a rectangular coordinate system, as defined by axes  $x'$  and  $y'$ . Determining the orientation angle for any value of  $x'$  is simple because the variation in orientation angle is linear. The necessary equations to determine the fiber-orientation angle,  $\theta(x')$ , are piecewise continuous linear functions.

$$\theta(x') = \begin{cases} \frac{2}{a}(T_1 - T_0)x' + T_0 - 2(T_0 - T_1), & \text{for } -a \leq x' \leq -\frac{a}{2} \\ \frac{2}{a}(T_0 - T_1)x' + T_0, & \text{for } -\frac{a}{2} \leq x' \leq 0 \\ \frac{2}{a}(T_1 - T_0)x' + T_0, & \text{for } 0 \leq x' \leq \frac{a}{2} \\ \frac{2}{a}(T_0 - T_1)x' + T_0 - 2(T_0 - T_1), & \text{for } \frac{a}{2} \leq x' \leq a \end{cases}$$

The resulting variation in the fiber-orientation angle can be plotted versus position along the x-axis. The piecewise-continuous nature of the orientation-angle variation, for  $T_0=0^\circ$  and  $T_1=45^\circ$ , is shown in Figure 2.7.

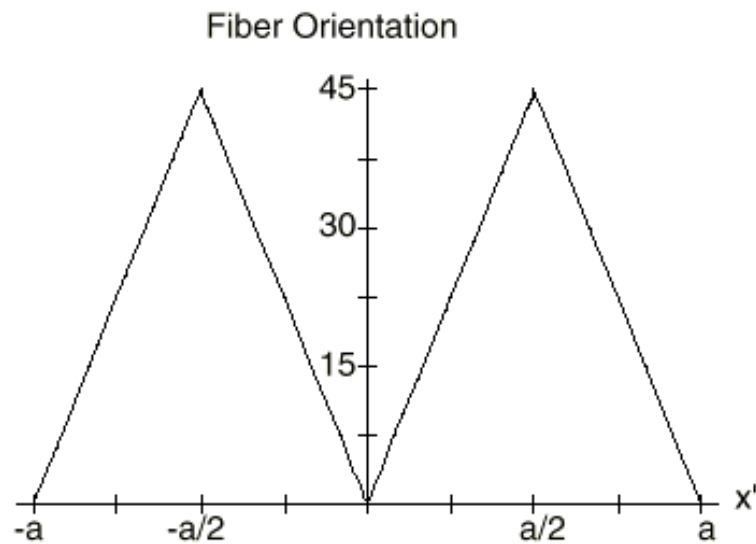


Figure 2.7 Linear variation of fiber-orientation angle for  $T_0=0^\circ$  and  $T_1=45^\circ$ , from Waldhart [11]

An example of a reference-path centerline, where  $\phi = 0^\circ$ ,  $T_0=0^\circ$  and  $T_1=45^\circ$ , is shown in Figure 2.8. Because  $\phi = 0^\circ$  in this first example, the x-y coordinate system and x'-y' coordinate system overlay each other. In this case, the tow-head-orientation angle,  $\beta$ , will be equal to the fiber-orientation angle,  $\theta$ , at all points along the centerline path. The values of the tow-head-orientation and the fiber-orientation angles are shown at the center and edges of the panel.

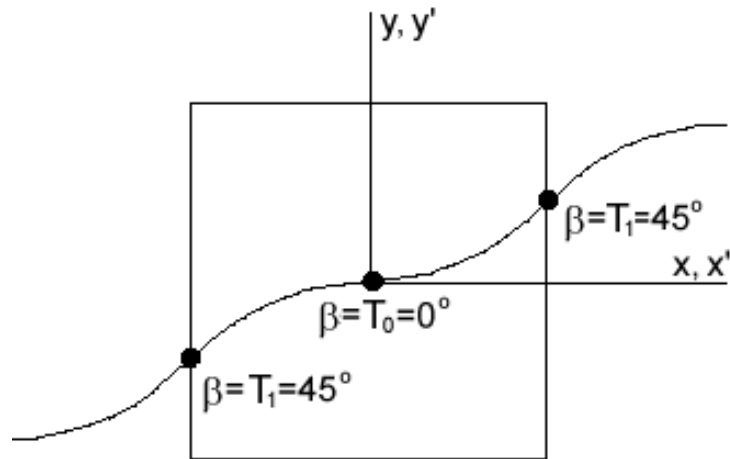


Figure 2.8 A reference-path centerline for  $\phi = 0^\circ$ ,  $T_0=0^\circ$  and  $T_1=45^\circ$

An example of a  $[90\langle 0/45 \rangle]$  lamina, where the axes of the reference-path centerline have been rotated  $90^\circ$  counter-clockwise from the panel axes, is shown in Figure 2.9. In this case, the tow-head-orientation angle,  $\beta$ , will differ from the fiber orientation angle,  $\theta$ , by the constant path-rotation angle,  $\phi$ . Once again, the values of the tow-head-orientation and the fiber-orientation angles are shown at the center and edges of the panel.

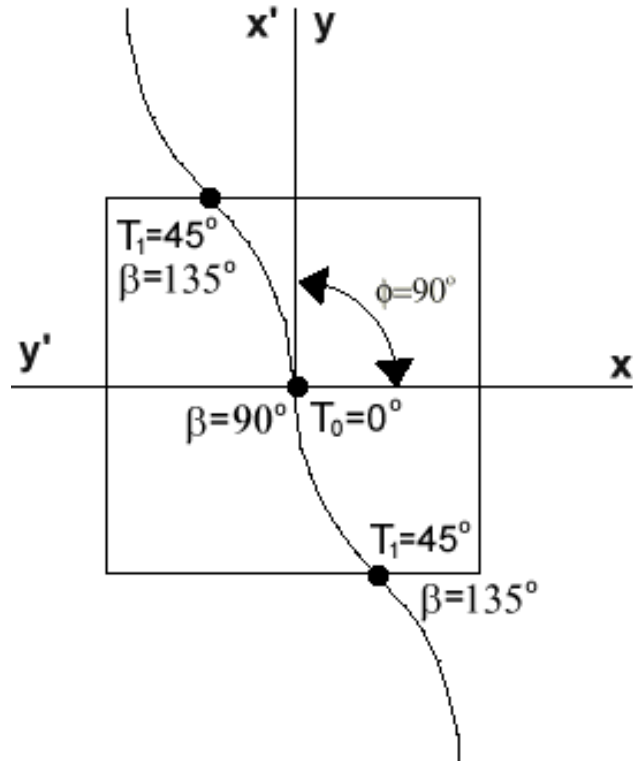


Figure 2.9 A reference-path centerline for  $\phi=90^\circ$ ,  $T_0=0^\circ$  and  $T_1=45^\circ$

### 2.2.3 Path Position Definition

The centerline of the reference-tow path will pass through the origin. The distance of the curvilinear-fiber path from the  $x'$  axis at various points is also defined as a function of  $x'$ . The position  $y'$  is defined by a set of parametric equations. These equations are complicated by the continuously changing fiber-orientation angle. Similar to the fiber-orientation-angle equations, the  $y'(x')$  position equations are piecewise continuous.



$$y'(x') = \begin{cases} \frac{a}{2(T_0 - T_1)} \left\{ \ln [\cos T_0] + \ln \left[ \cos \left( -T_0 + 2T_1 + \frac{2(T_1 - T_0)}{a} x' \right) \right] \right\}, & \text{for } -a \leq x' \leq -\frac{a}{2} \\ \frac{a}{2(T_1 - T_0)} \left\{ -\ln [\cos T_0] + \ln \left[ \cos \left( T_0 + \frac{2(T_0 - T_1)}{a} x' \right) \right] \right\}, & \text{for } -\frac{a}{2} \leq x' \leq 0 \\ \frac{a}{2(T_0 - T_1)} \left\{ -\ln [\cos T_0] + \ln \left[ \cos \left( T_0 + \frac{2(T_1 - T_0)}{a} x' \right) \right] \right\}, & \text{for } 0 \leq x' \leq \frac{a}{2} \\ \frac{a}{2(T_1 - T_0)} \left\{ \ln [\cos T_0] + \ln \left[ \cos \left( -T_0 + 2T_1 + \frac{2(T_0 - T_1)}{a} x' \right) \right] \right\}, & \text{for } \frac{a}{2} \leq x' \leq a \end{cases}$$

The parametric position equations can be used to determine the coordinates of any point along centerline path.

### 2.3 Shifted Fiber Paths

The reference-path is represented by the tow-path centerline. With tow-placement machines, each path has a width that is determined by the number of tows it contains. Once the reference-path centerline is defined, it is necessary to define the centerlines of additional paths that will fill the area of the lamina. To create additional paths, it is necessary to shift path centerlines identical to the reference path centerline along the  $y'$  axis a specified distance. The reference path and a single shifted path are shown in Figure 2.10. The small shift arrows in Figure 2.10 are of identical length. The nature of the curved paths creates an optical illusion which makes the arrows near the edges seem shorter.

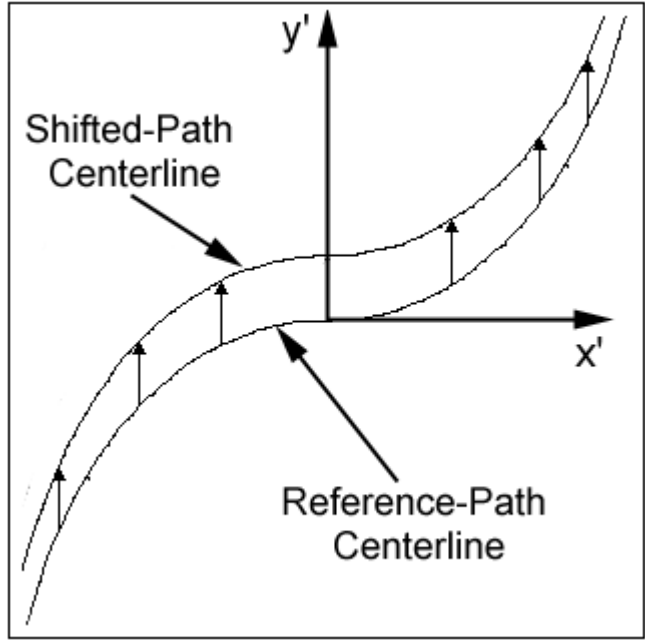


Figure 2.10 A single shifted-path centerline

The distance of the shift is typically equal to the width of the tow path at the center of the panel. The process of creating additional shifted paths is repeated until the panel is completely filled. The centerlines of all paths used to create an entire panel of variable-stiffness lamina, with  $T_0=0^\circ$  and  $T_1=45^\circ$ , is shown in Figure 2.11.

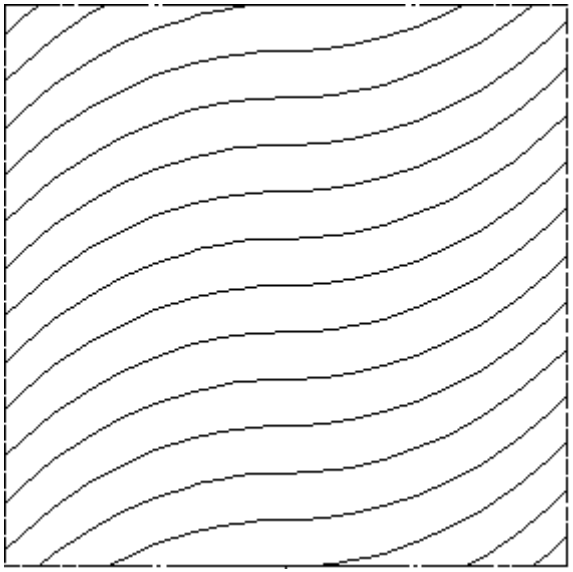


Figure 2.11 Path centerlines for a variable-stiffness lamina with  $T_0=0^\circ$  and  $T_1=45^\circ$

In previous research, it was assumed that the entire laminate maintained a single layer of thickness throughout each lamina, to simplify calculations [11]. In reality, adjacent tows paths will begin to overlap each other or have gaps between them. The formation of overlap and gap regions between tows leads to changes in laminate thickness throughout the area of the panel. Overlap occurs due to a change in the effective width of the path relative to the shift direction. The effective path width can be calculated using a simple equation.

$$W_{projected} = \frac{W_{nominal}}{\cos \theta}$$

The nominal width for  $\theta=0^\circ$  is represented by  $w_{nominal}$ . As  $\theta$  increases the effective width will also increase, as shown for a tow path, with  $T_0=0^\circ$  and  $T_1=60^\circ$ , in Figure 2.12. The nominal width in Figure 2.12 is 1.000, as shown at  $\theta=0^\circ$ .

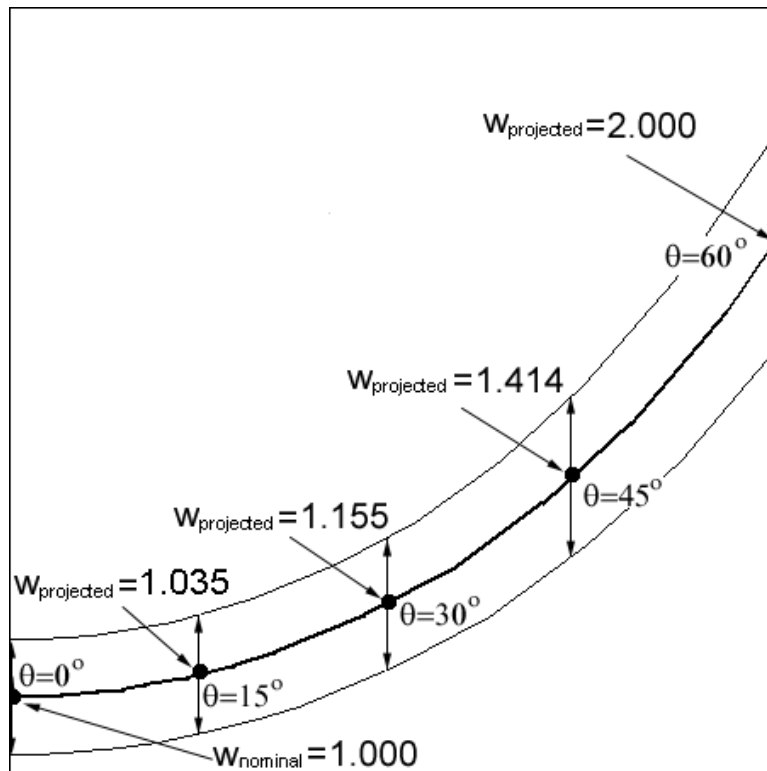


Figure 2.12 Change in projected tow path height for lamina

For a single thickness lamina, the shift distance at the center of the lamina is  $1.0w$  while at the right edge the shift distance would have to be  $2.0w$ . The shift is constant across the panel. Thus, if the shift distance is  $1.0w$ , then the center of the panel will have a single thickness, but the rest of the tow path will not be shifted far enough and will overlap the next path. Otherwise, if the shift distance is  $2.0w$ , then the right edge will have a single thickness, but elsewhere in the lamina, gaps will occur between tows. If the shift is chosen between  $1.0w$  and  $2.0w$ , there will be both overlap and gap regions.

If adjacent tow paths are placed such that they just touch each other at the center of the panel and  $T_0$  is less than  $T_1$ , adjacent tow paths will increasingly overlap as they move outward from the center of the panel, causing an increase in lamina thickness, as shown in Figure 2.13a. If  $T_0$  is greater than  $T_1$ , then adjacent paths will diverge as they move away from the center of the panel, resulting in a gap between the two paths, as in Figure 2.13b. Two sets of three tow paths are shown in Figure 2.13, that have been designed such that there is a single thickness region along the center of the panel,  $x'=0$ . The first is a set of three tow paths with  $T_0=0^\circ$  and  $T_1=45^\circ$  and the second is a set of three tow paths with  $T_0=45^\circ$  and  $T_1=0^\circ$ . The shaded region in Figure 2.13a marks the region where adjacent paths overlap. The shaded region between paths in Figure 2.13b marks the gap between adjacent paths.

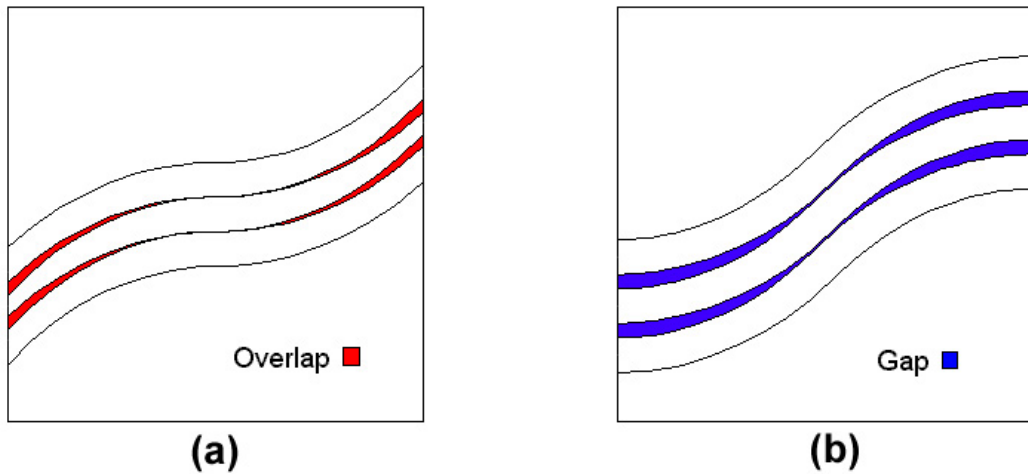


Figure 2.13 Laminates with single thickness at center  
 (a)  $T_0=0^\circ$  and  $T_1=45^\circ$   
 (b)  $T_0=45^\circ$  and  $T_1=0^\circ$

The amount of the shift can also be defined such that a single thickness region occurs at the edges of the panel,  $x'=a/2$ . Large gaps appear between adjacent paths in the center of the panel with  $T_0=0^\circ$  and  $T_1=45^\circ$ , in Figure 2.14a. The panel with  $T_0=45^\circ$  and  $T_1=0^\circ$  has an overlap region between adjacent paths. The same configurations, with single thickness regions at the edges, are shown in Figure 2.14. In this case, the shaded region in Figure 2.14a marks the gap between adjacent paths. The shaded region between paths in Figure 2.14b marks the region where adjacent paths overlap.

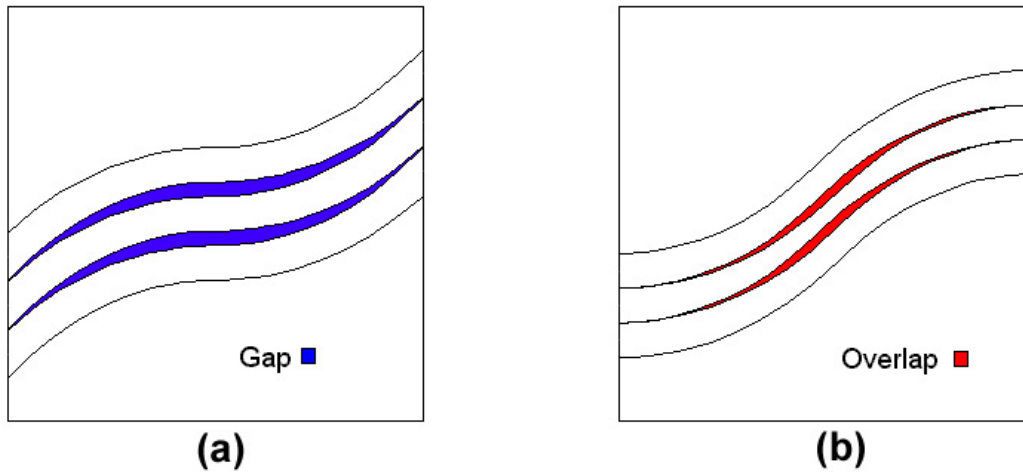


Figure 2.14 Laminates with single thickness at edge  
 (a)  $T_0=0^\circ$  and  $T_1=45^\circ$   
 (b)  $T_0=45^\circ$  and  $T_1=0^\circ$

The shift distance between adjacent paths and the values  $T_0$  and  $T_1$  affect the size of the overlap or gap regions. The thickness change corresponding to either gap or overlap regions could result in improved or degraded static response and adds another interesting feature to the design of a tow-placed variable-stiffness lamina. In this research, one of the goals is to examine how the thickness change corresponding to tow-path overlap can be used to increase the stiffness of the panel. The stiffness of the panel could be increased by using gap regions to redirect the load to other areas of the panel or by using overlap regions to carry load that cannot be carried by weak parts of the panel. While it is possible to create gaps between adjacent paths, designs with gaps were not examined in this research.

## 2.4 Variable-Stiffness-Lamina Nomenclature

One of the benefits of using linearly varying curves is that it allows for the fiber orientation throughout a single variable-stiffness lamina to be summarized with just three angles,  $T_0$ ,  $T_1$  and  $\phi$ , where  $T_0$  and  $T_1$  are the path orientation angles measured at the center of the panel and at  $x'=a/2$ , respectively, and  $\phi$  is the tow-path rotation angle. The standard method used to define linearly varying

curvilinear-fiber variable-stiffness lamina was established by Gürdal [10]. The entire variable-stiffness ply is represented as " $\phi \langle T_0|T_1 \rangle$ ." If the tow-path rotation angle,  $\phi$ , is zero, then the notation can be truncated to define only the fiber-orientation angles, " $\langle T_0|T_1 \rangle$ ."

Traditional composite laminae can be stacked together in a prescribed order to form a composite laminate. Variable-stiffness lamina can similarly be stacked to form a variable-stiffness laminate. Because of the thickness variation within a single variable-stiffness lamina, the thickness of a variable-stiffness laminate, composed of many variable-stiffness lamina, will also vary. Variable-stiffness laminates also require special nomenclature to specify the stacking sequence.

Traditional composite laminates use a nomenclature system where the fiber-orientation angles are listed inside a set of square brackets. Each layer is separated by slashes. An example of this nomenclature would be [45/-45/0/0/-45/45]. This design represents a six-layer laminate. This laminate could be summarized in a shorter form as  $[\pm 45/0]_s$ . In this case, the  $\pm$  correlates to the  $45^\circ$  and  $-45^\circ$  layers. The subscript "s" means that the laminate is symmetric, thus every layer is mirrored about the center plane of the laminate. Because traditional composite notation does not allow for variable fiber-orientation angles within each ply to be defined, it is necessary to use a modified version of this nomenclature convention.

Different layers can be added together in much the same way as traditional composites are. Instead of using multiple constant-orientation angles offset by slashes, the special angled brackets for each curvilinear-fiber variable-stiffness lamina are placed inside square brackets and offset by slashes, e.g.,

$$[ \langle 10/45 \rangle / \langle -10/-45 \rangle / \langle -10/-45 \rangle / \langle 10/45 \rangle ]$$

This method of nomenclature can be used with many of the conventions established for traditional composite laminates. A  $\pm$  outside of the square brackets or angle brackets denotes two variable stiffness layers. The first layer would have the signs shown in the brackets and the second layer would have the

opposite of the signs shown in the brackets. Thus a  $[\pm\langle 10/45 \rangle]$  would define two layers, a  $\langle 10/45 \rangle$  layer and a  $\langle -10/-45 \rangle$  layer. Additionally, a subscript "s" can be used to denote that each layer in a laminate has a symmetric layer associated with it. A  $[\pm\langle 10/45 \rangle]_s$  is exactly the same as the laminate listed explicitly above.



## Chapter 3

### Finite Element Modeling of Variable-Stiffness Laminates

The complex geometry of curvilinear-fiber variable-stiffness laminates makes analytically determining the response an impossible task. In previous research, models were simplified by ignoring the possibility of thickness variation within a ply. The problem was further simplified by assuming that the fiber paths were only dependent upon their distance along the  $x'$  axis. In reality, shifting the reference paths creates regions of overlap between adjacent paths, resulting in spatially varying thickness. In addition, the complexity is increased because the fiber-orientation angle depends on position within a specific tow path. To develop an analytical closed-form solution to a problem with spatially varying fiber orientations and thickness would be impossible. In this research, the finite element method will be used.

First, the boundary conditions of the finite element model will be covered. Next, the capabilities of the GENESIS analysis and design finite element package will be presented. Then, the method used to define the finite element model will be presented. Finally, the convergence criteria used to validate the model will be presented.

#### 3.1 Global Finite Element Model

The first step in developing the overall variable stiffness laminate is deciding what type of overall model will be used. This research will concentrate on uniform end shortening of square plates similar to the previous research. In these models, a square panel is subjected to a compressive displacement in the  $x$ -direction along two opposing edges at  $x = -a/2$  and  $x = a/2$ . In Case I, the top

and bottom edges are free to deform in the  $x$ - $y$  plane, as shown in Figure 3.1. In Case II, the top and bottom edges are constrained to zero displacement in the  $y$ -direction but free to deform in the  $x$ -direction as denoted by the double cross hatched regions along the boundaries, as shown in Figure 3.2.

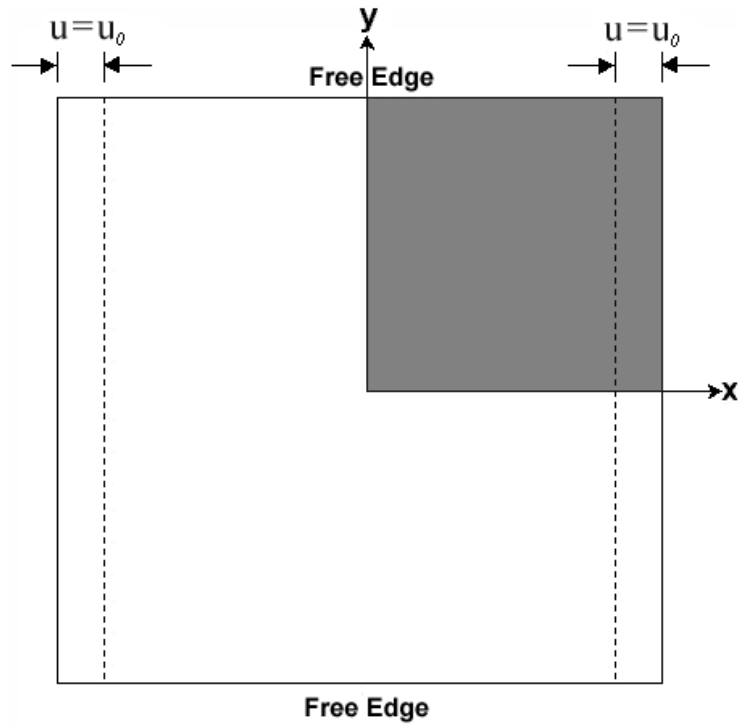


Figure 3.1 Case I: Uniform end shortening with free upper and lower edges

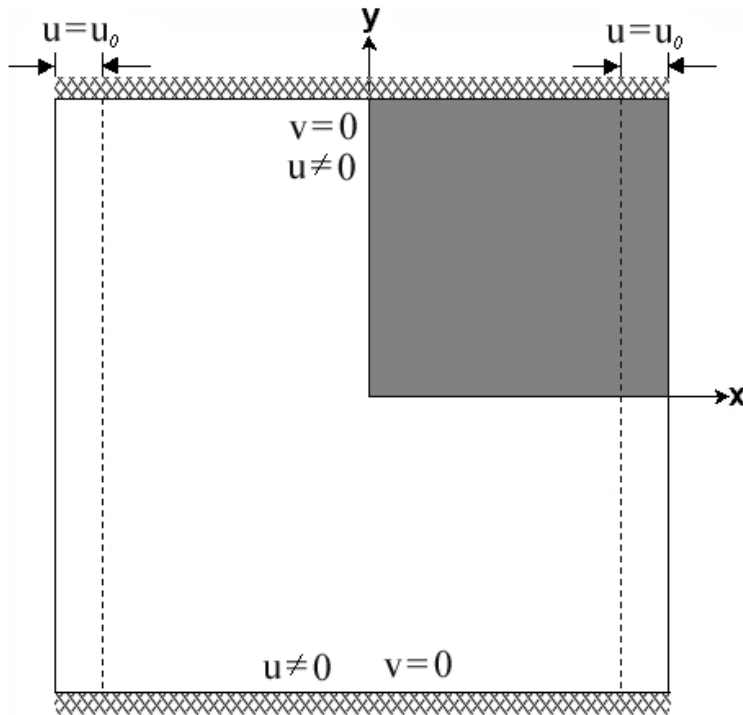


Figure 3.2 Case II: Uniform end shortening with constrained upper and lower edges

Frequently in finite element modeling, it is possible to take advantage of certain symmetries and reduce the size of the model, resulting in substantial computational savings. In this research, it is possible to accurately determine the response of the system by modeling only a quarter of the panel. The quarter of the panel modeled was the section in the upper right-hand quadrant. This quadrant is shaded in Figure 3.1 and Figure 3.2. In order to model the quarter panel, it is necessary to use special boundary conditions on the planes of symmetry along the  $x$  and  $y$  axes. The additional boundary conditions reflect the response that would result from elements in symmetric quadrants. The quarter panel models are shown in Figures 3.3 and 3.4.

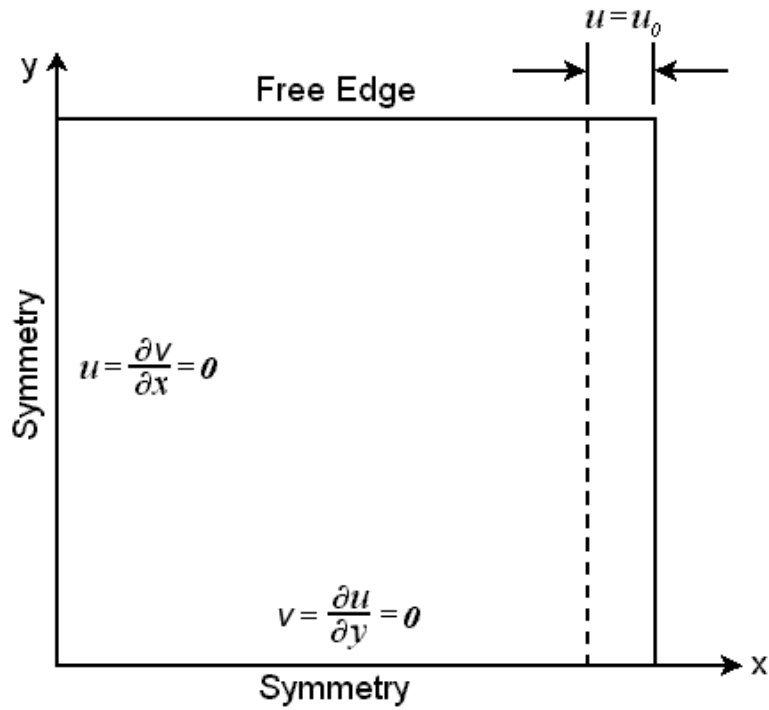


Figure 3.3 Case I: Quarter panel model

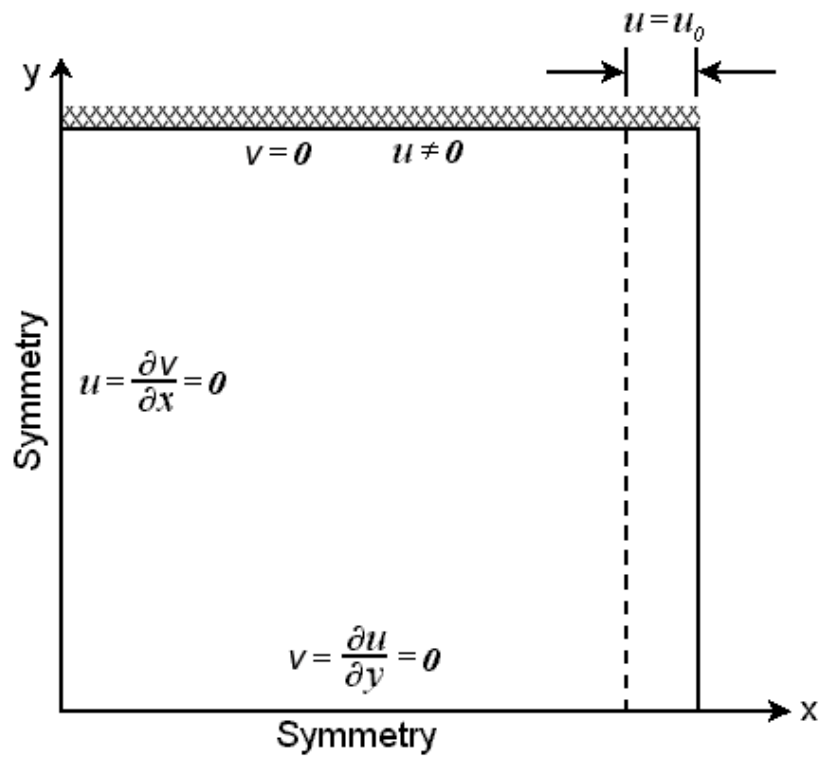


Figure 3.4 Case II: Quarter panel model

## 3.2 GENESIS

GENESIS is a commercially available finite element analysis and optimization program[13]. It allows a wide variety of different methods in both finite element analysis and various forms of design optimization for static, dynamic, vibration and heat transfer problems. Some of the finite element modeling and analysis features used in this research, will be explained in this section.

### *3.2.1 Element Geometry*

An initial finite element grid must be established which will define the locations of the initial nodes. After the initial grid points for the model were established, the elements were defined. GENESIS allows for approximately 16 different types of 2-D and 3-D elements. Of particular interest to this research is the availability of plate elements. These elements have in-plane, bending and in-plane/bending coupling stiffness [13]. The plate elements can be used in conjunction with special composite material property definitions to create a composite plate element. GENESIS allows for both quadrilateral and triangular composite plate elements.

The elements used in this research, were quadrilateral composite-plate elements. One of the benefits of these elements is that their position is defined by only four points; G1, G2, G3 and G4. Each element has a layer coordinate system, which allows for each layer to have a unique orientation angle. The layer coordinate system is used to represent the fiber orientation change from one element to another following the orientation-fiber angle definitions. A generalized quadrilateral composite element is shown in Figure 3.5. Where,  $\theta_i$  is the fiber-orientation angle, and must be determined for each layer of the element.

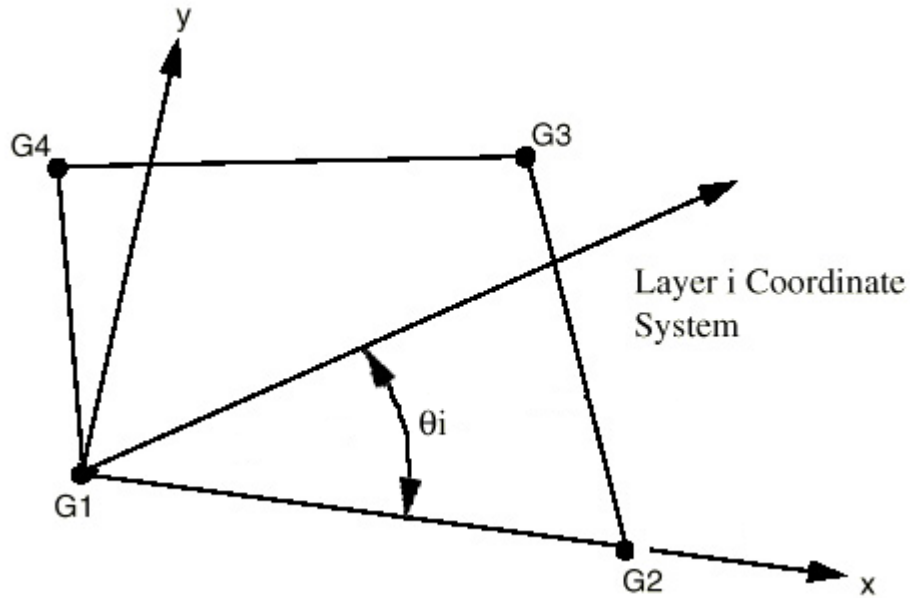


Figure 3.5 Generalized quadrilateral element, from GENESIS Manual [13]

The thickness of the elements and the orientation angles of each layer are determined in a property definition section. Additionally, each layer can have different material properties. For this research, all layers are made of the same composite material. A side view of a generalized element is shown in Figure 3.6. The position of grid points G1 and G2 can be seen and the reference plane of the element is offset by distance  $Z_{\text{offset}}$ . In this research, the offset distance is zero. The definition of layers uses a form common in composite analysis, where the first layer is defined in the negative z direction a distance  $-z_0$ . The layers then build up to the reference plane at  $z=0$  and on up to the  $n^{\text{th}}$  layer. In order to ensure symmetry, the laminate is defined from the first layer to the reference plane is defined, and then a symmetry condition is imposed which mirrors the design to the opposite side of the reference plane. The number of layers in each element can be specified independently which allows for thickness variation throughout the plate.

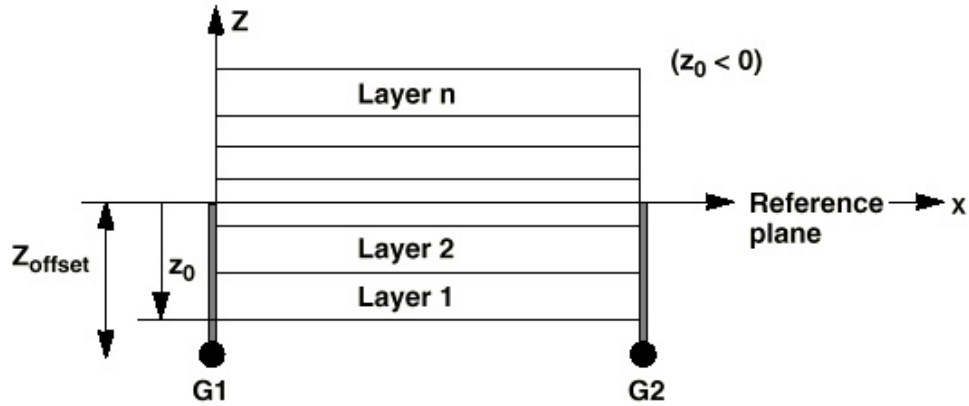


Figure 3.6 Through-the-thickness view of composite element, from GENESIS Manual [13]

### 3.2.2 Material Properties

In order to properly characterize a composite material, many material properties must be known. GENESIS allows for all of the engineering properties of a composite lamina to be input.

$E_1$	Modulus in the fiber direction
$E_2$	Modulus perpendicular to fibers
$\nu_{12}$	Poisson's ratio for expansion perpendicular to fiber direction due to compression in fiber direction
$G_{12}$	In-plane shear modulus
$X_T$	Tensile strength in fiber direction
$X_C$	Compressive strength in fiber direction
$Y_T$	Tensile strength transverse to fiber direction
$Y_C$	Compression strength transverse to fiber direction
$S$	Shear strength
$F_{12}$	Tsai-Wu interaction strength term

### 3.2.3 Failure Criteria

GENESIS calculates the stresses in each layer of each element by various methods including determining the stresses in the principal material system. The principal material system is defined as the set of coordinates that are aligned such that the 1-direction is aligned with the fibers and the 2 direction

is perpendicular to the fibers as shown in Figure 3.7. For orthotropic materials, such as fiber-reinforced composite laminates, converting stresses into these coordinates simplifies failure analysis. It is only necessary to determine the stresses in the fiber direction, perpendicular to the fiber direction and in shear. After the principal material direction stresses are determined, it is necessary to select a failure criterion.

GENESIS also has the ability to automatically calculate a failure index based on many different failure criteria commonly used in composite material analysis. The methods available include maximum strain, maximum stress, Tsai-Hill, Hoffman and Tsai-Wu failure theories. For each of the failure criterion, it is necessary to input the failure strength in tension and compression for both the fiber direction and transverse to the fiber direction and the shear failure strength. The failure index is then calculated according to each theory. If the failure index reaches a value of 1.0, then failure has occurred.

### **3.2.3.1 Maximum Strain Criterion**

The simplest of the methods is the maximum strain criterion. Only three distinct failure modes are considered, fiber-direction failure, perpendicular-to-the-fiber-direction failure and shear failure. For the fiber direction and perpendicular to the fiber direction, failure can occur in tension or compression. The strain in each mode is compared to the allowed strain for the associated failure mode. The failure index is the maximum of the ratios of actual stresses to respective strengths. One of the advantages of using this method is that GENESIS will also output which mode of failure caused failure. For the maximum strain criterion,  $X_1$  is the maximum strain in the fiber direction,  $X_2$  is the maximum strain perpendicular to the fiber direction and  $X_{12}$  is the maximum shear strain.  $\varepsilon_1$ ,  $\varepsilon_2$  and  $\gamma_{12}$  are the strain in the fiber direction, the strain perpendicular to the fiber direction and the in-plane shear strain, respectively. A conditional statement determines whether the compression or tension failure strains should be used for  $X_1$  and  $X_2$ . That is, the failure index is:



$$FI = MAX\left(\frac{\epsilon_1}{X_1}, \frac{\epsilon_2}{X_2}, \frac{\gamma_{12}}{X_{12}}\right)$$

### 3.2.3.2 Maximum Stress Criterion

Closely related to the maximum strain criterion is the maximum stress criterion. While not explicitly used in GENESIS, a form of the maximum stress criterion is used. Instead of comparing failure stresses to the stresses in each element, GENESIS converts the failure stresses into failure strains. The strain in the fiber direction, strain perpendicular to the fiber direction and shear strain can then be compared to these failure strains.  $X_1$  is the tensile strength in the fiber direction divided by  $E_1$  for tensile stress and is the compression strength in the fiber direction divided by  $E_1$  for compression stress. Similarly,  $X_2$  is the tensile strength perpendicular to the fiber direction divided by  $E_2$  for tensile stress and is the compression strength perpendicular to the fiber direction divided by  $E_2$  for compression stress.  $X_{12}$  is the shear strength divided by the shear modulus. GENESIS also allows for failure strains to be input directly foregoing the need for failure stresses.

$$FI = MAX\left(\frac{\epsilon_1}{X_1}, \frac{\epsilon_2}{X_2}, \frac{\gamma_{12}}{X_{12}}\right)$$

Whereas, the maximum stress criterion would normally be:

$$FI = MAX\left(\frac{\sigma_1}{X_1}, \frac{\sigma_2}{X_2}, \frac{\tau_{12}}{X_{12}}\right)$$

where  $X_1$ ,  $X_2$  and  $X_{12}$  represent the failure strengths in the fiber direction, perpendicular to the fiber direction and in shear. A conditional statement would select the compression or tensile strength depending on the loading conditions of each element.

### 3.2.3.3 Tsai-Hill Criterion

GENESIS requires that the lamina have equal strengths in tension and compression for the Tsai-Hill criterion. The Tsai-Hill criterion takes into account that failure can occur due to a combination of failure modes. Because failure is a

combination of various terms, it is not possible to determine definitively what mode of failure will occur. Clear determination of the failure mode is not possible in failure criteria where there is interaction between stresses in different directions. It is possible to determine which stresses or combination of stresses are contributing the most to the failure index and speculate on the mode of failure from the stress plots. The failure index is calculated with a single concise equation.

$$FI = \frac{\sigma_1^2}{X^2} - \frac{\sigma_1\sigma_2}{X^2} + \frac{\sigma_2^2}{Y^2} + \frac{\tau_{12}^2}{S^2}$$

In the Tsai-Hill criterion equation X represents the failure strength of the fibers, Y represents the failure strength transverse to the fibers and S represents the shear failure strength.

#### 3.2.3.4 Hoffman Criterion

Somewhat more complex is the Hoffman criterion, which allows for the failure strengths to differ in tension and compression. Similar to Tsai-Hill, failure can occur due to a combination of failure modes. The subscripts within the following failure index refer to failure strength in tension and compression:

$$FI = \sigma_1 \left( \frac{1}{X_T} + \frac{1}{X_C} \right) + \sigma_2 \left( \frac{1}{Y_T} + \frac{1}{Y_C} \right) - \frac{\sigma_1^2}{X_T X_C} - \frac{\sigma_2^2}{Y_T Y_C} + \frac{\tau_{12}^2}{S^2} + \frac{\sigma_1 \sigma_2}{X_C X_T}$$

#### 3.2.3.5 Tsai-Wu Criterion

Slightly different from the Hoffman formulation, Tsai-Wu replaces the final term in the Hoffman criterion equation, with an interaction parameter,  $F_{12}$ . Determining this interaction parameter is difficult and expensive because the parameter must be measured under a biaxial state of stress.

$$FI = \sigma_1 \left( \frac{1}{X_T} + \frac{1}{X_C} \right) + \sigma_2 \left( \frac{1}{Y_T} + \frac{1}{Y_C} \right) - \frac{\sigma_1^2}{X_T X_C} - \frac{\sigma_2^2}{Y_T Y_C} + \frac{\tau_{12}^2}{S^2} + 2F_{12}\sigma_1\sigma_2$$

### 3.3 Creation of Variable Stiffness Finite Element Model

The finite element method is an excellent tool for determining the static response of systems with complex geometry, or boundary conditions, such as variable-stiffness laminates. GENESIS allows for the complex geometry of a variable stiffness plate to be easily input and solved. The task is to develop a method that can be used to generate finite element input accurately and quickly for a wide range of designs.

The goal in creating a finite element model is to approximate the complex geometry with a simpler geometry and thus make it possible to solve. It is important to retain enough detail in the model such that it accurately reflects the original problem. FEM relies on providing an adequate model of the system that strikes a balance between simplicity and accuracy. The approach used to generate the finite element model, and how that approach was implemented, will be covered in this section. Furthermore, some of the implications of this formulation will be examined.

#### *3.3.1 Finite Element Modeling of a Reference Path*

The first step in creating a finite element model is to create a discrete reference path. Because quarter panels are modeled, it is only necessary to generate a reference path from the origin to positive values of  $x'$ . An area of discrete grid points large enough to define a full reference path (i.e., from  $T_0$  to  $T_1$  and back to  $T_0$ , as in Figure 2.2) is formed first. These discrete grid points form the corners of the square elements, which are all initialized to zero thickness. The complete grid forms an empty area that will be used to store the information defining a reference path.

The reference path is defined by determining which elements in the empty grid lie within the area of the tow path. The distance between the center of each element and the reference fiber path must be determined. The distance was determined using a Golden Section search to minimize the distance between the element center and the reference fiber path [14]. The Golden Section search is a

very computationally efficient interval search method that is carried out in two stages. The first is to bracket the unimodal minimum. The second step is to reduce the interval of uncertainty by comparing function evaluations at different points in the interval. The advantage of a golden section search is that it requires only one function evaluation between iterations, which results in rapid convergence.

The distance between the center of each element and the reference path centerline is determined to decide if the element belongs to the reference tow path. If the distance between the element center and the reference path was less than half of the tow width, then the thickness of that element is increased to a single thickness. The result is a tow path of a single layer of composite material which goes through the complete variation of fiber angle. A single  $\langle 0/45 \rangle$  reference tow path, based about the tow-path centerline, is shown Figure 3.7. The bounds of each potential element are delineated by the grid. The elements that actually belong to the tow path are filled with black. The discrete nature of the model is apparent along the top and bottom edges of the tow path.

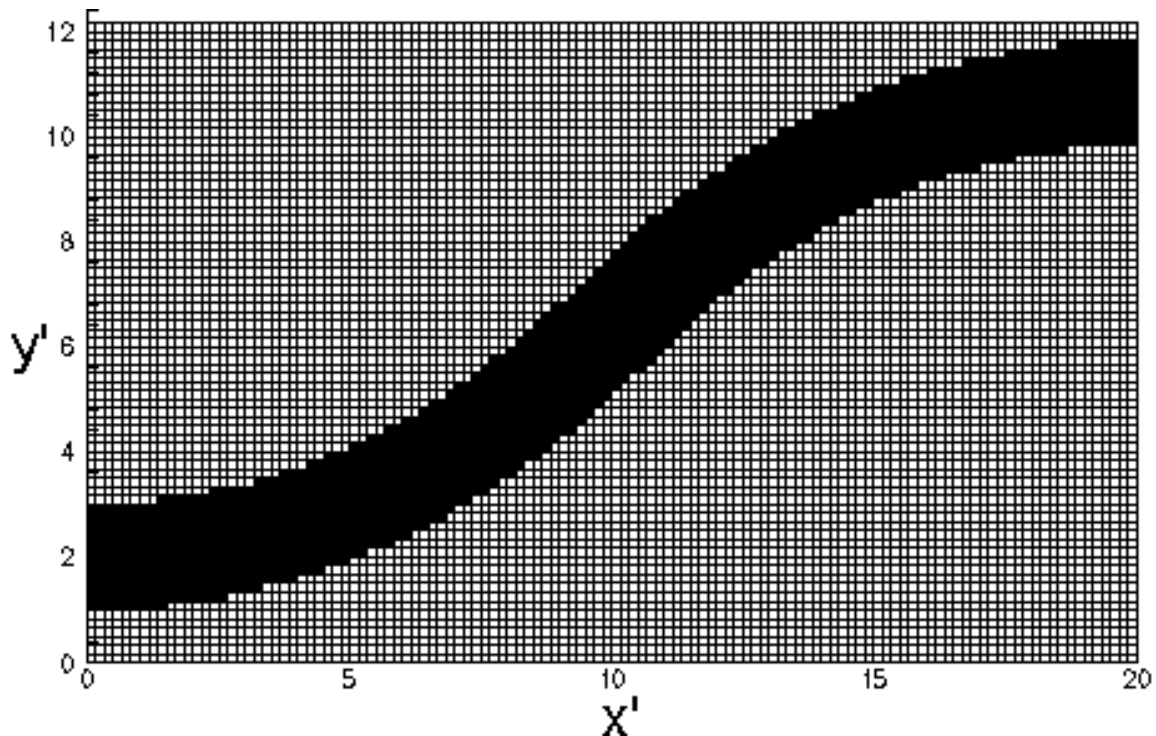


Figure 3.7 Discretized single  $\langle 0/45 \rangle$  reference tow path

In addition to determining the discretized path of the reference-tow path, it is necessary to know the angle in each element. The orientation angle is simple to determine with the Golden Section search. The minimum distance between the center of an element and the reference path results in a line perpendicular to the reference-path centerline. All points along the perpendicular line have the same orientation angle as the point the line crosses on the reference path. Using this method to define orientation angle means that for a constant value of  $x$  the fiber-orientation angle will change across a single tow path. A portion of a single tow path and the fiber-orientation angles at the top and bottom of the path are shown in Figure 3.8. The top and bottom of the tow path, for a constant value of  $x$ , will have different fiber-orientation angles, because they correlate to different points on the reference path. A point is defined on the centerline with the coordinate  $x'_0$ . Points along the upper edge of the tow will be perpendicular to the tow centerline at a higher value of  $x'$ , defined as  $x'_u$ . A point on the lower tow edge is perpendicular to the tow centerline at a lower value of  $x'$ , defined as  $x'_l$ . Because the orientation angles at these points are defined by the point on the centerline that they are perpendicular to, it is clear that the fiber-orientation angle along the vertical line at  $x'_0$  will be changing as the tow is crossed.

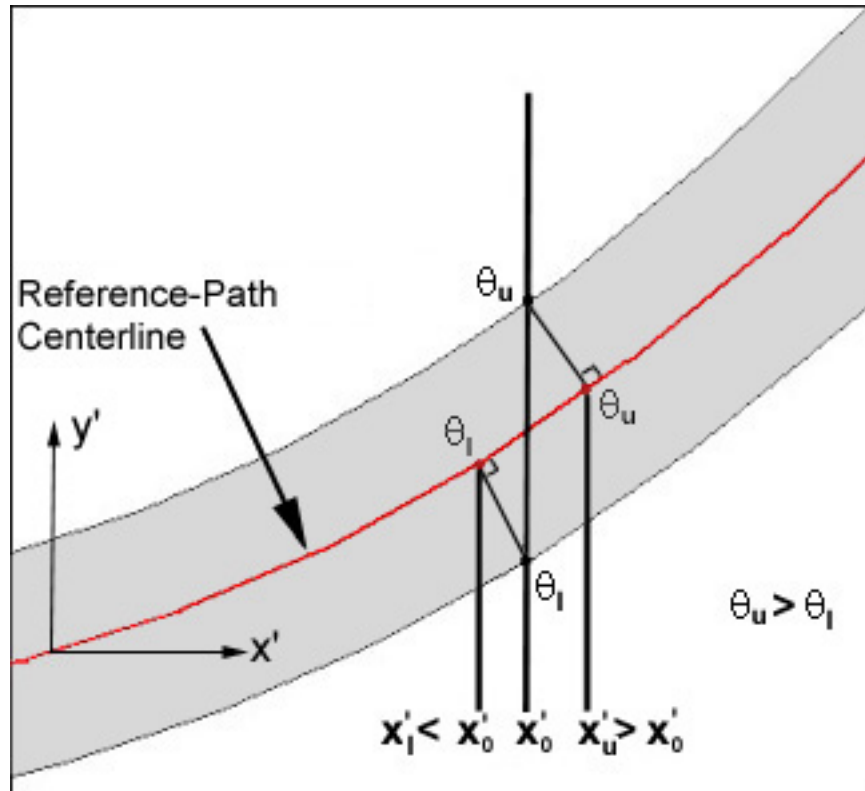


Figure 3.8 Variation of orientation angle across reference path for constant value of  $x'$

The information for the reference fiber path is stored in a text data file containing the thickness information and the orientation angle information for every element in the reference tow path. This file is used to create additional shifted paths in order to model the entire plate. Other reference paths can also be created in the same way for different layers.

One of the interesting features of this model is the nature of an individual reference path. While the centerlines of each path are strictly shifted in a manner similar to the previous research, the actual reference path is actually a set of parallel paths constructed in a manner similar to the Waldhart research on parallel shifting. The parallel nature of the fiber-orientation angles is evidenced by the changing direction of the color gradation in Figure 3.9. Figure 3.9 is also a concise graphical representation of the fiber orientation information for a  $\langle 0/45 \rangle$  reference path.

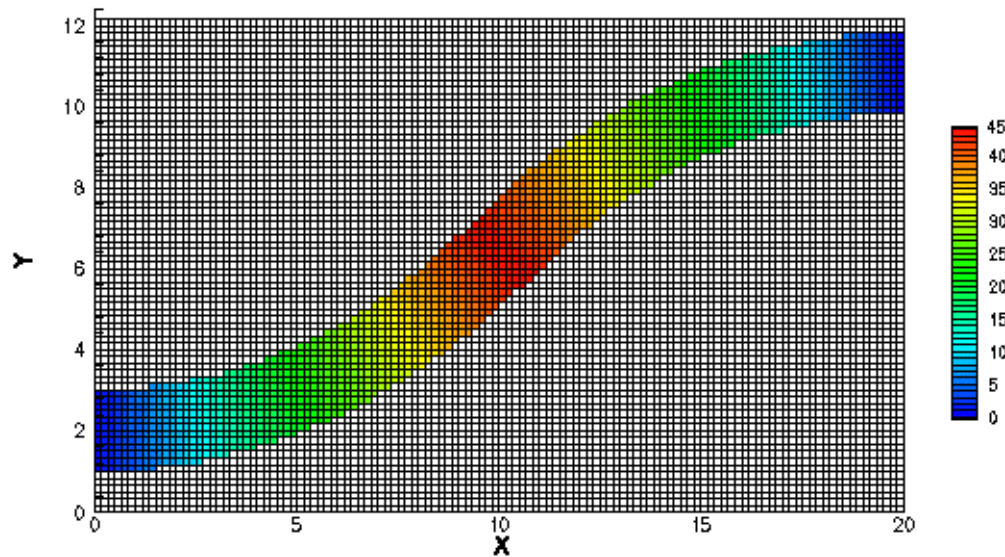


Figure 3.9 Variation of orientation angle for a single  $\langle 0/45 \rangle$  discretized path

### 3.3.2 Shifting of the Reference Path

Once the discretized reference path has been developed, it is necessary to use it to create the entire ply. Because all tow paths will be identical, all that is necessary to model the rest of the variable stiffness ply is to duplicate the reference tow path and shift the duplicate tow paths the correct distance. The shift distance is discretized by determining the number of elements in the x and y directions necessary to place an adjacent tow path. Once this is determined the values from the reference template are copied to the adjacent empty elements. If the elements are filled by the reference path then an additional layer is created. The process is repeated for the next path and so on until all of the elements of the panel are filled. The advantage of this process is that it can be handled very quickly. The process only requires placing the known values from the reference tow path data into an array that represents the entire plate. The disadvantage is that there is some loss in accuracy due to rounding error when discretizing the shift. This error decreases as the number of elements is increased.

Another advantage of this method is that it resembles how an actual laminate would be assembled by a tow placement machine. The order of the

shifting process is constant such that a new path one will always overlay a path which has already been laid down. This procedure is then repeated for additional layers until the entire laminate has been modeled. A thickness plot of a 4-layer  $\pm(0/45)_S$  laminate is shown in Figure 3.10. Some of the overlap regions, along the edge at  $x=a/2$ , have been marked.

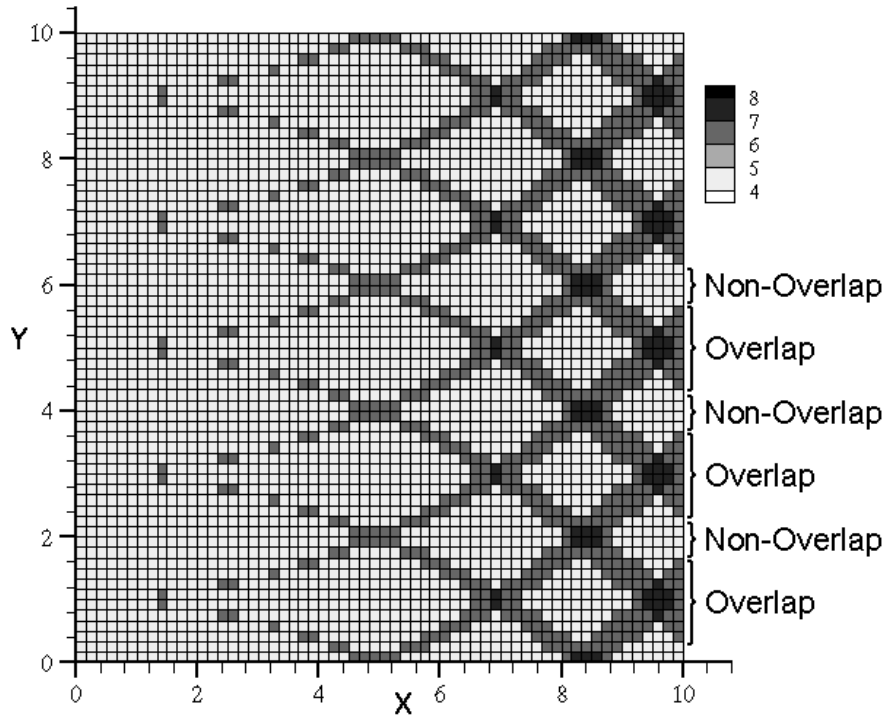


Figure 3.10 Thickness plot of  $[\pm(0/45)]_S$  laminate

An actual laminate created by a tow placement machine would most likely have one flat side regardless of thickness variation due to a flat mandrel. In areas where there was overlap the thickness changes would quickly stack up causing large changes in thickness. A view of how the outside edge,  $x=a/2$ , might look if viewed along the x -axis is shown in Figure 3.11. The thickness dimension has been exaggerated to demonstrate the overlap effect. A single tow path, viewed along its length, has been shaded. It is apparent that this type of laminate is non-symmetrical and large thickness changes possible. The overlap and non-overlap regions have also been marked.



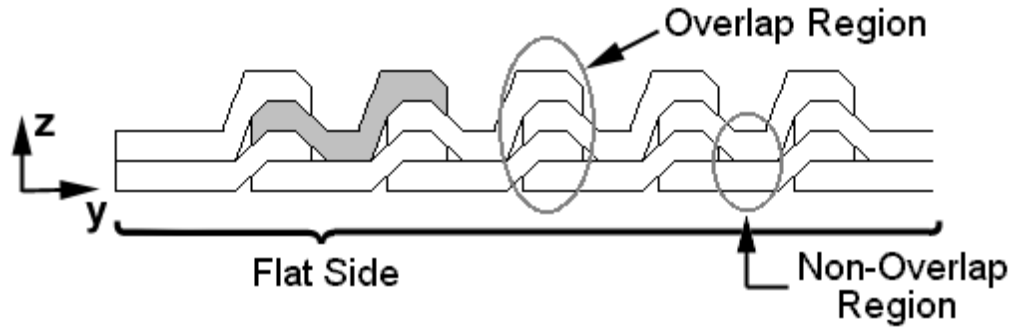


Figure 3.11 Two variable stiffness layers with one flat side

While it is possible in GENESIS to create laminates similar to the one shown in Figure 3.11, In this research, the laminates will be constrained to be midplane symmetric designs only. Because of that symmetry condition, there will not be a flat side. An example of a symmetric laminate as viewed along the x-axis is shown in Figure 3.12. The symmetry condition, while slightly less realistic, will simplify the model by ensuring there will be no bending coupling. Similar to Figure 3.11, a single tow path, viewed along its length, has been shaded, and the overlap and non-overlap regions have been marked.

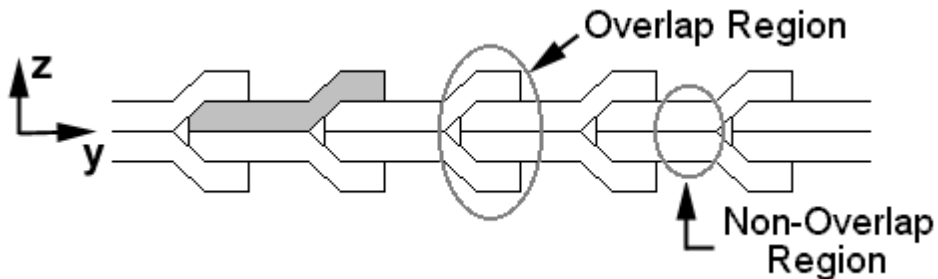


Figure 3.12 Two-layer midplane-symmetric variable-stiffness laminate

While Figures 3.11 and 3.12 show a small transition zone between thickness changes it should be noted that in the discrete model there is no transition. Additionally, there is no explicit continuity of each ply. That is to say, that layers of a ply do not stay connected when the entire laminate is stacked together. An example of how the edge of an discretized model would look is shown in Figure 3.13. Each of the small rectangles represents a single element. As noted earlier in Figure 3.8 the orientation angle along constant values of x will

change. As one looks along the edge of the variable stiffness laminate along the x-axis, each element will have a different orientation angle. In Figure 3.13 the largest fiber-orientation angle is denoted by red. For a constant value of x at the panel edge the largest fiber-orientation angle occurs at the element in the middle of the tow. The orientation angle decreases toward the edges of the tow path to a minimum value at the ends of each tow path, denoted by green. In the middle of Figure 3.13, a single tow path is highlighted to show exactly which path the element definitions are derived from. It is interesting to note that in the overlap region that angles in different layers can be quite different.

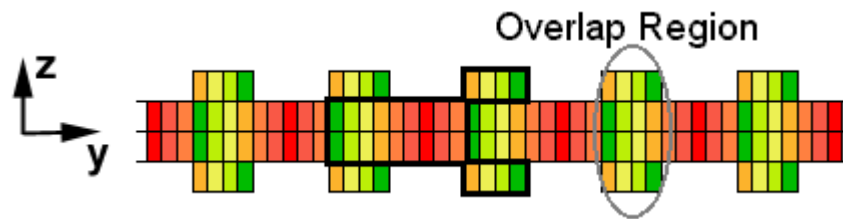


Figure 3.13 Edge of discretized two layer laminate

One practical limitation of this method is on the angle  $T_1$ . For a simple laminate,  $T_0 = 60^\circ$  and the shift distance equals half of the path width such that layers at the center of the composite panel have only a single layer of thickness. If  $|T_1| > |T_0|$ , there will be an overlap region in a continuous model and a possibility of overlap in a discrete model. As  $T_1$  approaches  $60^\circ$  each new path will overlap half of the previous path and will be half of the current path will be covered by the next path that is placed. This arrangement creates a region that has double thickness along the entire edge. Beyond,  $T_1 = 60^\circ$  the path will begin to overlap other paths causing the possibility for triple thickness or thicker regions. For a laminate with  $T_1 = 90^\circ$ , extreme increases in thickness would be seen. Because there is a step-wise transition between different thickness regions, it is desirable to minimize the amount of thickness change between adjacent layers. For this reason,  $T_0$  and  $T_1$  will be limited to values such that a single layer of variable stiffness composite never has more than double

thickness. This constraint varies with shift distance. For laminates where  $T_0=0^\circ$  and single thickness at  $x=0$ ,  $T_1 \leq 60^\circ$ .

Also important to note, is that occasionally when shifting paths small irregularly spaced gaps are created between paths. These holes are due to rounding off the shift distances during the discretization process. It will be assumed that there are never any zero-thickness regions in any layer. These gaps will be assumed to be of a single thickness and to have the same orientation angle as an adjacent element.

### 3.4 Evaluation of Results

Once the model has been defined, it is time to run GENESIS to determine the response of the model. The unknown quantities that need to be determined are the displacements. Once the displacements are determined, the resultant forces in each element and the strains and stresses in each layer of each element can be determined. GENESIS output includes all of these values. It is helpful to normalize the force resultants so that different variable stiffness configurations can be compared. Finally, the data must be used to determine the in-plane stiffness for the entire panel.

#### 3.4.1 Force Results

The force results are the force per unit width, in the direction denoted by the subscript, on each element edge. The force per unit width in the x direction is denoted by  $N_x$ . Similarly, the force results per unit width in the y direction and the shear force per unit width for each element are denoted by  $N_y$  and  $N_{xy}$ , respectively. Before the force on each element is plotted, it is useful to normalize the values with respect to the response of the following standard laminate:

$$\bar{N}_x = \frac{a}{2u_0 A_{11}(\pm 0^\circ)_s} N_x$$

$N_x$  represents the force resultant of a single element,  $a$  is the width of the entire plate and  $u_0$  is the prescribed displacement.  $A_{11}(\pm 0^\circ)_s$  is the in-plane

stiffness term in the x-direction for a four-layer  $0^\circ$  laminate. The  $0^\circ$  orientation was chosen as the basis for this normalization because it has the highest x-direction in-plane stiffness for a four-layer laminate. A normalized stiffness of zero would correspond to no force in the x direction and high compressive force is denoted by a negative number. The higher the compressive force on an element in the x direction, the more negative the number. Similarly  $N_y$  and  $N_{xy}$  can be normalized by replacing  $N_x$  with  $N_y$  or  $N_{xy}$ , respectively. Normalizing the values is useful because it provides us with a basis to compare plates of different sizes and thicknesses.

### *3.4.2 Stiffness Calculation*

The stiffness of the entire plate can be calculated by examining the force resultants along the displaced edge of the plate. For a straight-fiber laminate under uniform end shortening, this is a simple procedure because  $N_x$  is not a function of  $y$ . Variable-stiffness laminates do not show this simple response as shown in Figure 3.14. The normalized force resultant is a function of element fiber-orientation angle, element thickness along the edge and the effects of other local thickness changes.

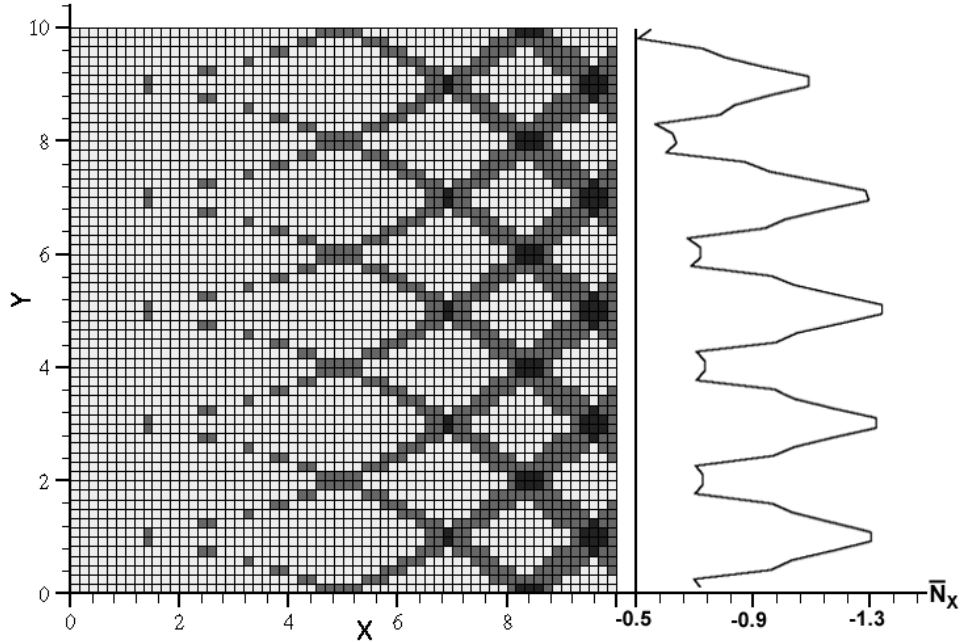


Figure 3.14  $N_x$  distribution along displaced edge

In order to quantify the stiffness of the plate, it is useful to determine the total force required to achieve the prescribed displacement. The total force resultant for the entire panel can be calculated by integrating the area under the  $N_x$  curve from  $y=0$  to  $y=b/2$  along the outside edge at  $x=a/2$ .

$$F_x = \int_0^{b/2} \bar{N}_x \left( \frac{a}{2}, y \right) dy$$

In practice this integration is most easily accomplished numerically, using the trapezoid rule. This procedure provides a basis to compare the overall response of variable stiffness plates with different orientation angle properties, thicknesses and shift distances. The average force per unit width can be calculated by dividing the total force by the original length of the side.

$$N_x^{avg} = \frac{F_x}{a/2}$$

Because the thickness of the variable-stiffness laminates can vary, it is necessary to keep the weight increase in mind. If a variable stiffness laminate is designed that is twice as stiff, but weighs three times more than a comparable straight fiber laminate, then nothing has been accomplished. The weight ratio is

calculated by taking the ratio of the variable-thickness laminate weight to the standard four-layer  $0^\circ$  laminate weight. Thus, a variable-stiffness laminate with thickness variation will always have a weight ratio greater than one.

$$\bar{W} = \frac{W_{VS}}{W_{(\pm 0)_s}}$$

The stiffness calculation yields a single number that can be used to summarize the stiffness of an entire panel. The weight ratio can be used to normalize the stiffness values, so that the weight-normalized stiffness can be compared to these of laminates with different thickness values. The weight ratio provides an objective function that can be maximized in an optimization problem.

### 3.5 Mesh Size Convergence

One of the most important considerations when creating a finite element model is determining how many elements, or what "mesh size", will be necessary to provide an accurate model of the system. If there are too few elements, it is possible that important details will be neglected thus rendering the analysis useless. If there are too many elements, the system will be accurately modeled, but excess computational time will be used. A convergence study was used to determine the number of elements necessary to achieve the desired results.

In this research, there are two main considerations that will dictate the mesh size. The first goal is to have enough elements to properly characterize the static response of the model. The second goal is to have enough elements to adequately model the thickness variation throughout the plate. For the sake of computational efficiency, it is desirable to use the bare minimum number of elements that will accomplish both of these goals.

#### 3.5.1 Static Response

The method used to achieve the first goal was to run simulations with various numbers of elements between 100 and 10,000. Each of the simulations was run on a  $[\pm(0|45)]_s$  laminate with a uniform end displacement of  $u_0 = -0.02$ ".

The results were converted to total force resultants to easily compare the different models. The percent difference is calculated by comparing the total force results for various models to the total force results for the 10,000-element model.

$$\text{Percent Difference} = \frac{|F_x^{10,000} - F_x|}{F_x^{10,000}} \times 100\%$$

Accurate results are achieved with as few as 400 elements. Little additional improvement is seen beyond 900 elements, as seen in Table 3-1. The 400-element model is a rough approximation of the actual structure while the 10,000-element model resolves more of these minute details. An example of the complex nature of  $N_x$  can be seen in Figure 3.14. Small fluctuations in the percent difference are seen when the mesh-size resolution becomes fine enough to resolve more of the intricate details of the thickness and fiber-orientation angle interaction. Overall, these small fluctuations have little effect on the final results.

Table 3-1 Convergence data for various mesh sizes.

<b>Number of Elements</b>	<b>Total Force (lbs.)</b>	<b>Percent Difference</b>
100	-4179.07	6.55%
400	-4410.66	1.38%
900	-4486.47	0.32%
1,600	-4469.45	0.06%
2,500	-4474.01	0.04%
3,600	-4458.89	0.30%
4,900	-4459.39	0.29%
6,400	-4446.29	0.58%
8,100	-4476.61	0.10%
10,000	-4472.17	0.00%

### 3.5.2 Thickness Resolution

It is also important to examine how well the thickness variation is represented using different mesh sizes. The nature of variable-stiffness laminates makes discretization of the thickness difficult. The difficulty arises

because in a continuous model there is an overlap region that extends across most of the composite panel. The overlap region in some parts of the panel is so infinitesimally small that it would take an infinite number of elements to adequately resolve. Resolution on this scale is impractical though, so the goal is to achieve the best resolution with the fewest elements.

For models with less than 10,000 elements, resolving a continuous overlap region is difficult for  $T_l \leq 25^\circ$ . A four-layer  $[\pm(0|30)]_s$  variable-stiffness laminate has an overlap region that is well represented by the 10,000-element model. Other mesh sizes are compared against this to see how well the thickness variation was resolved. The 100-element model proved insufficient. From the static response data, we know that at least 900 elements are necessary. From plots that are not shown, 900 -1,600 element models demonstrate no continuity of the overlap region. Because the laminates are symmetric and the maximum thickness for any one layer is double thickness, the discrete thickness can only have values of 4,6 or 8. Four layers will occur in areas where there is no overlap. Six layers will occur where a single set of symmetric layers each has an overlap region. Eight layers will exist only in those areas where all four layers have an overlap region. Thickness plots across entire panels for various mesh sizes are shown in Figures 3.15-3.18.



A 2,500 element model of the  $[\pm\langle 0|30\rangle]_s$  laminate is shown in Figure 3.15. While the 2,500 element convergence results were satisfactory, the thickness variation is disjointed for more than 75% of the plate. The 2,500 element model shows no regions with a thickness value of eight.

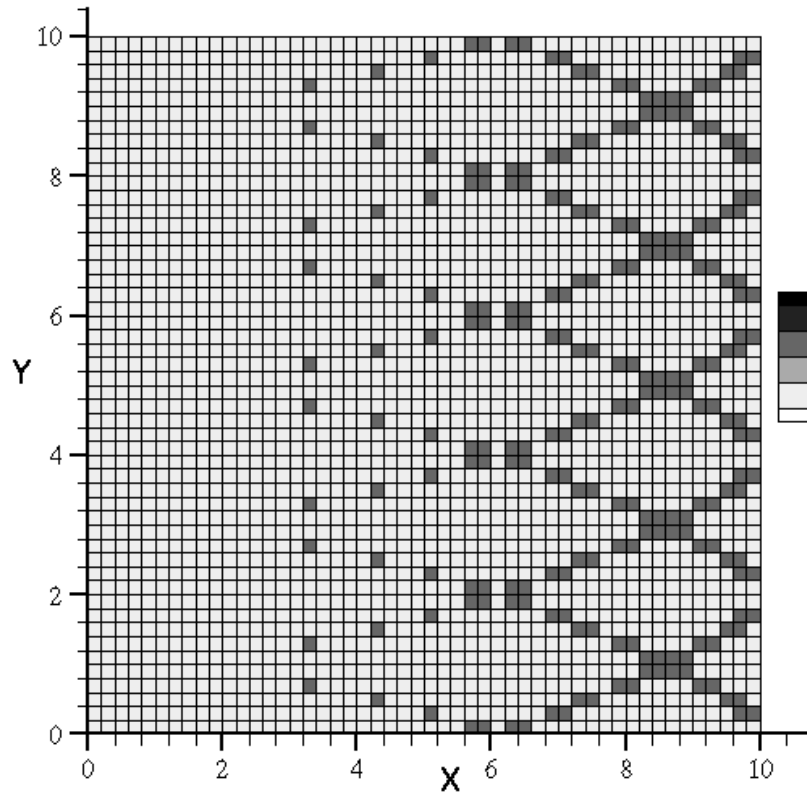


Figure 3.15 Thickness plot for 2,500 elements

The 3,600 element model of the  $[\pm\langle 0|30\rangle]_s$  laminate, in Figure 3.16, is the first model to resolve the eight thickness regions where overlap regions cross. Continuity of overlap regions is retained across approximately one third of the width of the model. The thickness variation becomes discontinuous after that point.

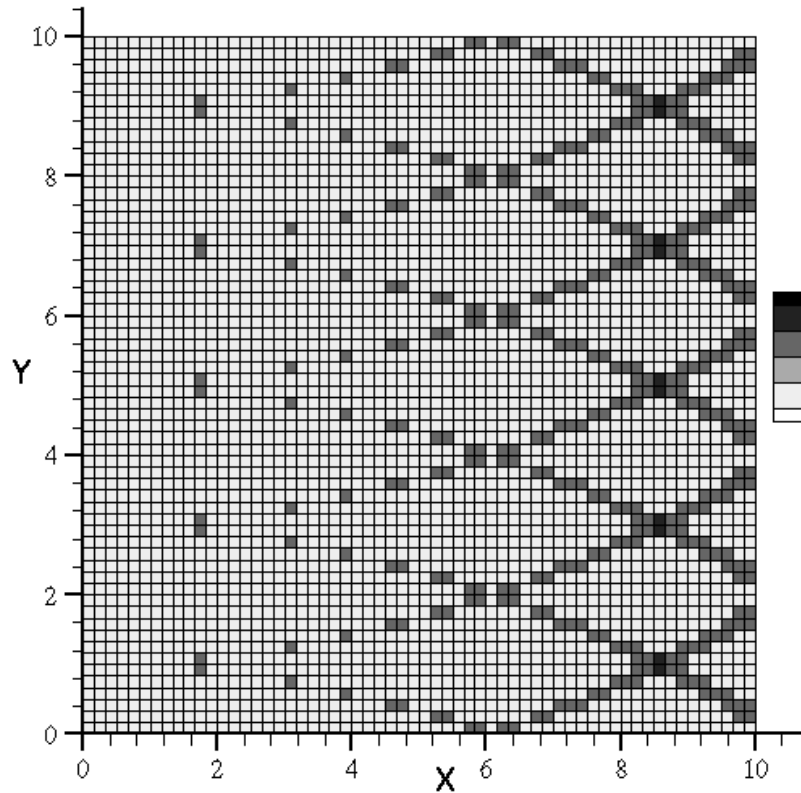


Figure 3.16 Thickness plot for 3,600 elements

An interesting comparison can also be made between the width of the overlap regions along the edge at  $x=a/2$  in Figure 3.16 and the overlap regions of the  $[\pm\langle 0|45\rangle]_s$  laminate shown in Figure 3.10. The smaller value of  $T_1$ , leads to narrower overlap regions and, thus, wider non-overlap regions.

A 4,900 element model of the  $[\pm\langle 0|30\rangle]_s$  laminate is shown in Figure 3.17. The 4,900 element model shows slightly better resolution than the 3,600 model with continuous double thickness regions extending about 40% of the width of the model.

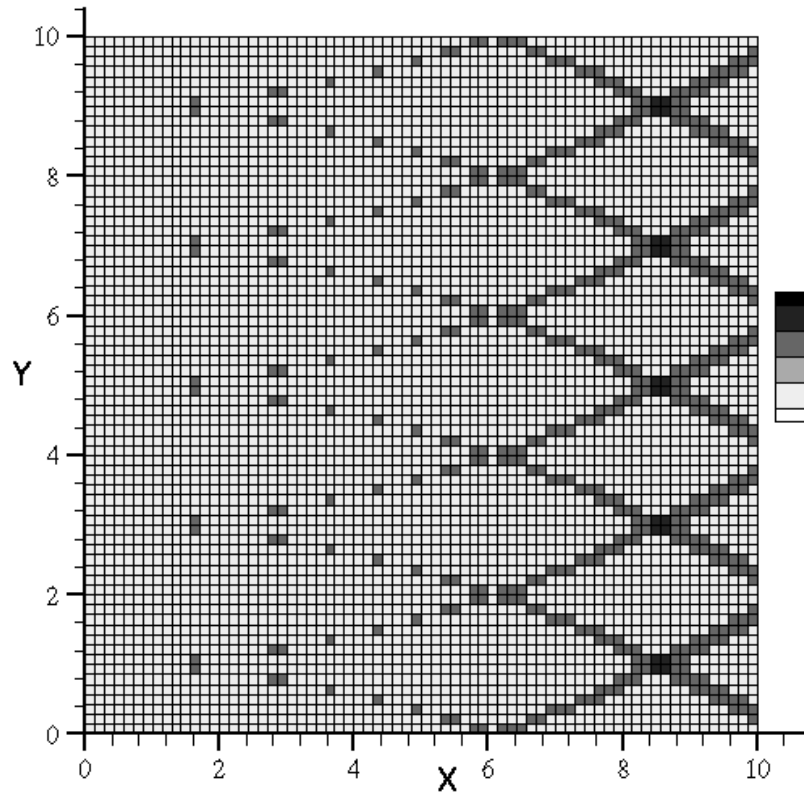


Figure 3.17 Thickness plot for 4,900 elements

Not surprisingly, the best model is the 10,000 element model, shown in Figure 3.18, which remains continuous across half of the model and only has a few isolated increased thickness elements beyond that. The disadvantage of the increased resolution is the substantial computation time necessary to solve the finite element problem.

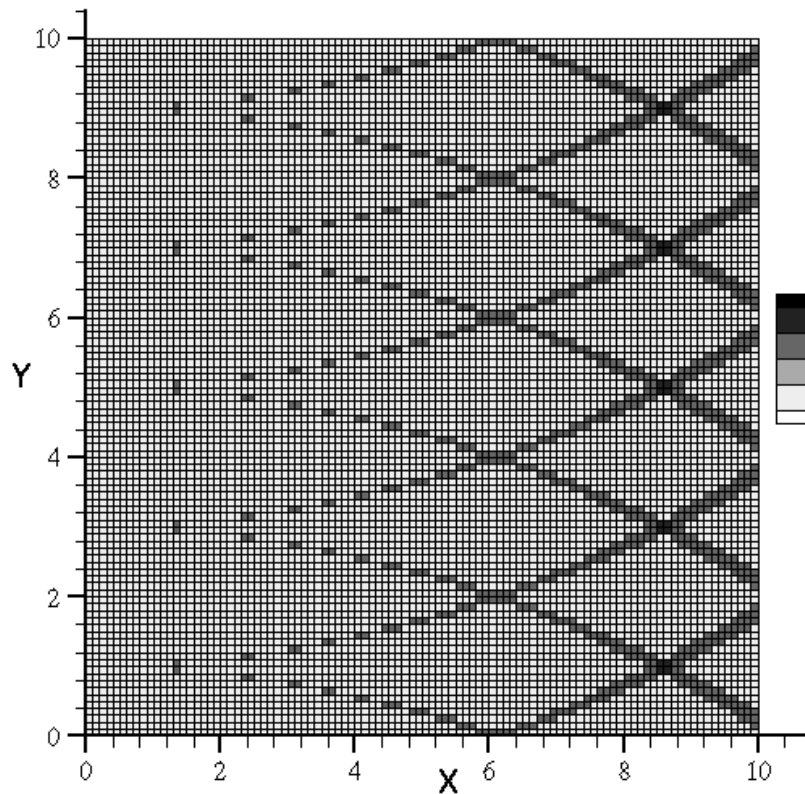


Figure 3.18 Thickness plot for 10,000 elements

The resultant force convergence data and thickness resolution data leads to the decision that a 3,600 element model provides the best compromise between accuracy and computational efficiency for this research.

## Chapter 4

### Results of Finite Element Analysis

Many different forms of response data are generated by the GENESIS finite element analysis. The most basic output is the displacement field, which must be solved for to determine the other static response quantities. One of the most important responses in the design of variable-stiffness composite laminates is the force resultant, which can be used to determine the axial stiffness of the plate. Additionally, the stresses in each layer of every element must be determined in order to check failure criteria. This section will first show typical output from a single GENESIS analysis. GENESIS results for shifted path variable-stiffness composite laminates will then be compared to results from previous research.

#### 4.1 In-plane Results for $[\pm 0/45]_s$ Variable Stiffness Laminate

In this section, the results obtained for a four-layer  $[\pm 0/45]_s$  laminate will be examined. First, the finite element model properties and material properties will be defined. Then, the displacement results will be examined. Next, the force resultants and stress results will be examined followed by the failure index data.

##### 4.1.1 Finite Element Model Definition

For this analysis, the Case I boundary conditions for uniform end shortening in the x direction with the transverse edges free to displace. The Case I boundary conditions for the quarter panel model were shown in Figure 3.3. The model contains 3600 composite plate elements in a 60 x 60 grid of

initially square elements as shown in Figure 4.1. The initial width of the panel,  $a$ , and height of the panel,  $b$ , are both 20 inches. Thus, the dimensions of the quarter panel are 10" x 10". The width of the tow path is 2". The distance of the tow shift is 2". The initial displacement,  $u_0$ , is -0.03".

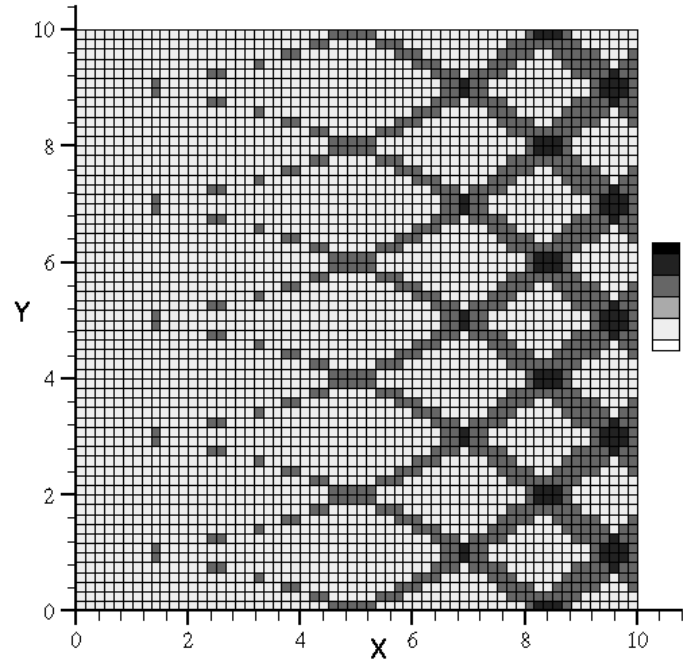


Figure 4.1 Thickness plot of  $[\pm(0|45)]_s$

The elastic properties for the composite material tested are:

$$E_1 = 21.0 \text{ Msi}$$

$$E_2 = 1.4 \text{ Msi}$$

$$G_{12} = 0.8 \text{ Msi}$$

$$\nu_{12} = 0.34$$

$$t = 0.0055 \text{ in}$$

The failure theory used for this model was the Tsai-Hill, which requires the tensile and compressive strengths to be the same for both the fiber direction and transverse to the fiber direction. The failure strengths used in this analysis were:

$$\sigma_1^C = 200.0 \text{ ksi}$$

$$\sigma_1^T = -200.0 \text{ ksi}$$

$$\sigma_2^C = 15.0 \text{ ksi}$$

$$\sigma_2^T = -15.0 \text{ ksi}$$

$$\tau_{12}^F = \pm 15.0 \text{ ksi}$$

#### *4.1.2 Displacement Results*

The unknowns in the finite element system of equations are the displacements of each node. Once the displacements of the nodes are determined, they can be used to calculate the other response quantities such as, strains, stresses and force resultants. For the Case I boundary conditions with the free upper edge and the given material properties, the displacements are too small to be visibly discernable at the scale shown. To better illustrate displacement results, a second analysis was run with a larger displacement ( $u_0 = -0.5$ ). The displacement in the x-direction is relatively consistent. Perpendicular to the axial shortening, there is a large lateral expansion near the displaced edge and somewhat smaller lateral expansion near the panel center, at  $x=0$ , as shown in Figure 4.2.

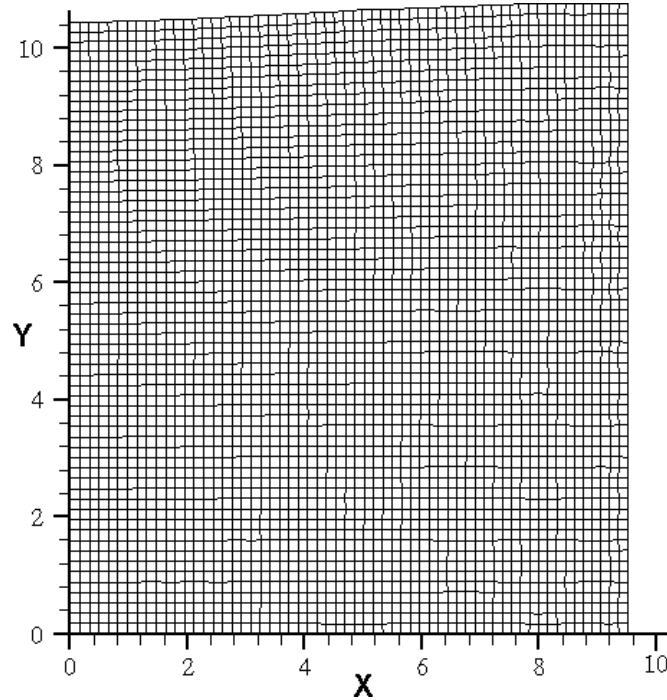


Figure 4.2 Displacement of  $[\pm(0|45)]_s$  for  $u_0=-0.5''$

In reality, the laminate would have failed well before it reached this level of deformation, but the large deformation gives a better idea of how the displacements vary. In a typical straight-fiber laminate, the displacements for these boundary conditions would be expected to be uniform, resulting in a rectangular shape. It is obvious that this is not the case for variable-stiffness laminates. The central portion of the panel,  $x=0$ , the fibers are oriented in the direction of the applied displacement and the Poisson's ratio is very small. Near the edge at  $x=a/2$ , the effective Poisson's ratio is much larger than at the center of the panel, and more lateral expansion results.

#### 4.1.3 Force Resultants

Once the displacements of the nodes have been determined, it is possible to determine the force resultants in each element. The different normalized force resultant distributions across a  $[\pm(0|45)]_s$  quarter panel model are shown in Figures 4.3 - 4.5.



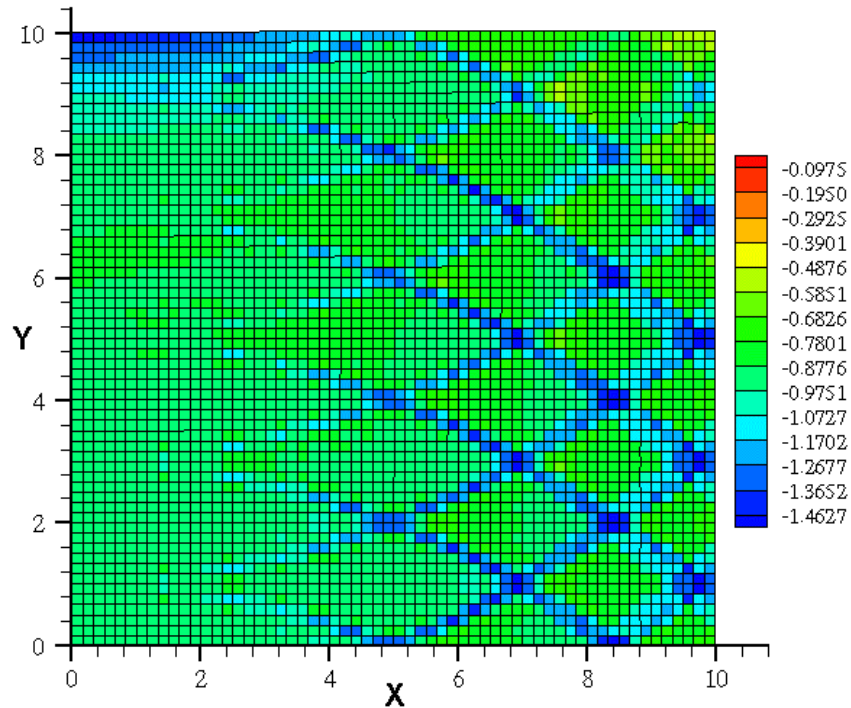


Figure 4.3  $N_x$  distribution across  $[\pm(0|45)]_s$  panel

The variation of  $N_x$  throughout the panel, shown in Figure 4.3, has many interesting features. The most pronounced characteristic is the crisscrossing arcs, where the overlap of adjacent tows occurs. As expected the thicker regions bear a proportionally larger part of the load, effectively redistributing the load toward the center of the panel. Upon closer inspection, it is apparent that the angle variation in the overlap region results in a change in stiffness. Between  $x=5''$  and  $x=7''$  the overlap region elements have values of  $N_x \approx 1.40$ . Between  $x=7''$  and  $x=8''$  the values seem to drop to  $N_x \approx 1.20$  and elements nearer the edge have values approaching  $N_x = 1.0$ . Along the free edge, there is a considerable drop in stiffness near the displaced edge. The drop in stiffness is due to the high level of transverse strain. Toward the center of the panel ( $x=0$ ), along the free edge, there is an increase in compressive load. The increased force-resultant values along the free edge result from having a smaller neighborhood of local elements to carry to load transferred along the overlap

regions. The load transferred to the elements near the center of the panel can be distributed to more elements, thus the force resultants are somewhat smaller.

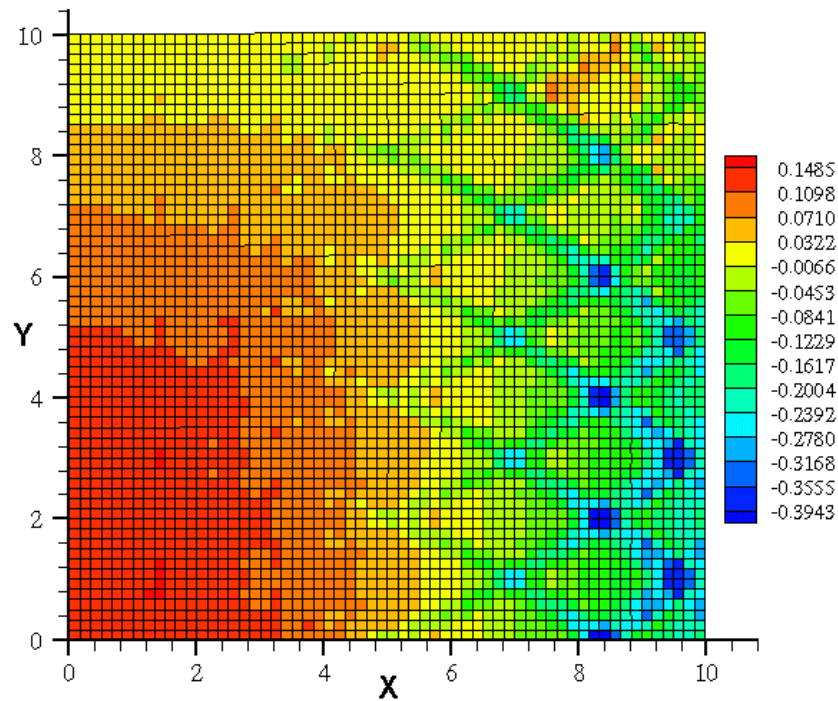


Figure 4.4  $N_y$  distribution for  $[\pm(0|45)]_s$  panel

Both compressive force resultants and tensile force resultants are evident in the  $N_y$  distribution. Once again, the overlap regions can be identified and tend to carry a compressive load. In the center of the quarter panel, a tensile load is evident. The tensile load is distributed consistently in a rectangular area near the center of the plate, resulting in little gradation of color. Along the free edges,  $N_y$  approaches zero, which is to be expected because this edge is not loaded in the  $y$ -direction.

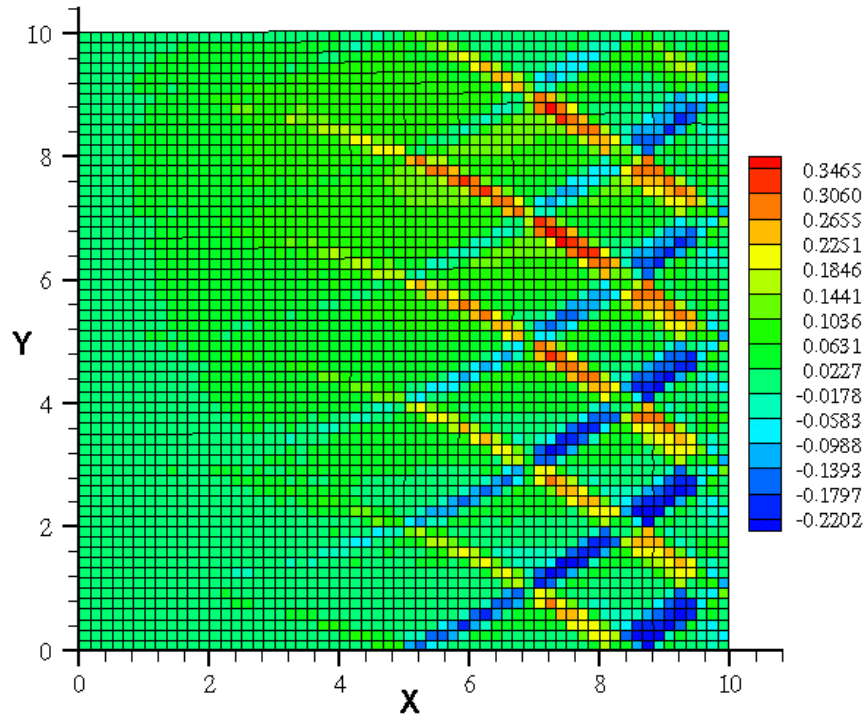


Figure 4.5  $N_{xy}$  distribution across  $[\pm(0|45)]_s$  panel

The shear force resultant on most elements is approximately zero. Along the free edge, the shear resultant is also approximately zero because there is no shear force at the boundary, similar to the  $N_y$  distribution along the free edge. The overlap regions are the exception to the near-zero values. The reason they differ is that they are locally unbalanced regions of the composite. In these regions, the stacking sequence is approximately  $[-\theta/-\theta/\theta]_s$  or  $[-\theta/\theta/\theta]_s$ . When a compressive load is applied to an unbalanced composite element it will have a tendency to shear as shown in Figure 4.6.

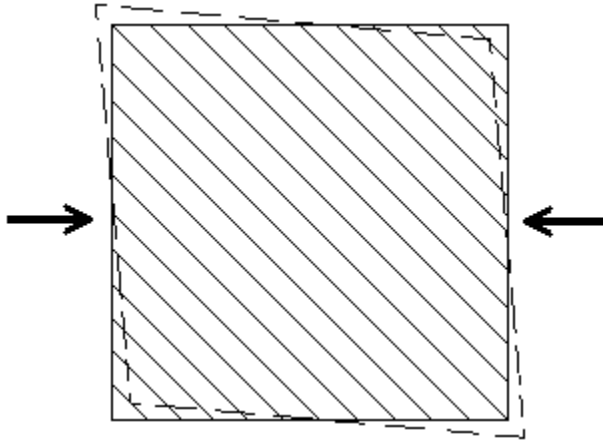


Figure 4.6 Shearing of an axially compressed  $-45^\circ$  element

The shear deformation of the unbalanced element is restrained by the balanced elements surrounding it. The force from the balanced elements result in a positive shear force per unit length that will attempt to maintain the shape of the element, as shown in Figure 4.7. For an element with a positive orientation angle, the shear force will be negative.

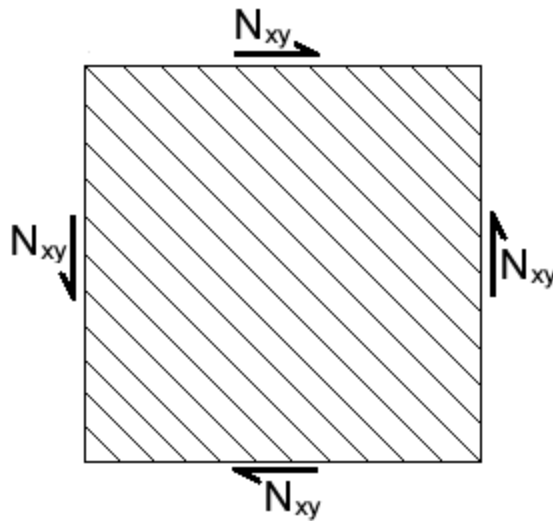


Figure 4.7 Positive shear force per unit length

Although not explicitly shown in Figure 4.7, there will be some shear deformation in the element. Along the displaced edge at  $x=a/2$ , there is less shear force because the unbalanced elements are surrounded by fewer balanced elements than internally located overlap regions, and are not constrained from

shearing by the boundary conditions. In the areas where the overlap regions cross, the elements become balanced again and there is very little shear force resultant.

The equations to determine the total resultant force,  $F_x$ , on the panel were used to quantify the stiffness of various panel configurations. For optimization problems, the weight normalized stiffness would represent the value of the objective function that could be maximized. It is also necessary to consider the weight variation. The total force resultants and weight ratios for various laminate configurations are shown in table 4.1. The final column in Table 4.1 is the total force normalized by the weight ratio.

Table 4-1 Case I total force and weight ratio results for selected laminates

Laminate	Total Force (lbs.)	Weight Ratio	Weight Normalized Total Force
$[\pm 0]_s$	-13,874	1.00000	-13,874
$[\pm 30]_s$	-4,926	1.00000	-4,926
$[\pm 45]_s$	-1,863	1.00000	-1,863
$[\pm \langle 0/30 \rangle]_s$	-10,512	1.05278	-9,986
$[\pm \langle 0/45 \rangle]_s$	-6,699	1.12083	-5,977
$[\pm \langle 0/60 \rangle]_s$	-4,585	1.26111	-3,636

The highest total axial force necessary to achieve the prescribed deformation occurs in the straight fiber  $[\pm 0]_s$  laminate. For axial stiffness in this case, variable stiffness laminates do not seem to offer any advantages. The axial stiffness is determined by the amount of fibers oriented in the direction of the displacement.

A second set of variable-stiffness and straight-fiber models was designed to be run using the Case II boundary conditions shown in Figure 3.4. Case II constrains the top edge,  $y=b/2$ , to zero displacement. In this case, there is a value of axial stiffness, total force x, and a value of transverse stiffness, total force y. In this comparison the  $[\pm 0]_s$  still shows the highest axial stiffness. Most of the variable-stiffness laminates show comparable axial stiffness. Additionally,

most of them show much higher stiffness in the transverse direction. The results of these analyses are shown in Table 4.2. This stiffness information could be used to maximize transverse stiffness, while maintaining an axial compressive stiffness of at least -10,000 lbs. For the laminates shown, the  $\pm[0/45]_s$  is the best design.

Table 4-2 Case II total force and weight ratio results for selected laminates

Laminate	Total Force X (lbs.)	Total Force Y (lbs.)	Weight Ratio
$[\pm 0]_s$	-13967.6	-318.3	1.0000
$[\pm\langle 0/15 \rangle]_s$	-13505.1	-599.1	1.0111
$[\pm\langle 0/30 \rangle]_s$	-12262.3	-1412.0	1.0528
$[\pm\langle 0/45 \rangle]_s$	-10209.6	-2536.4	1.1208
$[\pm 15]_s$	-12325.4	-1077.0	1.0000
$[\pm\langle 15/30 \rangle]_s$	-10881.3	-1989.4	1.0556
$[\pm\langle 15/45 \rangle]_s$	-8851.6	-3092.7	1.1417
$[\pm 30]_s$	-8429.7	-2609.2	1.0000
$[\pm\langle 30/45 \rangle]_s$	-6701.7	-3465.7	1.0967
$[\pm 45]_s$	-4411.0	-3372.81	1.0000

#### 4.1.4 Failure Results

For an optimization problem, the total force resultant represents an objective function that can be maximized for a chosen set of boundary conditions. Without constraints, the axial displacement could be increased without restriction in order to increase the total force. In this research, stress limits and failure indices are used to constrain the optimization problem.

Three stresses are output for each layer of each element,  $\sigma_1$  the stress in the fiber direction,  $\sigma_2$  the stress perpendicular to the fibers and  $\tau_{12}$  the shear stress in the principal material coordinate system. For the  $[\pm\langle 0/45 \rangle]_s$  laminate there are three plots for each layer, resulting in 24 different stress states to analyze. To compare the stresses in each element to failure strengths would be

an overwhelming task for this simple laminate, not to mention that most laminates would have many more layers. Additionally, interpreting the stress data is complicated by the interactions of different stresses and the thickness and orientation variation of the variable stiffness model. Fortunately, using failure criteria gives insight as to where failure will most likely occur and at what load it will occur.

The stresses are then checked against the failure criteria designated in the GENESIS input file. If a failure index exceeds a value of 1.0 then the element has exceeded the specified failure strength. The failure indices across the panel in the second layer and the fourth (i.e., central) layer are shown in Figures 4.8 and 4.9, respectively. The effect variable thickness has on the results is also evident in Figure 4.8. White squares represent areas where the elements do not exist in that layer of the total laminate. In the central layers, every element is represented. In the outermost layers, only the overlap regions exist.

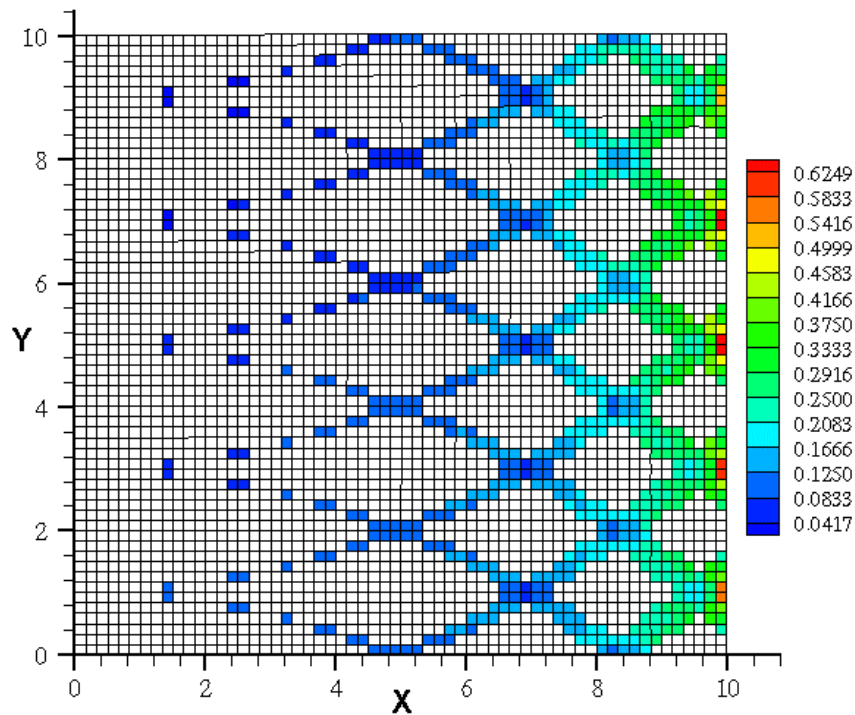


Figure 4.8 Failure indices in second layer of  $[\pm(0|45)]_s$  panel

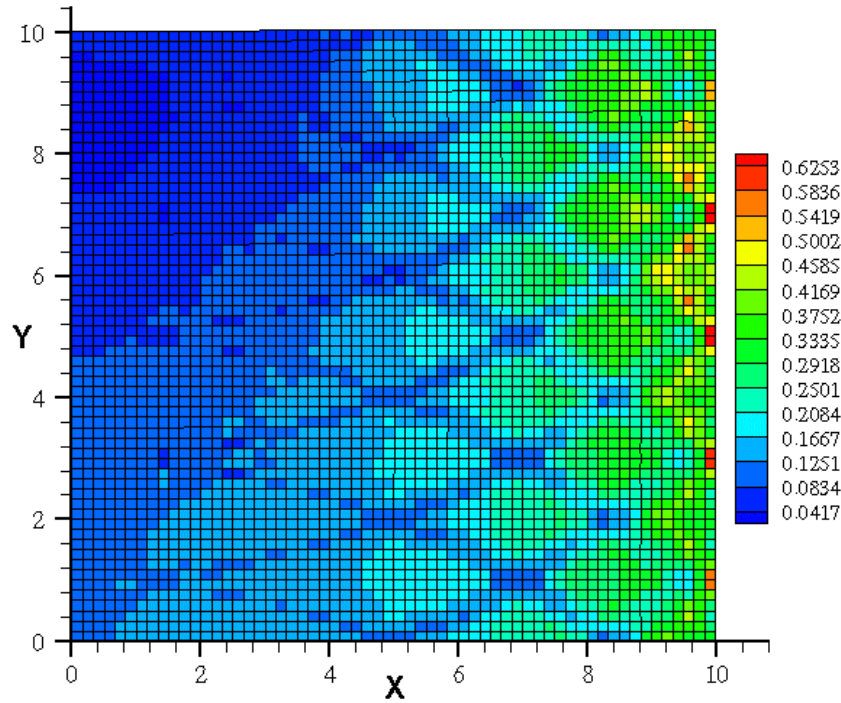


Figure 4.9 Failure indices in central layer of  $[\pm(0/45)]_s$  panel

In both plots it is obvious that failure is going to occur first along the displaced edge, at  $x=a/2$ , in elements between the overlap regions. Because GENESIS cannot determine what the mode of failure will be explicitly, it is necessary to look at the stress distributions. The failure data can be used with the stress data to get an idea of why failure is going to occur. In this case, the stresses in the fiber direction and transverse to the fiber direction are relatively low compared to the failure strengths in those directions. The shear stress attains values much closer to its failure strength along the displaced edge. The stresses in the fiber direction, transverse to the fiber direction and shear stresses vary through the central layer of the  $[\pm(0/45)]_s$  panel are shown in Figures 4.10 through 4.12.



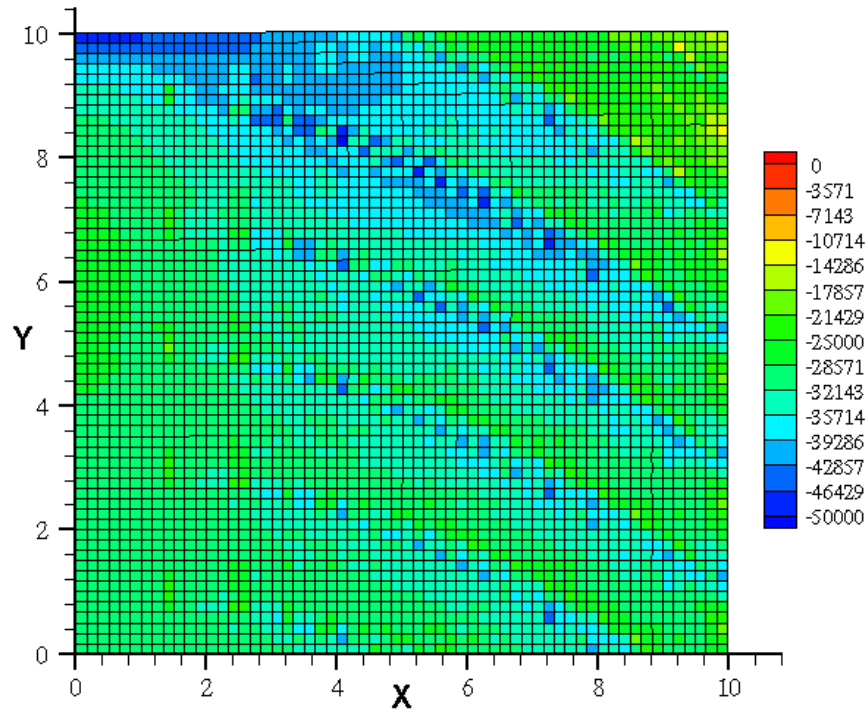


Figure 4.10 Stresses in fiber direction,  $\sigma_1$ , of the middle layer

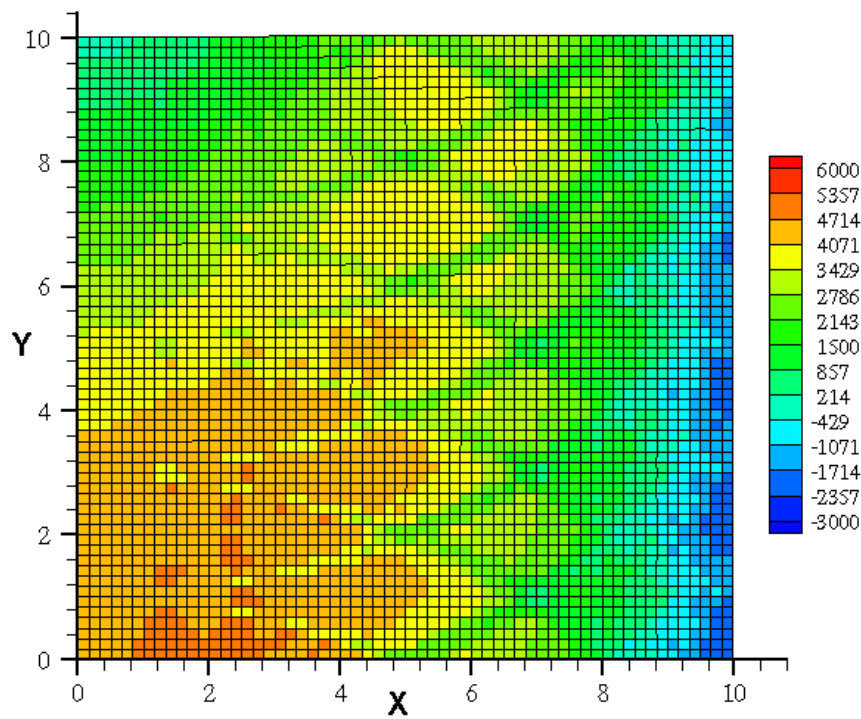


Figure 4.11 Stresses transverse to fiber direction,  $\sigma_2$ , in middle layer

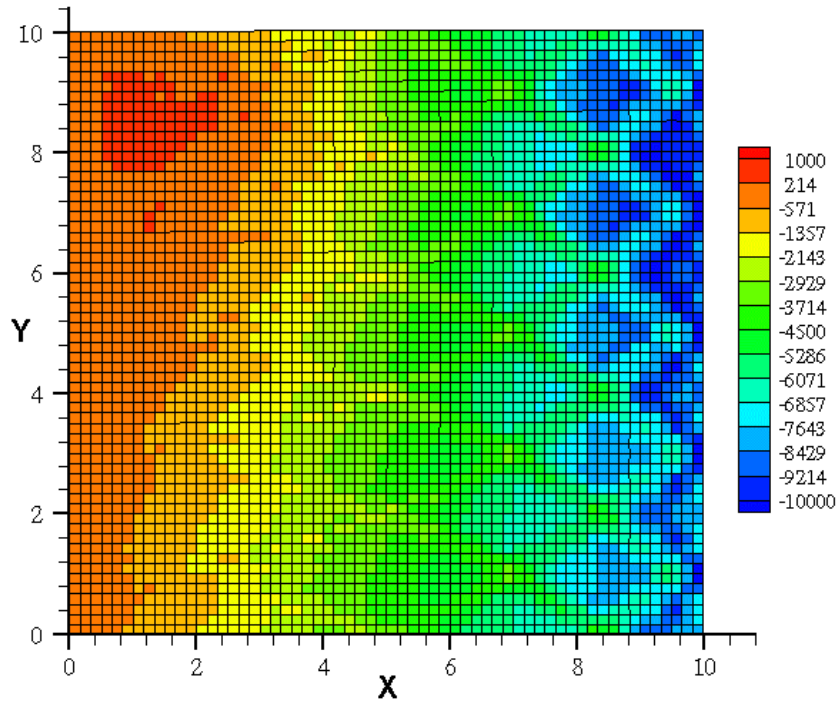


Figure 4.12 Shear stresses,  $\tau_{12}$ , in middle layer

Along the displaced edge, it is apparent that the forces in the fiber direction and transverse to the fiber direction are relatively low compared to the failure strengths in those directions. They are both approximately 20% of the failure strength. The shear stress on the other hand reaches values of approximately 60% of the shear failure stress. Thus, it can be concluded that failure will occur due to a shearing mode along the displaced edge.

#### 4.1.5 Stresses in Tow Paths

One other interesting plot is the variation in stress through a single tow path. Once the stresses in every layer are known it is possible to go back and recover the stresses for a single tow path. Figure 4.13 shows the variation of stress in the fiber direction for a single tow path.

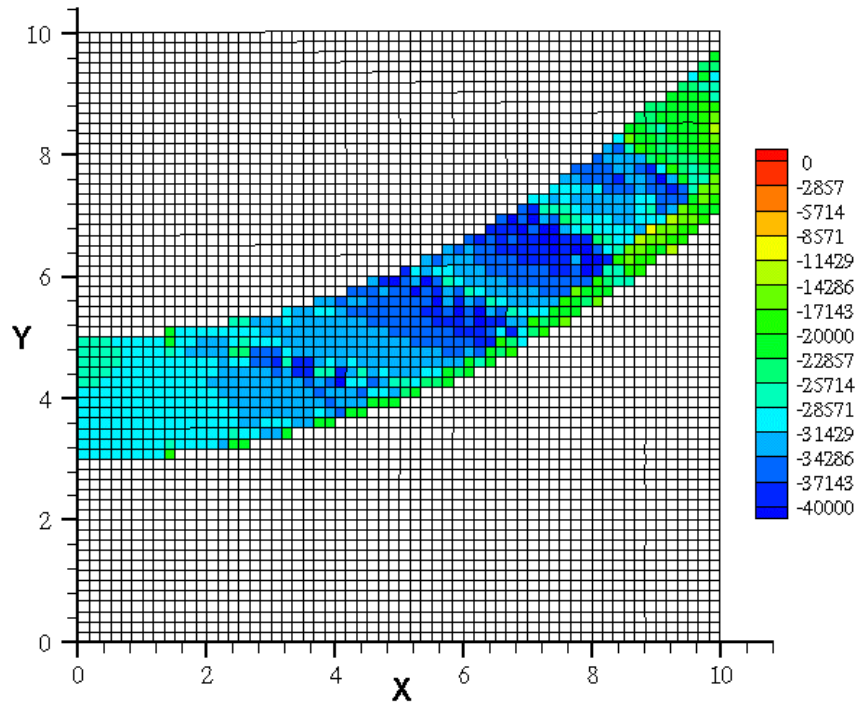


Figure 4.13 Variation of  $\sigma_1$  for a single  $\langle 0|45 \rangle$  path

In this path, the overlap region from one of the overlap regions is clearly visible as the green band on the lower edge of the path. The overlap regions that cross over this tow path are also visible as faint lines. It is also interesting to note how the stresses change between overlap regions and how they change as the fiber angle changes. The stresses in the fiber direction increase as the fiber orientation changes approaching the displaced edge. The fiber stress drops dramatically each time an overlap region crosses the tow path. It then begins to increase again until the next overlap region crosses.

The data reflect the complex nature of variable-stiffness laminates and allows an insight into some of the factors that must be considered in the design of such laminates. The interaction of the thickness changes and the fiber changes results in very complex behavior. The stiffness results can be used to determine objective function evaluations and the failure results as constraint criteria it is possible to formulate design optimization problems using variable-stiffness laminates.

## 4.2 Comparison to Previous Research

Previous research by Waldhart [11] studied the axial stiffness of variable stiffness panels created using shifted tow paths and parallel tow paths. The response of shifted path was solved in a closed-form by making some assumptions about the panel geometry. The first assumption was that tow paths could be represented by individual fiber paths. The angle at any point in the tow path is not dependent on which path it belongs to. The angle at any point in the panel is only a function of position along the x-axis. The second assumption was that there was no thickness change in the laminate. Once these assumptions were made it was possible to determine the in-plane response and buckling behavior of different variable stiffness configurations with a closed-form solution.

Using finite element methods, allows for a more accurate representation of the laminate where these two assumptions are not necessary. By using specific tow reference paths, the angle in each layer of every element is determined using the Golden section search. These orientation angles are based not on position along the x-axes, but they are determined based on position within a specific tow path. The thickness variation can be determined by allowing adjacent tow paths to overlap each other. The result is a more complex and more accurate model of variable-stiffness composite structure.

While there are some fundamental differences in the models created in the previous research and the model developed in this research, we still expect results between the two models to be comparable. Waldhart investigated the axial response of two shifted-path variable-stiffness laminate configurations in detail. The configurations examined were a  $[0\pm\langle 45/75 \rangle]_{9s}$  and a  $[90\pm\langle 45/75 \rangle]_{9s}$  laminate. For each of these laminates, plots were made of the normalized force resultants  $N_x$ ,  $N_y$  and  $N_{xy}$ . Similar laminates have been created using the methods put forth in this research, and solved using GENESIS for comparison.

The material constants and overall panel parameters are identical to the  $[\pm\langle 0/45 \rangle]_s$  example. The only difference to the previous example is that the shift distance has been increased from 2.0 inches to 2.82843 inches so that the

resulting laminate would have a single thickness at  $x=0$ . In order to reduce the amount of computation time and output data, the finite element models that are used are only four layers thick;  $[0\pm\langle 45/75 \rangle]_s$  and  $[90\pm\langle 45/75 \rangle]_s$ . The difference in the number of layers is compensated for by normalizing the data as shown earlier. It is important to note that  $\langle 45/75 \rangle$  variable stiffness paths will overlap the two previous paths creating regions of triple thickness near the displaced edge at  $x=a/2$ . The finite element model currently does not account for these small triple-thickness regions.

It is also important to note that Waldhart used a normalization calculation based on the fiber orientation at the center of the variable stiffness plate, instead of a  $0^\circ$  laminate. This difference will only change the axial stiffness term  $A_{11}$ . Thus, the normalization calculation becomes:

$$\bar{N}_x = \frac{a}{2u_0 A_{11}(\pm 45^\circ)_s} N_x$$

The result is that the normalized force resultants will be higher as compared to previous results in this research. For this comparison, the finite element results also used this normalization equation, so that they could be compared to the previous research on an equal basis.

#### 4.2.1 Comparison of $N_x$ Results for $[90\pm\langle 45/75 \rangle]_s$ Model

The thickness variation for the  $[90\pm\langle 45/75 \rangle]_s$  model is shown in Figure 4.13. The effect of angles approaching  $90^\circ$  can be seen by the large areas of overlap denoted by black. The top of the panel is a large region where the overlapping paths in both directions cross each other creating an area that is double the thickness.

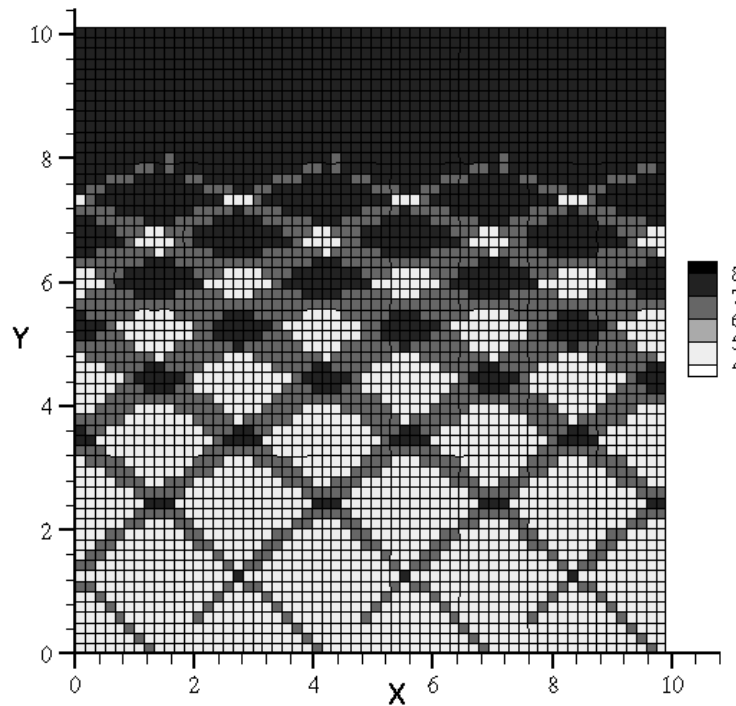


Figure 4.14 Thickness plot of  $[90\pm(45/75)]_s$  panel

Once again, there is a uniform compressive displacement applied in the  $x$ -direction. The results of this displacement on the force resultant  $N_x$  for the quarter panel  $[90\pm(45/75)]_s$  are shown in Figure 4.14. The results from the closed-form solution of the quarter panel  $[90\pm(45/75)]_{9s}$  are shown in Figure 4.15. The distribution of the forces is similar in the two models. The finite element model shows a less consistent distribution due to the crisscrossing overlap regions. The  $N_x$  results are approximately twice as high along the upper edge due to the thickness increase. Along the center at  $y=0$ , the values of  $N_x$  differ by approximately 25%. The finite element model has a nominal thickness of four layers in this region.

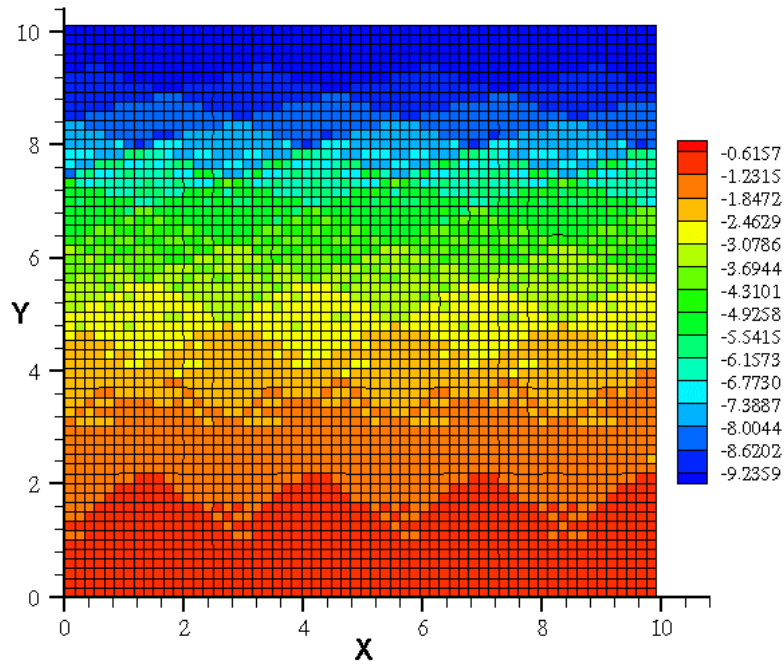


Figure 4.15  $N_x$  distribution for  $[90\pm(45/75)]_s$  panel

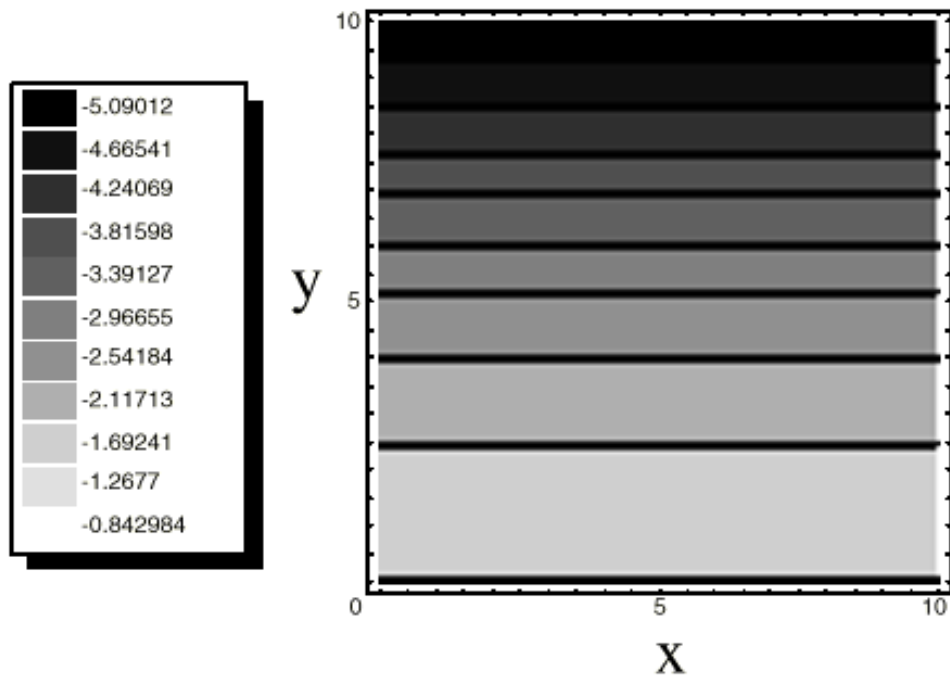


Figure 4.16 Closed-form  $N_x$  solution for  $[90\pm(45/75)]_{9s}$ , from Waldhart [11]

#### 4.2.2 $N_y$ and $N_{xy}$ Comparison Results for $[90\pm\langle 45|75\rangle]_s$

Results for  $N_y$  and  $N_{xy}$  for  $[90\pm\langle 45|75\rangle]_s$  were also compared with the closed-form  $N_y$  and  $N_{xy}$  results for the  $[90\pm\langle 45|75\rangle]_{9s}$ . The boundary conditions for the closed-form model set  $N_y$  and  $N_{xy}$  to zero along the top edge. The boundary conditions resulted in both  $N_y$  and  $N_{xy}$  being zero throughout the plate. The results of the finite element model closely resemble the closed-form solutions with values that approach zero. The local changes in geometry result in some small locally high values of  $N_y$  and  $N_{xy}$ . Overall, the results agree well with the previous research. Because these results were approximately zero throughout all models, these results are not shown here.

#### 4.2.3 Comparison of $N_x$ Results for $[0\pm\langle 45|75\rangle]_s$ Model

The thickness distribution for this model is identical to the previous example except that it is rotated  $90^\circ$  clockwise as shown in Figure 4.16. The same areas of path overlap and region of double thickness are apparent.



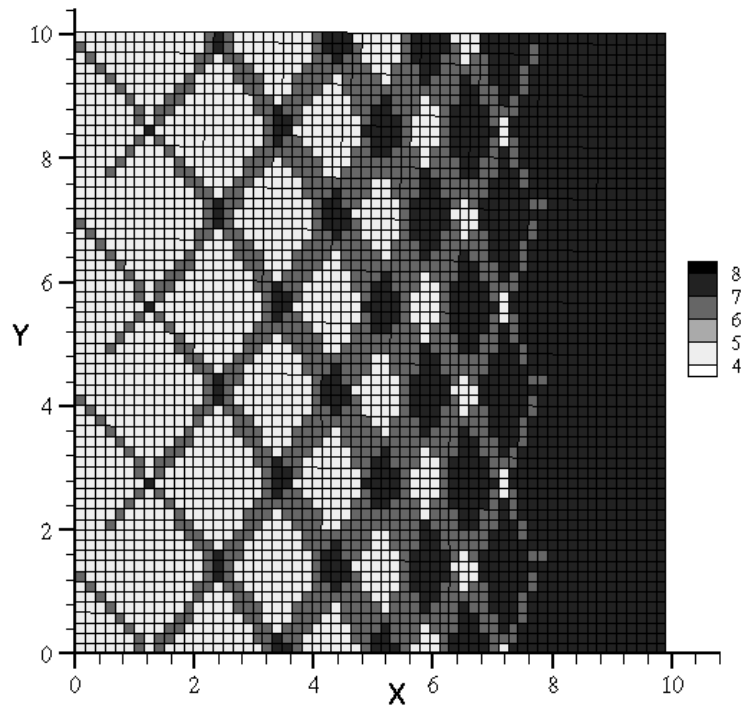


Figure 4.17 Thickness plot of for  $[0\pm(45/75)]_s$  panel

In this case, the distribution of  $N_x$  is more complex for both the finite element model and the closed-form solution. The finite element quarter panel results are shown in Figure 4.17 while the closed-form quarter-panel solution results are shown in Figure 4.18. Once again, the distribution of  $N_x$  shows some of the same general characteristics. The upper right corner is the stiffest area in both models. Once again, the finite element model results are approximately double the force resultant values from the closed-form results due to the thickness increase. Near the center of the panel, i.e., near (0,0), is another area where both models show high values of  $N_x$ . The finite element results seem to be slightly higher due to the increased thickness elements in the region. These elements appear to carry a higher portion of the load. These results also demonstrate how the more complex geometry of the finite element model can lead to local irregularities that cannot be captured with the flat closed-form solution.

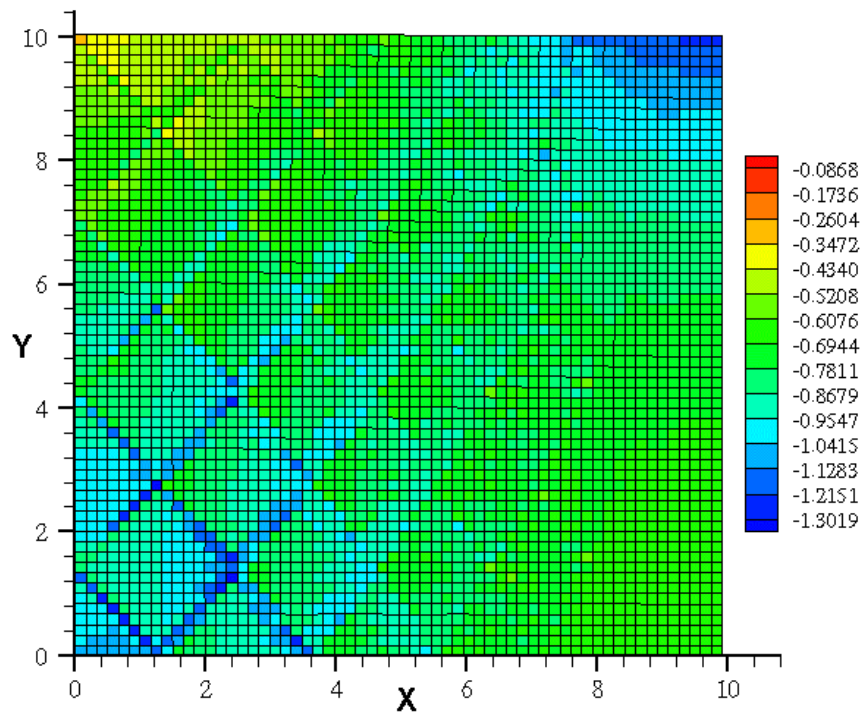


Figure 4.18  $N_x$  distribution for  $[0\pm(45/75)]_s$  quarter panel

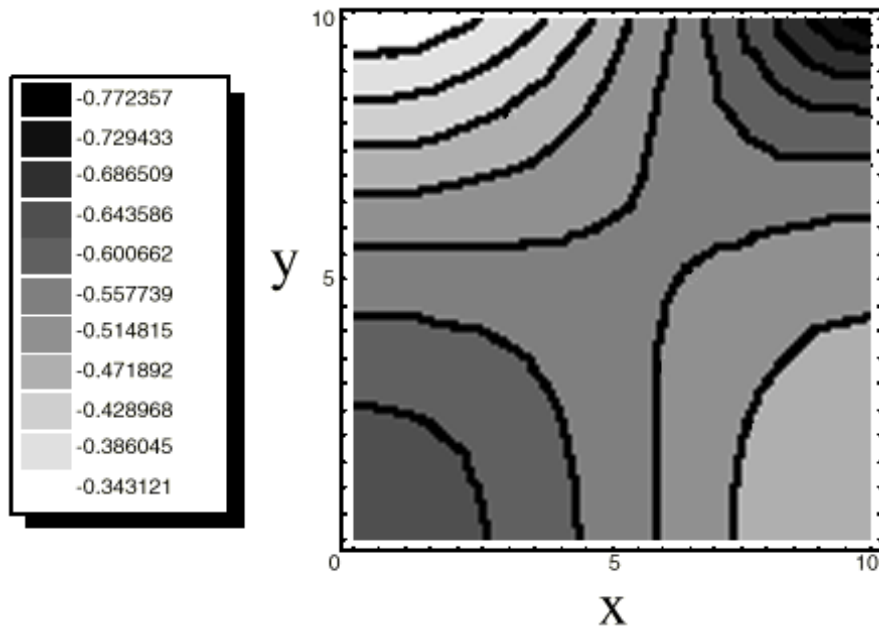


Figure 4.19 Closed-form  $N_x$  solution for  $[0\pm(45/75)]_{9s}$ , from Waldhart [11]

In both models, there are also two regions of lower  $N_x$  values. The region near (10,0) at the bottom right hand corner of the finite element quarter-panel model shows a slight decrease in  $N_x$  similar to the closed-form model. The upper-left-hand corner of the finite element model shows a larger drop in  $N_x$ , which has values that approach those seen in the closed-form solution.

#### *4.2.4 Comparison of $N_y$ Results for $[0\pm\langle 45|75 \rangle]_s$ Model*

In this case, the results for  $N_y$  in the closed for solution are not zero. The finite element quarter panel results are shown in Figure 4.19. Many of the same general trends are evident in the finite element results as are seen in the closed-form results, shown in Figure 4.20. Along the displaced edge, there is a region of high tensile force due to the high lateral displacement. The finite element values along this edge are slightly less than double the values of the closed-form solution. Near the center of the panel, there is a region of high compressive force carried in large part by the overlap elements. In this area, the force resultant values are substantially higher than the closed-form solution. Along the top edge, the force resultant approaches zero in both models, because it is a free edge.

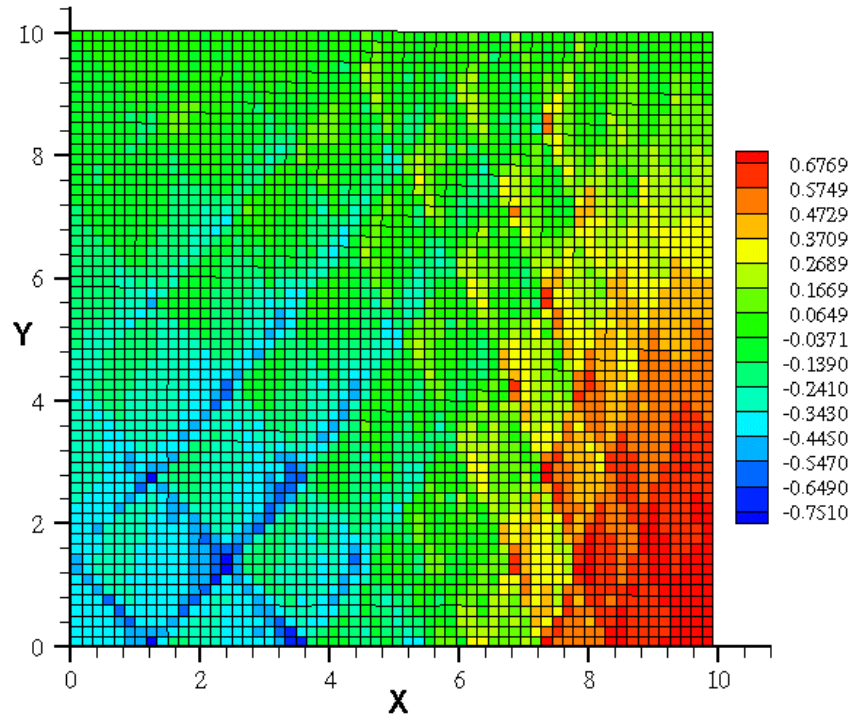


Figure 4.20  $N_y$  distribution for  $[0\pm(45/75)]_s$  quarter panel

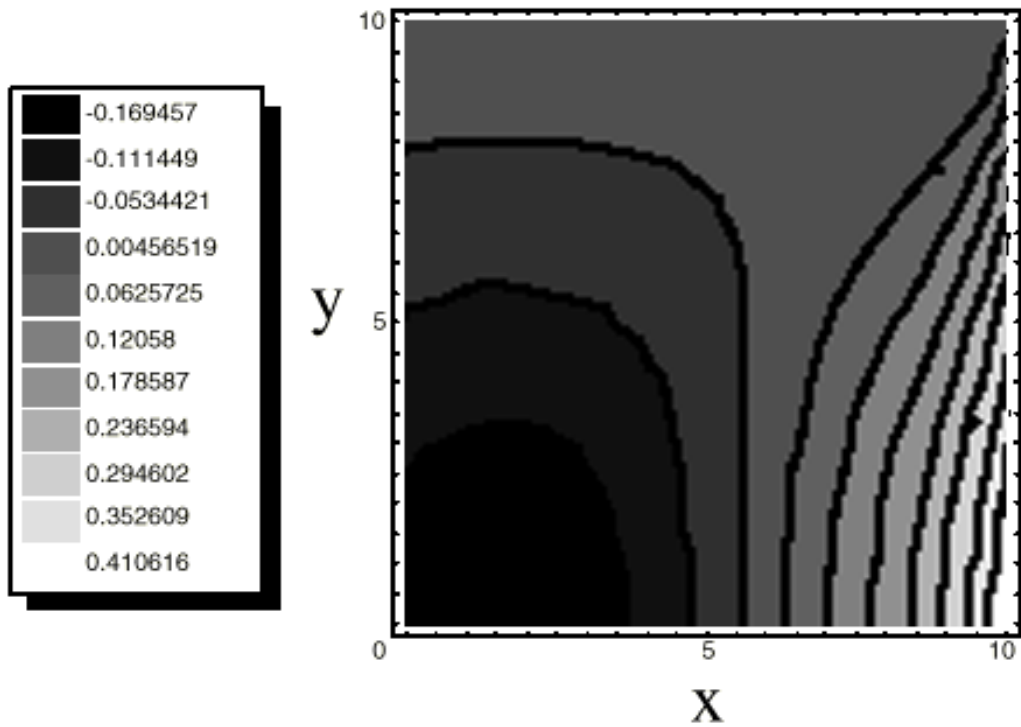


Figure 4.21 Closed-form  $N_y$  distribution for  $[0\pm(45/75)]_{9s}$  panel, from Waldhart [11]

#### *4.2.5 Comparison of $N_{xy}$ Results for $[0\pm\langle 45/75 \rangle]_s$ Model*

Similar to the  $N_y$  results, the  $N_{xy}$  are more complex in the  $[0\pm\langle 45/75 \rangle]_s$  model. The  $N_{xy}$  distribution for the finite element quarter-panel model is shown in Figure 4.21. The  $N_{xy}$  distribution for the closed-form quarter-panel model is shown in Figure 4.22. Once again, the same general trends can be seen. In this case, the overlap regions have a more pronounced effect. The overlap regions carry the majority of the shear load in the area at the center of the quarter-panel model. In the closed-form model, the shear load is evenly distributed in the same area. In both models the area around the edges is approximately zero. The closed-form solutions shows no shear forces in the center of the plate, while the finite element model shows some local shear forces due to overlap. Overall, the results from the two models compare very favorably in spite of the fundamental differences in how the models were developed.

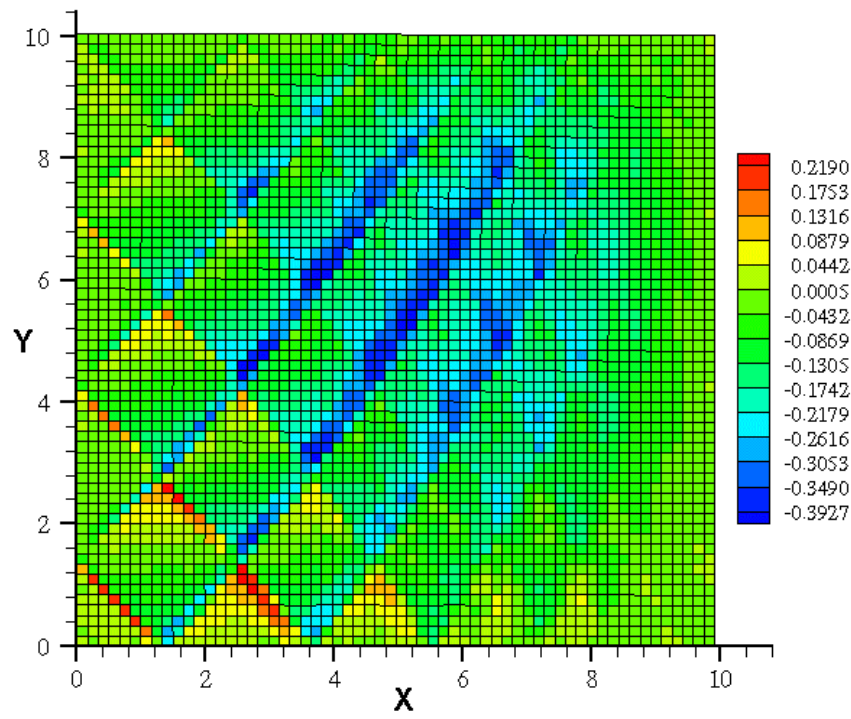


Figure 4.22  $N_{xy}$  distribution for  $[0\pm(45/75)]_s$  panel

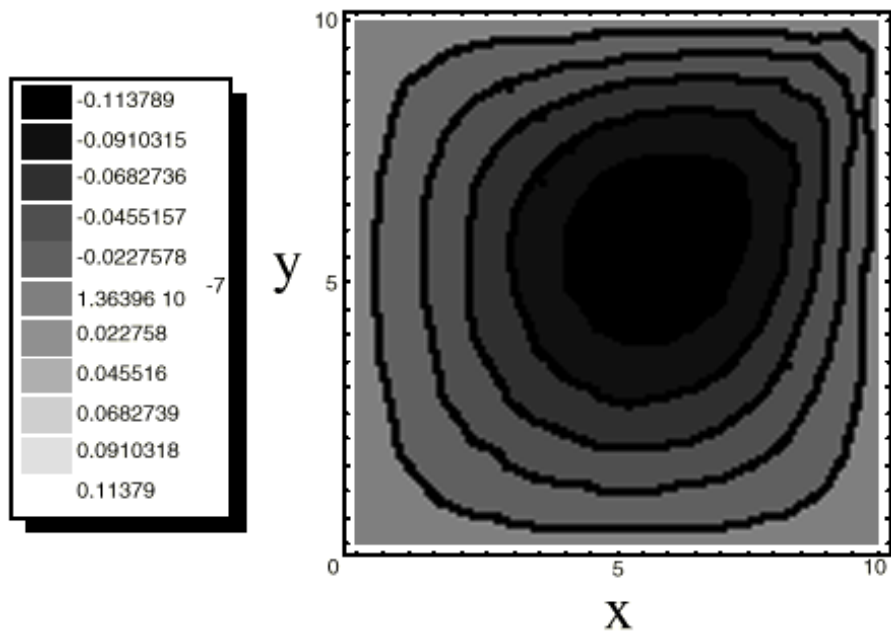


Figure 4.23 Closed-form  $N_{xy}$  distribution for  $[0\pm(45/75)]_s$  panel, from Waldhart [11]

## Chapter 5

### Additional Design Capabilities

One of the goals in developing the program used to create the finite element models of various variable-stiffness laminates was to provide a high level of flexibility to the designer. By their very nature, variable-stiffness laminates allow an incredible variety of design possibilities. The method developed allows for many different variables to be changed to create a wide range of possible laminate designs. In addition, GENESIS allows for a wide range of composite material design parameters and material properties to be entered. Up to this point, the laminates have been fairly simple symmetric, quasi-balanced four layer laminates. The program has many capabilities, which will be demonstrated, in this section.

#### 5.1 $T_0$ and $T_1$ Variation

The values of  $T_0$  and  $T_1$  can be designed with values between  $-90^\circ$  and  $90^\circ$ . Because the overlap region is only allowed to create up to double thickness, care must be taken in using values near these. It is also possible to mix positive  $T_0$  with negative values of  $T_1$ . A  $\langle +25|-45 \rangle$  tow path is shown in Figure 5.1.

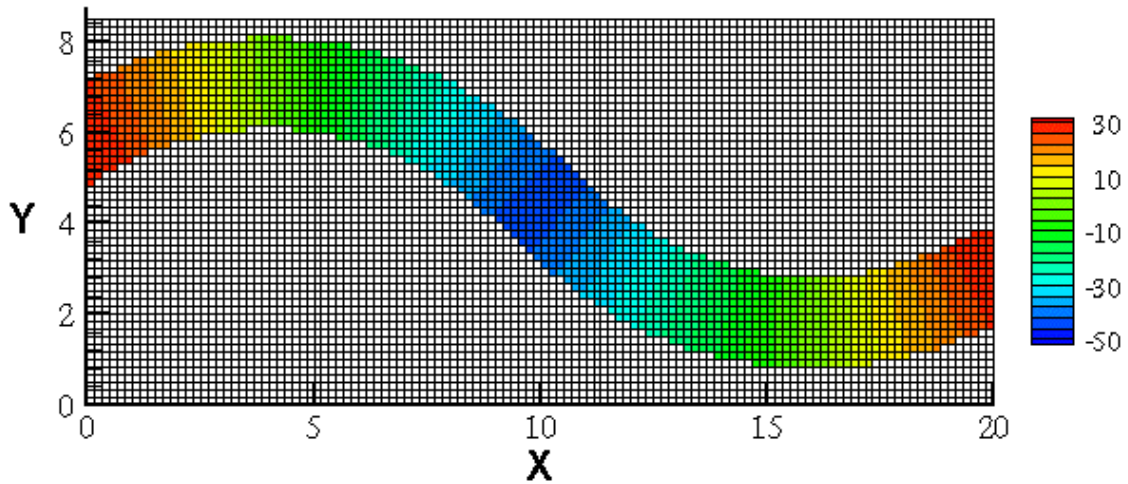


Figure 5.1 Orientation angle of  $\langle +25|-45 \rangle$  tow path

This type of tow path results in a quarter panel model as shown in Figure 5.2. The interesting feature of this design is the reinforcing overlap regions at the center of the panel. Additionally, the possibility of tailoring the position of fibers of a certain orientation, such as the  $0^\circ$  fibers at  $x \approx 4''$ , is shown.



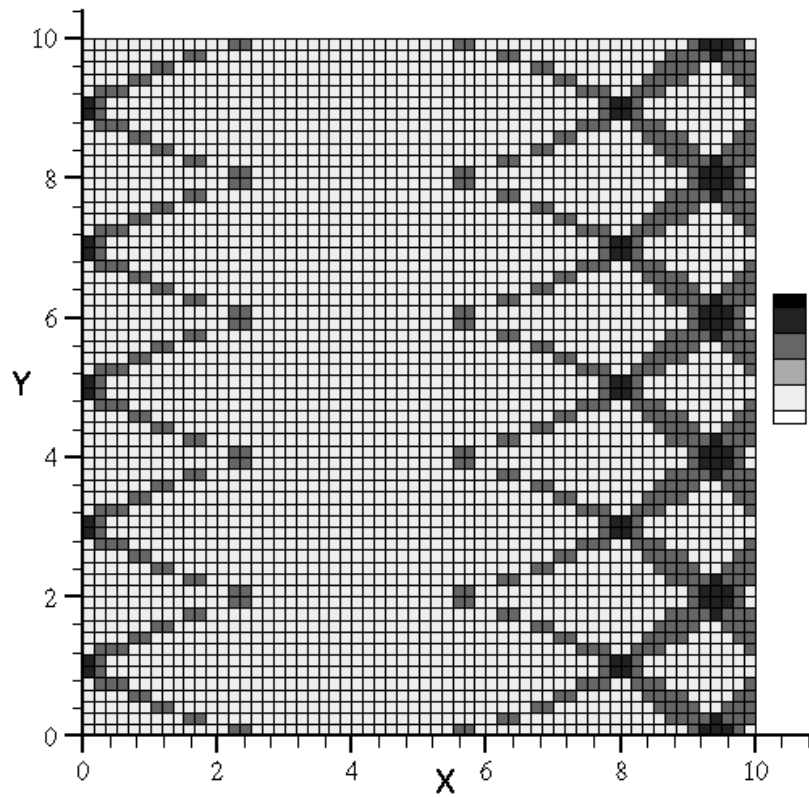


Figure 5.2 Thickness distribution of [(±25|±45)<sub>s</sub>] panel

## 5.2 Shift Variation

Another possible design variable is the shift distance. By increasing or decreasing the shift distance, it is possible to tailor the amount of overlap region. Once again, with the current method it is not possible to decrease the shift distance such that more than double thickness occurs. A straight fiber [±45]<sub>s</sub> laminate with a path width of 2" and a shift distance of 2" is shown in Figure 5.3. The shift results in an overlap region that forms a network of increased thickness regions.

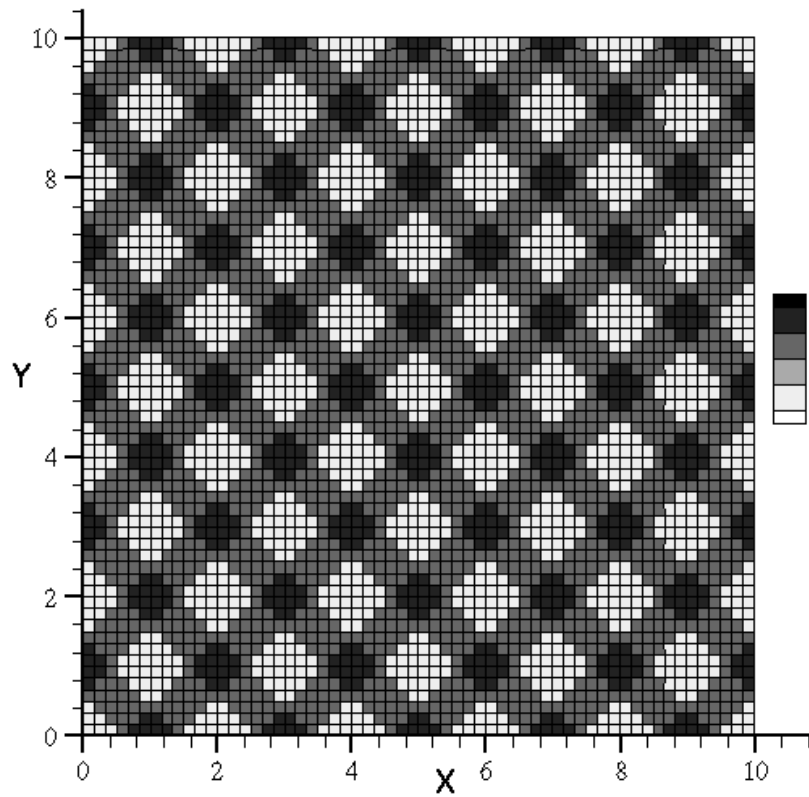


Figure 5.3 Thickness plot of  $[\pm 45]_s$  panel with 2" shift

When subjected to uniform end shortening, the increased thickness regions carry a higher part of the axial load. The  $N_x$  distribution is shown in Figure 5.4.

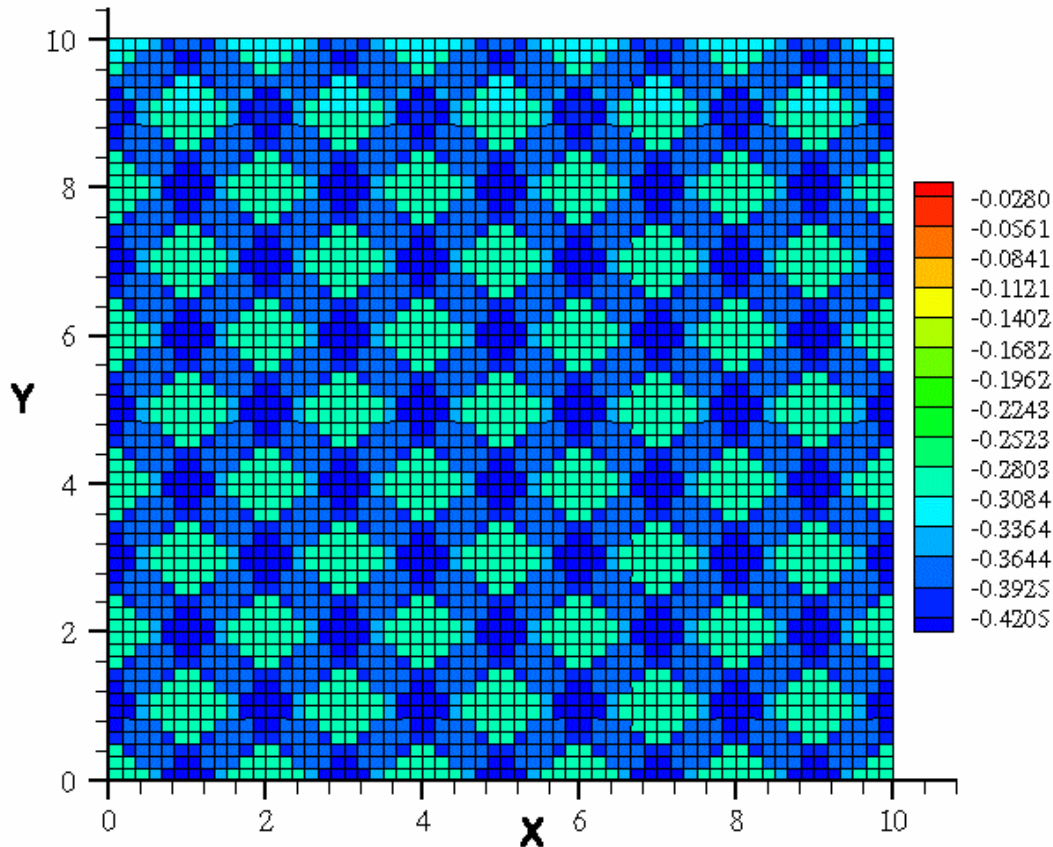


Figure 5.4  $N_x$  distribution for  $[\pm 45]_s$  panel with 2" shift

### 5.3 Mixed Lay-up Analysis

Optimizing the axial response of a four layer laminate for a set of given boundary conditions represents a relatively simple design problem. For the case of uniform end shortening with free transverse edges, the best design is typically a  $0^\circ$  straight fiber laminate. If the boundary conditions are more complex, this may not always be the case. Combinations of variable-stiffness laminate configurations may offer advantages that straight fiber laminates cannot. It is also possible that combination of a variable stiffness laminate and a straight fiber laminate may improve performance. For example, it might be favorable to use a straight-fiber laminate for high axial stiffness in conjunction with variable-stiffness plies for a good combination of transverse and axial stiffness. A 6400 element example of two variable-stiffness laminates combined is shown in Figure

5.5. The outer layers are  $[90 \langle 0|\pm 25 \rangle]$  combined with inner layers of a  $[0 \langle 0|\pm 45 \rangle]$  laminate.

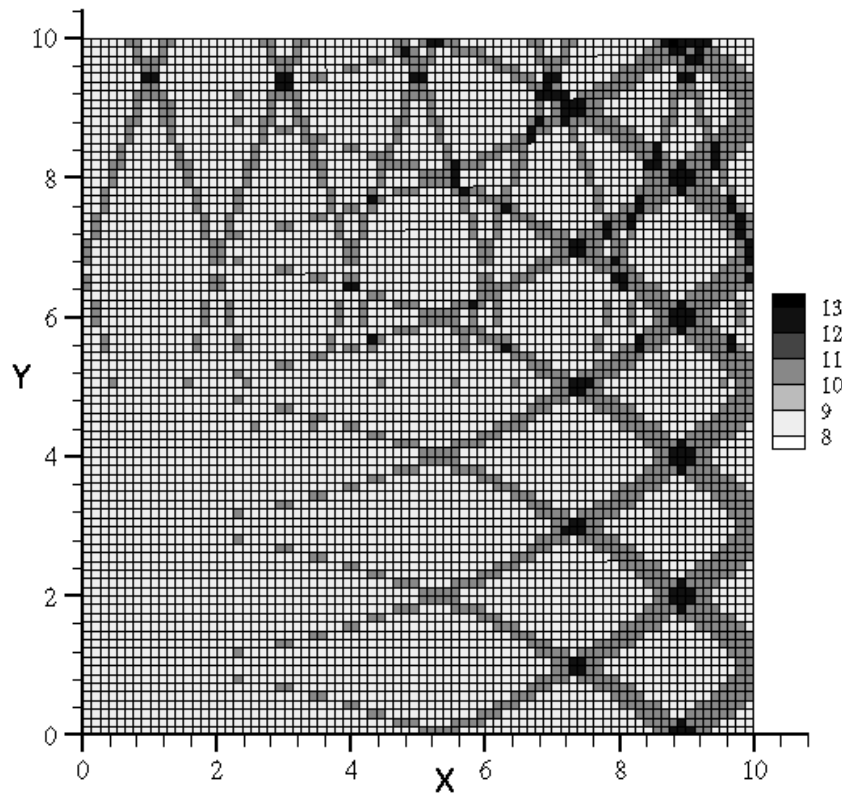


Figure 5.5 Thickness of  $[[90 \langle 0|\pm 25 \rangle] / [0 \langle 0|\pm 45 \rangle]]_s$  Laminate

More elements were used to produce better resolution. As the number of layers increases it can become more difficult to distinguish one layer from the next. The overlap regions also become very complex which will lead to unusual stress distributions.

#### 5.4 Parallel-Fiber Methods and Shifted-Fiber Methods

Waldhart [11] examined the difference between two different methods of tow path placement. The two methods investigated were the shifted path method and parallel path method. As mentioned earlier, the shifted path method creates additional paths by shifting the entire reference path a set distance. The parallel path method creates additional paths by forming paths parallel to the reference

path. While the shifted path method can and usually will result in some thickness variation, the parallel path method cannot have any thickness variation. Parallel paths, by definition, can never cross each other.

While this research has concentrated on the shifted path method it is important to realize that the method used for creating adjacent paths is really a combination of the parallel path method and the shifted path method. The reference tow path represents a set of parallel fibers. This set of parallel fibers is then shifted to create additional paths.

The method used In this research, to model variable-stiffness laminates can also be used to create fully parallel path models or to create nearly continuous shifted path models. Parallel paths can be created by increasing the tow width to a size larger than the panel dimensions and using a shift distance such that only one path will cross the panel dimensions. An example of a parallel-path layer is shown in Figure 5.6. At point A the orientation angle is defined as  $0^\circ$ , and at point B the orientation angle is  $45^\circ$ . All other points in the panel are defined such that they are parallel to the reference path.

On the other hand, if the tow width is defined such that it will only be a few elements wide and the shift distance is decreased such that the model can be filled with elements it is possible to get purely shifted fiber results. It is important to fix the thickness to a single layer, so there is no variation in thickness due to overlap. An example of such a flat shifted laminate is shown in Figure 5.7. In this case, the orientation angle is only a function of position along the x axis.

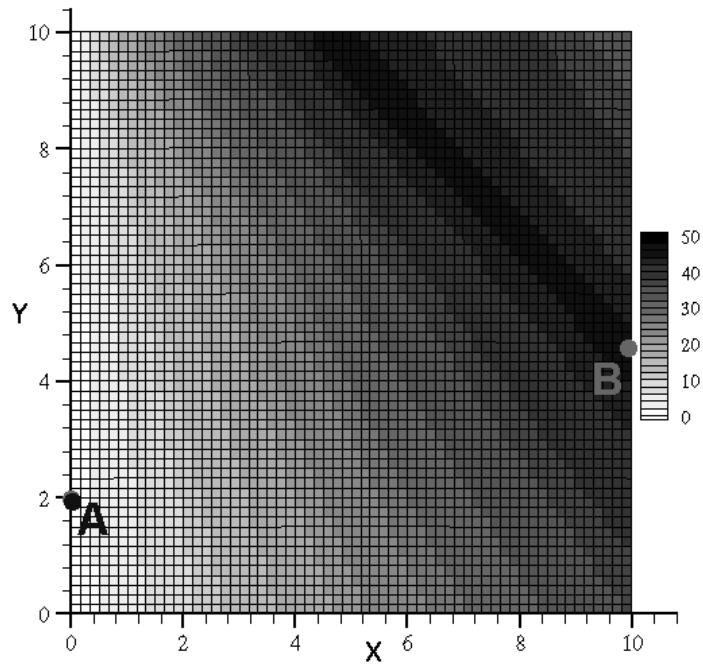


Figure 5.6 Orientation angle variation in a  $[\pm 0|45]_s$  layer of parallel tow paths

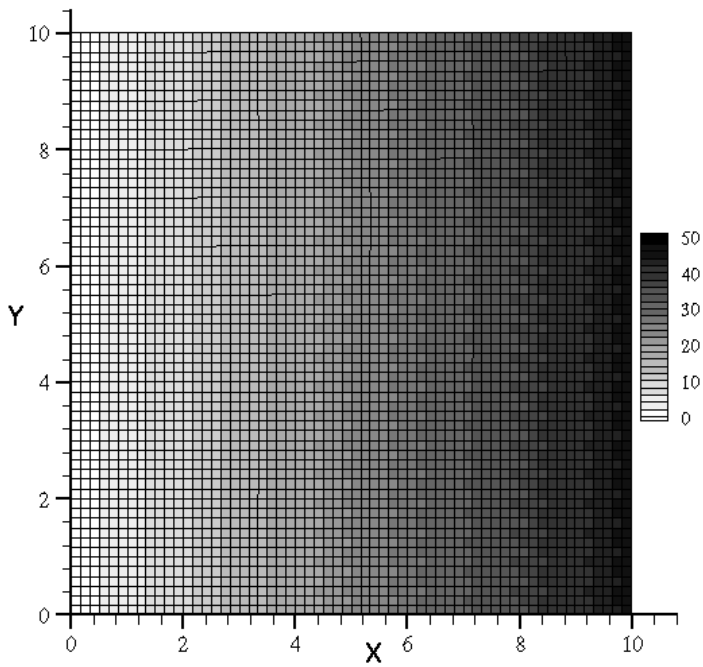


Figure 5.7 Orientation angle variation in a  $[\pm 0|45]_s$  layer of flat-shifted paths

The  $N_x$  distributions differ quite radically. The force-resultant distribution, for the flat shifted-path laminate, is very similar to the results shown previously for the  $[\pm\langle 0|45\rangle]_s$  laminate. The distribution is relatively consistent except for a small region of higher axial force in the upper left-hand corner. The parallel-path results are more complex. There is also a region of higher axial force in the upper right-hand corner. Additionally, there is more change in the force resultants, from point to point, in the parallel-path laminate. The  $N_x$  results, for the parallel-path laminate and the shifted-path laminate, are shown in Figures 5.8 and 5.9, respectively.

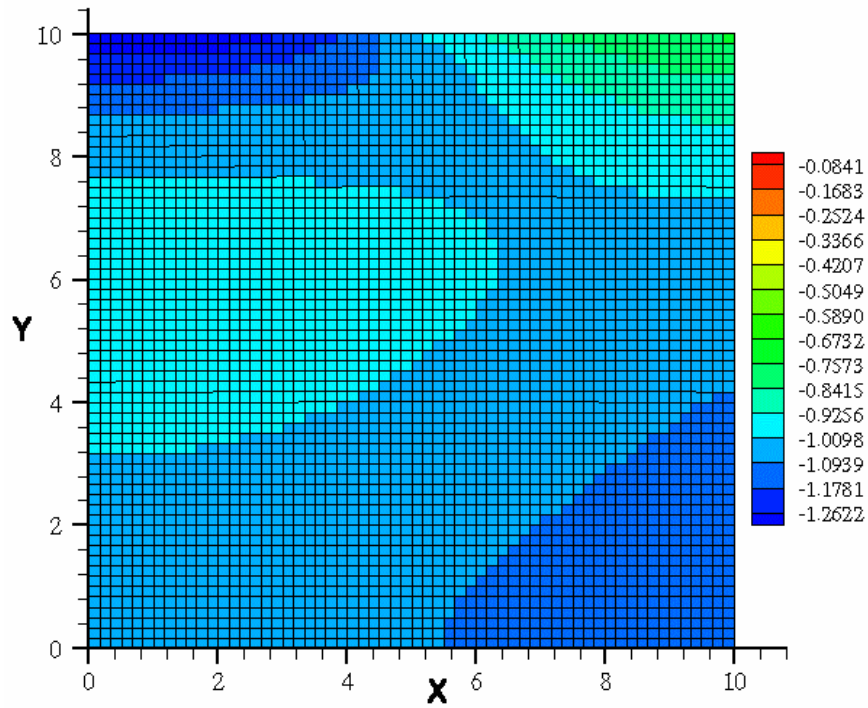


Figure 5.8  $N_x$  distribution for parallel  $[\pm(0)45]_s$  laminate

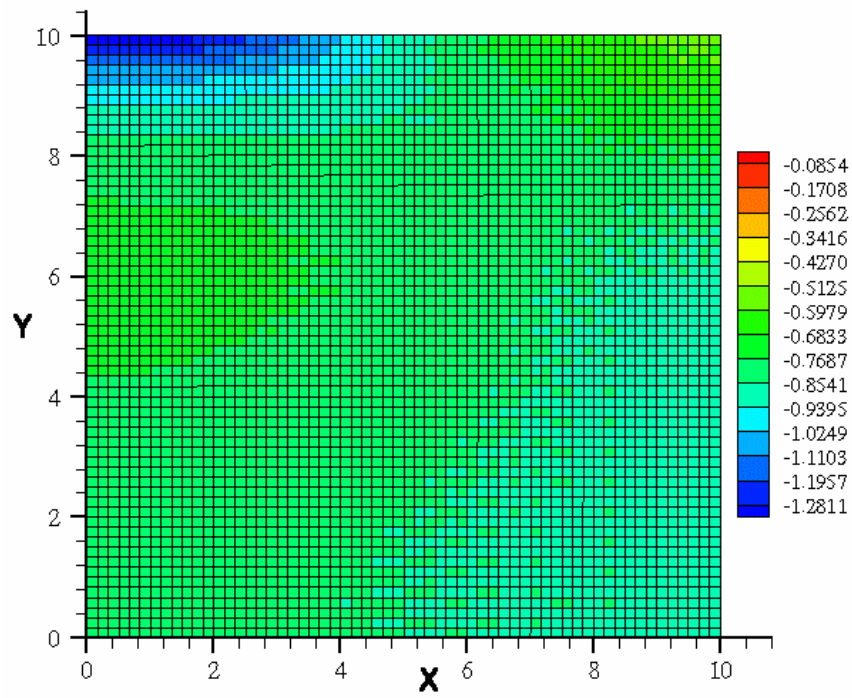


Figure 5.9  $N_x$  distribution for flat-shifted  $[\pm(0)45]_s$  laminate



The total force that results from a displacement  $u_0 = -0.02$ , for the shifted fiber laminate is -3886.32 while for the parallel fiber laminate the force resultant is -4841.23. It is also important to note that, the failure index for the parallel fiber laminate is 30% lower than that of the shifted fiber laminate.

## Chapter 6

### Concluding Remarks

Tow-placement machines have made it possible to economically manufacture composite structures, which have spatially varying fiber orientation and thickness. When curvilinear paths are shifted in a plane to create a variable-stiffness laminate, there will be overlaps or gaps between adjacent tow paths, causing a change in thickness, and the fiber-orientation angle will depend on the position of a point within a specific tow path. This research has developed the tools necessary to generate a finite element model to accurately treat thickness variation, due to overlaps, throughout the laminate and the orientation angle changes within each tow path, for a tow-placed shifted-path laminate. Tow-placed variable-stiffness laminates with gaps are not addressed in this research.

The finite element modeling method developed in this research, creates a discretized reference path using a Golden Section search to determine the distance between the center of each element and the centerline of the reference tow path, and the orientation angle at the center of each element. Once the discretized reference path is created, it can be shifted to create additional tow paths to create a single variable-stiffness lamina. The thickness and the orientation angle of the elements that make up the finite element model of the panel are defined from these data. The data necessary to model different lamina are then combined to form a variable-stiffness laminate.

The GENESIS finite element analysis and design package was used to determine the response of various variable stiffness configurations. The results of the analyses were used to determine the overall stiffness of the panel. This stiffness can be used as an objective function that can be maximized in a design

optimization problem. Additionally, the failure index of each element can be calculated, using one of many common failure criteria, to determine the possibility of failure. The maximum failure index can then be used to determine the maximum load that can be applied to the variable stiffness panel before failure. The results of this research show how this process can be used to determine the failure load of a  $[\pm(0|45)]_s$  laminate.

Additional finite element results were compared to closed-form analytical results from previous research. The finite element results show very similar trends to the previous research and results that closely match the previous results in the nominal thickness areas. Expected differences occurred between the two models where the finite element model, due to overlap of tow paths, had increased thicknesses, that were not addressed in the previous research.

Finally, additional capabilities of the finite element modeling program were demonstrated. Examples were given that showed how the path-orientation angles could be changed, how the shift distance could affect laminate thickness, how various variable stiffness configurations could be combined and how the program could be used to create both parallel-fiber laminae and continuous shifted-fiber laminae.

The finite element modeling tool presented in this research, allows for a wide range of designs to be quickly and accurately generated. In addition, it provides a resource to obtain results in future research of tow-placed variable-stiffness laminates. When used in conjunction with the GENESIS finite element analysis and design software, it provides a wealth of information and insight into some of the complex mechanisms underlying the response of variable-stiffness laminates, such as the interaction between thickness variation and fiber-orientation angle variation or the effects of geometry changes on stress levels.

The primary goal of this work was to create and validate a tool that could be used in future research. The methods developed provide an efficient and accurate tool that can be used to model the complex geometry of variable-stiffness laminates. Most of the previous research of variable-stiffness laminates has acknowledged their potential to raise the buckling load of laminated panel.

In this area, the tow-placed variable-stiffness laminates developed in this research may show the most potential benefit. The overlap regions could act as built-in stiffeners that raise the buckling load. Currently, GENESIS does not have the capability to perform buckling-load analysis, but future versions of the software are expected to have this capability though.

The need for more experimental research of tow-placed variable-stiffness laminates is also necessary to validate the theoretical models. Manufacturing of laminates similar to those modeled in this research is necessary to determine how tow-placement machines perform on such complex parts. Experimental research could also give more insight into the effects of potentially dramatic changes in thickness. Similarly, the failure behavior of tow-placed variable-stiffness composite laminates should be measured and compared with theoretical predictions.

Another goal of this research was to show how the information static from analysis could be used in the formulation of structural optimization problems. Currently, the finite element model can be used to determine the stiffness for a variety of variable-stiffness configurations. This stiffness can be maximized using the failure index information provided by the GENESIS analysis. The function could be sampled at many points using various design variables and a response surface could be created and searched for optimal values of the design variables.

As mentioned earlier, GENESIS can also be used to perform finite element optimization by many different methods. Use of this finite element model in GENESIS could provide a very powerful tool for structural optimization and design of tow-placed variable-stiffness laminates.

Another area of potential research is in determining the thermal and vibrational response of tow-placed variable-stiffness laminates. GENESIS provides tools that can be used in these types of analyses. Variable-stiffness laminates could be used to direct heat conduction in a manner similar to the way they can be used to redistribute loads. Leissa and Martin [1] demonstrated that variable fiber spacing could be used to raise or lower the fundamental frequency

of a laminate. The complex geometry of tow-placed variable-stiffness laminates might have a similar effect on raising or lowering the fundamental frequency.

## Bibliography

- [1] W. Leissa and A. F. Martin, "Vibration and Buckling of Rectangular Composite Plates with Variable Fiber Spacing," *Composite Structures*, Vol. 14, No. 4, 1990, pp. 339-357.
- [2] M. T. DiNardo and P. A. Lagace, "Buckling and Postbuckling of Laminated Composites with Ply Dropoffs," *AIAA Journal*, Vol. 27 No. 10, October 1989, pp. 1392-1398.
- [3] M. W. Hyer and H.H. Lee, "The Use of Curvilinear-fiber Format to Improve Buckling Resistance of Composite Plates with Central Circular Holes." *Composite Structures*, Vol. 18, No. 3, 1991, pp. 239-261.
- [4] D. O. Evans, M. M. Vanigila, and P.C. Hopkins, "Fiber Placement Process Study," *34<sup>th</sup> International SAMPE Symposium*. Vol. 34, Book 2, May 1989, pp. 1822-1833.
- [5] J. R. Barth, "Fabrication of Complex Composite Structures Using Advanced Fiber Placement Technology," *35th International SAMPE Symposium*, Vol. 35, Book 1, April 1990, pp. 710-720.
- [6] F. Bullock, S. Kowalski, and R. Young, "Automated Prepreg Tow-Placement For Composite Structures," *35th International SAMPE Symposium*, Vol. 35, Book 1, April 1990, pp. 734-743.
- [7] M. L. Enders and P. C. Hopkins, "Developments in the Fiber Placement Process," *35th International SAMPE Symposium*, Vol. 36, Book 1, April 1991, pp. 778-790.
- [8] S. Nagendra, S. Kodiyalam, J.E. Davis and V.N. Parthasarathy, "Optimization of Tow Fiber Paths for Composite Design," *Proceedings of the AIAA/ASME/ASCE/AHS/ASC 36<sup>th</sup> SDM Conference*, April 10-13, 1995, New Orleans, LA, pp. 1031-1041.

- [9] Z. Gürdal and R. Olmedo, "In-Plane Response of Laminates with Spatially Varying Fiber Orientations: Variable Stiffness Concept," *AIAA Journal*, Vol. 31, No. 4, April 1993, pp. 751-758.
- [10] Z. Gürdal, "Design of Variable Stiffness Panels," *Proceedings of the 10<sup>th</sup> DOD/NASA/FAA Conference on Fibrous Composites in Structural Design*, 1994, Vol. 1, pp. 1-14.
- [11] C. Waldhart, *Analysis of Tow-Placed Variable-Stiffness Laminates*, Virginia Polytechnic Institute and State University. June, 1996.
- [12] R.T. Haftka and Z. Gürdal, *Elements of Structural Optimization*, Kluwer Academic Publishers, Boston, 1992.
- [13] *GENSIS User Manual*, VMA Engineering. Colorado Springs, November 1998.
- [14] J.S. Arora, *Introduction to Engineering Optimization*, McGraw-Hill, Inc., New York, 1989.

## **Appendix A: Layer\_Def.txt**



```

60          Number of Elements
20.         Width of Plate(a)
20.         Height of Plate(b)
2.0        Width of Path
2.0        Path Shift Distance
0.0        Path Shift Angle(Lambda)  LAMBDA WILL DEFAULT TO -PHI
2          Number of Layers(Half for Symmetric Laminate)
1          1=symmetric(define half)   0=non-symm(define full)
21000000.  E1 composite
1400000.   E2 composite
0.34      nul2 composite
800000.   G12 composite
0.0055    Layer thickness
.000001   Thermal expansion of fibers
.000001   Thermal expansion of matrix
HILL      Failure Theory(STRN,HILL,HOFF,TSAI)
50000000. Fiber Tensile Failure(XT)
-50000000. Fiber Compression Failure(XC)
50000000. Matrix Tensile Failure(YT)
-50000000. Matrix Compression Failure(YC)
50000000. Allowable Shear or Von Mises(S)
0.0       Tsai-Wu Interaction term
-0.1      X Displacement
0.0       Y Displacement
0         Case I (0) | Case II (1) | Case III (2)
1         Variable thickness?  1=Yes 0=No

```

```

Layer Name Phi T0   T1
NUM1 0.0 45.0 -45.0
NUM2 0.0 -45.0 45.0

```

All of the layer names must be different

```

Case I - X-displacement prescribed, top edge free
Case II - X-displacement and Y-displacement prescribed, no free edges
Case III - Y-displacement prescribed, right edge free

```

## Appendix B: RT.f90

```

MODULE GLOBALS
  REAL A !LAMINATE DIMENSION IN X-DIRECTION
  REAL B !LAMINATE DIMENSION IN Y-DIRECTION
  REAL HW !TOW WIDTH
  REAL T0 !orientation ANGLE @ R=0
  REAL T1 !orientation ANGLE @ LOCL
  REAL PHI !ROTATION OF R-S COOR WRT X-Y
  REAL LOCL !CHARACTERISTIC DISTANCE ROTATED PHI
  REAL ORIGIN(2) !SHIFT CENTER OF TOW FROM 0,0 IN XY
  REAL LAMBDA !ANGLE OF SHIFT OFF R DIRECTION
  REAL WIDTH
  DOUBLE PRECISION :: PI=3.141592653589793
END MODULE GLOBALS

PROGRAM THICK

  USE GLOBALS
  REAL POINTX, POINTY !POINT WHERE THICKNESS IS TO BE EVALUATED
  INTEGER I,J,K,L !Counter for number of tows crossing point (x,y)
  REAL SHFT !Distance of shift
  REAL R !x' distance in rotated coordinate system
  REAL MIN_DIST !Minimum distance from golden section search
  LOGICAL REP_CHECK,REP2_CHECK !False when pattern begins to repeat
  CHARACTER(1) YORN !Choice to continue
  INTEGER PLATE(100,100) !Array to measure thickness across entire plate
  INTEGER PLATE_TEMP(100,100) !Used to transform plate for phi=90
  REAL ANGLE !Fiber orientation angle from golden section
  REAL ORNT(100,100,2) !Fiber orientations throughout plate
  REAL ORNT_TEMP(100,100,2) !Temporary orientations for phi=90
  INTEGER PIDX(100,100,2) !Thickness Index
  INTEGER PIDX_TEMP(100,100,2) !Temp thickness Index for phi=90
  REAL PATH_ORNT(500,500) !Fiber orientations throughout path
  INTEGER PATH(500,500) !Array containing thickness data for typical path
  INTEGER M,N !Loop counters
  INTEGER THICKNESS !Thickness of laminate at a point
  REAL CLOSEST !Stops calculations after value is found
  REAL XMAX,XMIN,XLENGTH !Boundary and element defining parameters
  REAL ELEM_SIZE !Size of elements
  INTEGER PATH_NUM !Path number to use as Reference path
  REAL YMAX,YMIN,YLENGTH !Parameters for establishing y elements
  INTEGER Y_ELEM,X_ELEM !Elements in x&y direction
  INTEGER X_SHFT,Y_SHFT !Number of elements to shift path
  LOGICAL PLATE_CHECK !Check if path is on plate
  INTEGER PLATE_MAX !Size for full size plate
  INTEGER Y_DIFF,Y_LEFT,Y_RIGHT !Parameters to determine how to connect path
  INTEGER ADD_X !Additional elements to create a full length path
  LOGICAL STOPPER !Stops Measuring Y_DIFF
  LOGICAL BOUND_CHK !Makes sure that path template is within bounds
  INTEGER Q1,Q2 !Path coordinate simplifications
  INTEGER BUMP !Correction for left side path continuation
  INTEGER X_NODES,Y_NODES !Number of nodes in x and y directions
  INTEGER PATH_Y_ELEM !Number of elements in single path
  INTEGER ICK !Index for cycling through each layer
  INTEGER G1,G2,G3,G4 !Nodes of elements
  REAL LTHK !Thickness of a single layer

  TYPE LAYER
    INTEGER ELEMX
    REAL WIDTHA
    REAL HEIGHTB
    REAL PATHWIDTH
    REAL PATHSHIFT
    REAL PATHSHFTANGLE
    INTEGER NUM_LAYER
    REAL E1_COMP
    REAL E2_COMP
    REAL NU12_COMP
    REAL G12_COMP
    REAL LAY_THK
    INTEGER SYMMETRIC

```

```

REAL THERMX
REAL THERMY
CHARACTER*4 FAILURE
REAL XT
REAL XC
REAL YT
REAL YC
REAL SHEAR
REAL TSAIWU
REAL X_DISP
REAL Y_DISP
INTEGER CASENUM
INTEGER VARTHICK
CHARACTER*20 IDX(8)
REAL PHIX(20)
REAL T0X(20)
REAL T1X(20)

END TYPE

TYPE(LAYER) LAYERS

OPEN(96,FILE='LAYER_DEF.TXT')
READ(96,*)LAYERS%ELEMX
READ(96,*)LAYERS%WIDTHA
READ(96,*)LAYERS%HEIGHTB
READ(96,*)LAYERS%PATHWIDTH
READ(96,*)LAYERS%PATHSHIFT
READ(96,*)LAYERS%PATHSHFTANGLE
READ(96,*)LAYERS%NUM_LAYER
READ(96,*)LAYERS%SYMMETRIC
READ(96,*)LAYERS%E1_COMP
READ(96,*)LAYERS%E2_COMP
READ(96,*)LAYERS%NU12_COMP
READ(96,*)LAYERS%G12_COMP
READ(96,*)LAYERS%LAY_THK
READ(96,*)LAYERS%THERMX
READ(96,*)LAYERS%THERMY
READ(96,*)LAYERS%FAILURE
READ(96,*)LAYERS%XT
READ(96,*)LAYERS%XC
READ(96,*)LAYERS%YT
READ(96,*)LAYERS%YC
READ(96,*)LAYERS%SHEAR
READ(96,*)LAYERS%TSAIWU
READ(96,*)LAYERS%X_DISP
READ(96,*)LAYERS%Y_DISP
READ(96,*)LAYERS%CASENUM
READ(96,*)LAYERS%VARTHICK
READ(96,*)
READ(96,*)

HW=LAYERS%PATHWIDTH
A=LAYERS%WIDTHA
B=LAYERS%HEIGHTB
LOC1=A/2.0
WIDTH=0
ORIGIN(1)=0
ORIGIN(2)=0
SHFT=LAYERS%PATHSHIFT
LTHK=LAYERS%LAY_THK

X_ELEM=LAYERS%ELEMX
X_NODES=X_ELEM+1
ELEM_SIZE=A/2.0/X_ELEM
Y_ELEM=ANINT(B/2.0/ELEM_SIZE)
Y_NODES=Y_ELEM+1

DO 30 ICK=1,LAYERS%NUM_LAYER !Cycles through each layer of the laminate

READ(96,*)LAYERS%IDX(ICK),LAYERS%PHIX(ICK),LAYERS%T0X(ICK),LAYERS%T1X(ICK)

```

```

LAYERS%IDX(ICK)=TRIM(LAYERS%IDX(ICK))
IF(LAYERS%PHIX(ICK).EQ.90)THEN
  PHI=0.0
ELSE
  PHI=LAYERS%PHIX(ICK)
ENDIF
T0=LAYERS%T0X(ICK)
T1=LAYERS%T1X(ICK)
LAMBDA=-PHI
PLATE=0

!Decides how many paths and which ones are checked
!For shifted laminates it is only necessary to use 1 path
  PATH_NUM=1
  PATH_ORNT=0
  PATH=0
  PLATE=0
  ORNT=0
  BOUND_CHK=.TRUE.

  XMAX=X(2*LOC1,PATH_NUM*SHFT)
  XMIN=A/2.0
  XLENGTH=XMAX-XMIN
  ADD_X=ANINT(XLENGTH/ELEM_SIZE)
!This checks to insure that reference path doesn't run out of template area
  DO WHILE(BOUND_CHK)
    BOUND_CHK=.FALSE.
    J=1
    I=1
    DO WHILE(I.LE.X_NODES+ADD_X)
      CALL GOLDEN((I-0.5)*ELEM_SIZE,(J-
0.5)*ELEM_SIZE/2.0,PATH_NUM,SHFT,MIN_DIST,ANGLE)
      IF(MIN_DIST.LE.HW/2.0)THEN
        PATH_NUM=PATH_NUM+1
        BOUND_CHK=.TRUE.
        PATH=0
        PATH_ORNT=0
        I=X_NODES+ADD_X+100!Resets loop
      ENDIF
      I=I+1
    ENDDO
  ENDDO

  PATH_Y_ELEM=1
  I=X_NODES+ADD_X
  DO WHILE(I.GT.0)
    REP_CHECK=.TRUE.
    REP2_CHECK=.TRUE.
    J=2
    DO WHILE(REP_CHECK)
      K=0

      CALL GOLDEN((I-0.5)*ELEM_SIZE,(J-0.5)*ELEM_SIZE,PATH_NUM,SHFT,MIN_DIST,ANGLE)

      IF(MIN_DIST.LE.HW/2.0)THEN
        K=K+1
        PATH(I,J)=K
        PATH_ORNT(I,J)=ANGLE
      ENDIF

      J=J+1

      IF(J.GT.500)THEN
        REP_CHECK=.FALSE.
        WRITE(6,*)'Possible Anomaly in column -',I !checks for incomplete paths
      ENDIF
      IF(PATH(I,J-1).EQ.0.AND.PATH(I,J-2).EQ.1)THEN !If Phi + T1 > 90 won't work
        REP_CHECK=.FALSE.

```

```

        IF (J.GT.PATH_Y_ELEM) THEN
            PATH_Y_ELEM=J
            IF (PATH_Y_ELEM.GT.500) THEN
                PATH_Y_ELEM=500
            ENDIF
        ENDIF
    ENDDO
    I=I-1
ENDDO

!Calculations reduced by stopping after the single thickness region is crossed
!Doesn't allow for Phi + T1 >90
65     FORMAT(F10.6,1X,F10.6,1X,I2,1X,F10.3)

    OPEN(99,FILE='SINGLE_PATH.DAT')!Writes data file for single path and angle

    WRITE(99,*)'TITLE = "Single Path Data"'
    WRITE(99,*)'VARIABLES = "X", "Y", "Thickness","Angle"'
    WRITE(99,*)'ZONE I=',X_NODES+ADD_X+1,' J=',PATH_Y_ELEM+1,' F=POINT'
    WRITE(99,*)

    DO 17 M=1,PATH_Y_ELEM+1
        DO 18 N=1,X_NODES+ADD_X+1
            IF(N.LT.X_NODES+ADD_X.AND.M.LT.PATH_Y_ELEM) THEN
                IF (PATH_ORNT(N,M).NE.0) THEN
                    WRITE(99,65)(N-1)*ELEM_SIZE,(M-1)*ELEM_SIZE,1,PATH_ORNT(N,M)
                ELSE
                    WRITE(99,65)(N-1)*ELEM_SIZE,(M-1)*ELEM_SIZE,0,-1000.0
                ENDIF
            ELSE
                WRITE(99,65)(N-1)*ELEM_SIZE,(M-1)*ELEM_SIZE,0,-1000.0
            ENDIF
        CONTINUE
    CONTINUE
    CLOSE(99)

    WRITE(6,*)'Single Path Generated'

    PLATE_CHECK=.TRUE.
    M=-INT(PATH_Y_ELEM*ELEM_SIZE/SHFT)-10

    BUMP=ANINT(TAN(RADIAN(PHI+T0)))

    DO WHILE(PLATE_CHECK)
! Discretizes the shift into a number of x and y points
        X_SHFT=ANINT(X(0,M*SHFT)/ELEM_SIZE)
        Y_SHFT=ANINT(Y(0,M*SHFT)/ELEM_SIZE)
        DO 15 I=1,X_NODES+ADD_X
            DO 16 J=1,PATH_Y_ELEM+1

IF((I+X_SHFT.GT.0.AND.J+Y_SHFT.GT.0).AND.(I+X_SHFT.LE.X_ELEM.AND.J+Y_SHFT.LE.Y_ELEM)) THEN
                PLATE(I+X_SHFT,J+Y_SHFT)=PLATE(I+X_SHFT,J+Y_SHFT)+PATH(I,J)
                IF (PLATE(I+X_SHFT,J+Y_SHFT).EQ.1.AND.PATH(I,J).EQ.1) THEN
                    ORNT(I+X_SHFT,J+Y_SHFT,1)=PATH_ORNT(I,J)
                    PIDX(I+X_SHFT,J+Y_SHFT,1)=M
                ELSEIF (PLATE(I+X_SHFT,J+Y_SHFT).EQ.2.AND.PATH(I,J).EQ.1) THEN
                    PIDX(I+X_SHFT,J+Y_SHFT,2)=M
                    ORNT(I+X_SHFT,J+Y_SHFT,2)=PATH_ORNT(I,J)
                ENDIF
                !If path points plus shift are inside panel they are added to panel
            ENDIF

                !Adds points from paths coming from left IF LAMBDA IS NOT -PHI
                Q1=I+X_SHFT-(X_NODES+ADD_X)
                Q2=J+Y_SHFT-Y_DIFF-BUMP
                IF(Q1.GT.0.AND.Q2.GT.0) THEN
                    PLATE(Q1,Q2)=PLATE(Q1,Q2)+PATH(I,J)
                    IF (PLATE(Q1,Q2).EQ.1) THEN
                        ORNT(Q1,Q2,1)=PATH_ORNT(I,J)
                    ENDIF
                ENDIF
            ENDDO
        ENDDO
    ENDWHILE

```

```

        PIDX(Q1,Q2,1)=M
        ELSEIF(PLATE(Q1,Q2).EQ.2)THEN
            ORNT(Q1,Q2,2)=PATH_ORNT(I,J)
            PIDX(Q1,Q2,2)=M
        ENDIF
    ENDIF
16     CONTINUE
15     CONTINUE
        M=M+1
        IF(M*SHFT-(PATH_Y_ELEM-1).GT.B/2.0)THEN !Shifted outside of panel
            PLATE_CHECK=.FALSE.
        ENDIF

ENDDO

IF(LAYERS%PHIX(ICK).EQ.90)THEN !Transforms matrix of angles/thickness if phi=90
    DO 666 I=1,Y_ELEM
        DO 667 J=1,X_ELEM
            ORNT_TEMP(I,J,1)=ORNT(J,I,1)+90.0
            ORNT_TEMP(I,J,2)=ORNT(J,I,2)+90.0
            PLATE_TEMP(I,J)=PLATE(J,I)
            PIDX_TEMP(I,J,1)=PIDX(J,I,1)
            PIDX_TEMP(I,J,2)=PIDX(J,I,2)
667     CONTINUE
666     CONTINUE

        DO 668 I=1,X_ELEM
            DO 669 J=1,Y_ELEM
                ORNT(I,J,1)=ORNT_TEMP(I,J,1)
                ORNT(I,J,2)=ORNT_TEMP(I,J,2)
                PLATE(I,J)=PLATE_TEMP(I,J)
                PIDX(I,J,1)=PIDX_TEMP(I,J,1)
                PIDX(I,J,2)=PIDX_TEMP(I,J,2)
669     CONTINUE
668     CONTINUE
        ENDIF

!This builds the layer definition files that will be used to
!generate GENESIS input file
        OPEN(95,FILE=LAYERS%IDX(ICK)//'.ILD')
        WRITE(95,*)'Number of Elements -',X_ELEM
        WRITE(95,*)'HW -',HW
        WRITE(95,*)'Shift',SHFT
        K=1
49     FORMAT(A8,I8,I8,I8,I8,I8,I8,I2,1X,I2,1X,I4,1X,F8.5,1X,F8.4,1X,I2,1X,I4,1X,F8.5,1X,
F8.4)
        DO 31 J=1,Y_ELEM
            DO 32 I=1,X_ELEM
                G1=(J-1)*Y_NODES+I
                G2=(J-1)*Y_NODES+I+1
                G3=J*Y_NODES+I+1
                G4=J*Y_NODES+I
                IF(PLATE(I,J).EQ.1)THEN
                    WRITE(95,49)'CQUAD4 ',K,(J-
1)*Y_ELEM+I,G1,G2,G3,G4,1,1,PIDX(I,J,1),LTHK,ORNT(I,J,1)
                    ELSEIF(PLATE(I,J).EQ.2.AND.LAYERS%VARTHICK.NE.0)THEN
                        WRITE(95,49)'CQUAD4 ',K,(J-
1)*Y_ELEM+I,G1,G2,G3,G4,2,1,PIDX(I,J,1),LTHK,ORNT(I,J,1),1,PIDX(I,J,2),LTHK,ORNT(I,J,2)
                    ELSEIF(PLATE(I,J).LT.1)THEN !ASSUMES THAT THERE ARE NO 0 THICKNESS REGIONS
                        PLATE(I,J)=1
                        WRITE(95,49)'CQUAD4 ',K,(J-1)*Y_ELEM+I,G1,G2,G3,G4,1,1,PIDX(I,J,1),LTHK,ORNT(I-
1,J,1)
                    ELSEIF(PLATE(I,J).GT.2.AND.LAYERS%VARTHICK.NE.0)THEN !NO 3+ THICK REGIONS
                        PLATE(I,J)=2
                        WRITE(95,49)'CQUAD4 ',K,(J-
1)*Y_ELEM+I,G1,G2,G3,G4,2,1,PIDX(I,J,1),LTHK,ORNT(I,J,1),1,PIDX(I,J,2),LTHK,ORNT(I,J,2)
                    ELSEIF(PLATE(I,J).GE.2.AND.LAYERS%VARTHICK.EQ.0)THEN ! NO THICKNESS VARY
                        PLATE(I,J)=1
                        WRITE(95,49)'CQUAD4 ',K,(J-
1)*Y_ELEM+I,G1,G2,G3,G4,1,1,PIDX(I,J,1),LTHK,ORNT(I,J,1)

```

```

                ENDIF
                K=K+1
32          CONTINUE
31          CONTINUE
            CLOSE(95)
30          CONTINUE
            CLOSE(96)

            CALL GENESIS_INPUT(PLATE,ORNT,X_ELEM,Y_ELEM,X_NODES,Y_NODES,ELEM_SIZE,LAYERS)
            END

SUBROUTINE GOLDEN(POINTX,POINTY,PATH_INDEX,SHFT,MIN_DIST,ANGLE)
!*****
!*
!*   This subroutine uses a golden section search to determine
!*   the minimum distance between the specified point (x,y) and
!*   tow path I.  When this distance converges the minimum distance is
!*   returned to be compared to the tow width.
!*
!*****
USE GLOBALS
REAL SHFT           !Distance of shift
REAL R              !x' distance in rotated coordinate system
REAL POINTX,POINTY !minimize distance to this point
REAL RLOW,RHIGH    !Brackets containing minimum
REAL XA,YA         !Coordinates of point A
REAL XB,YB         !Coordinates of point B
REAL RA,RB         !XA and XB in R-S coord.
REAL,PARAMETER :: TAU=0.618033988749894902
REAL INTERVAL      !Total bracketed distance
LOGICAL CONVERGE   !Convergence?
REAL LAST_DIST     !Last calculated distance
REAL DISTANCE_A,DISTANCE_B !Distances between (x,y) and points A & B
DOUBLE PRECISION EPS !Convergence criteria epsilon
INTEGER PATH_INDEX !which number path is being checked
REAL MIN_DIST      !The minimum distance
REAL ANGLE         !Orientation angle of fiber at (x,y)

CONVERGE=.TRUE.
EPS=0.001

! BRACKET MINIMUM AND INITIALIZE VALUES
RLOW=-A/(2*COS(RADIAN(PHI)))*2
RHIGH=A/(2*COS(RADIAN(PHI)))*2
INTERVAL=RHIGH-RLOW
RA=RHIGH-TAU*INTERVAL
RB=RLOW+TAU*INTERVAL
LAST_DIST=1E6

XA=X(RA,SHFT*PATH_INDEX)
YA=Y(RA,SHFT*PATH_INDEX)
XB=X(RB,SHFT*PATH_INDEX)
YB=Y(RB,SHFT*PATH_INDEX)

DISTANCE_A=DISTANCE(POINTX,POINTY,XA,YA)
DISTANCE_B=DISTANCE(POINTX,POINTY,XB,YB)

DO WHILE(CONVERGE)
    IF(DISTANCE_B.GT.DISTANCE_A)THEN
        IF((INTERVAL).LT.EPS)THEN
            CONVERGE=.FALSE.
        ENDIF
        LAST_DIST=DISTANCE_A
        RHIGH=RB
        RB=RA
        DISTANCE_B=DISTANCE_A
        INTERVAL=RHIGH-RLOW
        RA=RHIGH-TAU*INTERVAL
        XA=X(RA,SHFT*PATH_INDEX)
        YA=Y(RA,SHFT*PATH_INDEX)
    ENDIF
END DO

```



```

        DISTANCE_A=DISTANCE ( POINTX , POINTY , XA , YA )
        R=RA
    ELSE
        IF ( ( INTERVAL ) .LT. EPS ) THEN
            CONVERGE= .FALSE.
        ENDIF
        LAST_DIST=DISTANCE_B
        RLOW=RA
        RA=RB
        DISTANCE_A=DISTANCE_B
        INTERVAL=RHIGH-RLOW
        RB=RLOW+TAU*INTERVAL
        XB=X ( RB , SHFT*PATH_INDEX )
        YB=Y ( RB , SHFT*PATH_INDEX )
        DISTANCE_B=DISTANCE ( POINTX , POINTY , XB , YB )
        R=RB
    ENDIF
ENDDO
MIN_DIST=LAST_DIST
ANGLE=180.0*THETAXY(R)/PI
END

REAL FUNCTION DISTANCE(X1,Y1,X2,Y2)
!Determines distance between a set of points
    REAL X1,X2,Y1,Y2
    DISTANCE=SQRT( (X1-X2)**2+(Y1-Y2)**2)
    RETURN
END

REAL FUNCTION RADIAN(ANGLE)
!Changes degrees to radians
    USE GLOBALS
    REAL ANGLE

    RADIAN=ANGLE*PI/180
    RETURN
END FUNCTION RADIAN

REAL FUNCTION PSI(R)

    USE GLOBALS
    REAL R
    INTEGER K
    REAL ADD

    IF (T0.EQ.T1) THEN
        PSI=R*TAN(RADIAN(T0))
    ELSE
        K=CEILING(R/LOC1)
        ADD=LOC1*LOG(COS(RADIAN(T1))/COS(RADIAN(T0)))/RADIAN(T0-T1)
        IF(MOD(K,2).EQ.0) THEN
            PSI=(K-1)*ADD-LOC1*LOG(COS(THETA(R))/COS(RADIAN(T1)))/RADIAN(T0-T1)
        ELSE
            PSI=(K-1)*ADD+LOC1*LOG(COS(THETA(R))/COS(RADIAN(T0)))/RADIAN(T0-T1)
        ENDIF
    ENDIF
    RETURN
END FUNCTION PSI

REAL FUNCTION THETA(R)
!Determines theta in rotated RS coordinates
    USE GLOBALS
    REAL R
    INTEGER K

    K=CEILING(R/LOC1)

    IF(MOD(K,2).EQ.0) THEN
        THETA=(RADIAN(T0-T1)*(R-(K-1)*LOC1))/LOC1+RADIAN(T1)
    ELSE
        THETA=(RADIAN(T1-T0)*(R-(K-1)*LOC1))/LOC1+RADIAN(T0)
    ENDIF
END FUNCTION THETA

```

```

        ENDIF
        RETURN
    END FUNCTION THETA

REAL FUNCTION THETAXY(R)
!Determines theta in XY coordinates
    USE GLOBALS
    REAL SHFT                !DISTANCE OF SHIFT
    REAL R                   !RADIAL DISTANCE ALONG ROTATED COOR

    THETAXY=RADIAN(PHI)+THETA(R)
    RETURN
    END FUNCTION THETAXY

REAL FUNCTION S(R)
!Determines coordinate S in RS Coordinates
    USE GLOBALS
    REAL R

    IF(R.GT.0)THEN
        S=PSI(R)
    ELSE
        S=-PSI(-R)
    ENDIF
    RETURN
    END FUNCTION S

REAL FUNCTION X(R,SHFT)
!Determines X for XY coordinates
    USE GLOBALS
    REAL SSTAR                !DISTANCE IN S DIRECTION
    REAL THETASTAR
    REAL SHFT                !DISTANCE OF SHIFT
    REAL R                   !RADIAL DISTANCE ALONG ROTATED COOR

    SSTAR=S(R)+SHFT*COS(RADIAN(LAMBDA))
    RSTAR=R-SHFT*SIN(RADIAN(LAMBDA))
    THETASTAR=THETAXY(R)

    X=RSTAR*COS(RADIAN(PHI))-SSTAR*SIN(RADIAN(PHI))-WIDTH*SIN(THETASTAR)+ORIGIN(1)

    RETURN
    END FUNCTION X

REAL FUNCTION Y(R,SHFT)
!Determines Y for XY coordinates
    USE GLOBALS
    REAL SSTAR                !DISTANCE IN S DIRECTION
    REAL THETASTAR
    REAL SHFT                !DISTANCE OF SHIFT
    REAL R                   !x' DISTANCE ALONG ROTATED COOR

    SSTAR=S(R)+SHFT*COS(RADIAN(LAMBDA))
    RSTAR=R-SHFT*SIN(RADIAN(LAMBDA))
    THETASTAR=THETAXY(R)

    Y=RSTAR*SIN(RADIAN(PHI))+SSTAR*COS(RADIAN(PHI))+WIDTH*COS(THETASTAR)+ORIGIN(2)

    RETURN
    END FUNCTION Y

SUBROUTINE GENESIS_INPUT(PLATE,ORNT,X_ELEM,Y_ELEM,X_NODES,Y_NODES,ELEM_SIZE,LAYERS)
!*****
!*      Generates GENESIS Input file for Static Analysis
!*
!*
!*****

    INTEGER PLATE(100,100)        !Array to measure thickness across entire plate
    REAL ORNT(100,100,2)        !Fiber orientations throughout plate
    INTEGER X_ELEM,Y_ELEM
    INTEGER Y_NODES,X_NODES

```

```

REAL ELEM_SIZE
INTEGER I,J,K,L
INTEGER G1,G2,G3,G4          !Grid connctivity vector
REAL DISP
CHARACTER*56 ELEM_DATA
INTEGER MAT1,MAT2,PATH1,PATH2,THK_NUM
REAL THK1,THK2
REAL THETA1,THETA2
INTEGER R_EDGE(101)
INTEGER PLATE_TOPO(10000)

TYPE PCOMP_LIST
  INTEGER M
  REAL TA
  REAL TB
END TYPE

TYPE(PCOMP_LIST) PCP(40)

TYPE LAYER
  INTEGER ELEMX
  REAL WIDTHA
  REAL HEIGHTB
  REAL PATHWIDTH
  REAL PATHSHIFT
  REAL PATHSHFTANGLE
  INTEGER NUM_LAYER
  REAL E1_COMP
  REAL E2_COMP
  REAL NU12_COMP
  REAL G12_COMP
  REAL LAY_THK
  INTEGER SYMMETRIC
  REAL THERMX
  REAL THERMY
  CHARACTER*4 FAILURE
  REAL XT
  REAL XC
  REAL YT
  REAL YC
  REAL SHEAR
  REAL TSAIWU
  REAL X_DISP
  REAL Y_DISP
  INTEGER CASENUM
  INTEGER VARTHICK
  CHARACTER*20 IDX(8)
  REAL PHIX(20)
  REAL T0X(20)
  REAL T1X(20)

END TYPE

TYPE(LAYER) LAYERS

OPEN(96,FILE='VS01.DAT')
50  FORMAT(A8,8X,I8,8X,8X,8X,I8,I8,8X)
51  FORMAT(A8,I8,8X,F8.4,F8.4,F8.4,I8,I8)
52  FORMAT(A8,I8,I8,I8,I8,I8,I8,8X,8X)
53  FORMAT(A8,I8,24X,A8,16X,A8)
60  FORMAT(A8,I8,F8.5,F8.3,A8,I8,F8.5,F8.3,A8)
54  FORMAT(A8,I8,E8.3,E8.3,F8.5,E8.3,8X,8X,F8.4)
55  FORMAT(A8,I8,I8,I8,F8.5,I8,I8,F8.5,8X)
56  FORMAT(A8,8X,I8,I8,F8.5,I8,I8,F8.5,8X)
57  FORMAT(A8,I8,I8,I8,I8,I8,I8,I8)
58  FORMAT(A56)
59  FORMAT(56X,I2,1X,I2,1X,I4,1X,F8.5,1X,F8.4,1X,I2,1X,I4,1X,F8.5,1X,F8.4)
61  FORMAT(I8)
62  FORMAT(A8,I8,I8,I8,A8,I8)
63  FORMAT(A8,48X,I8)

```

```

64     FORMAT(I3,1X)
67     FORMAT(F10.5,1X,F10.5,1X,I3)
68     FORMAT(A8,E8.3,E8.3,8X,E8.3,E8.2,E8.3,E8.2,E8.3)
69     FORMAT(A8,8X,E8.3)

!Executive Control Parameters
WRITE(96,*)'ID VS01'
! WRITE(96,*)'CHECK'
WRITE(96,*)'POST=FORMAT'
WRITE(96,*)'CEND'

!Solution Control Parameters (Load cases)
WRITE(96,*)'TITLE=VARIABLE STIFFNESS COMPOSITE PLATE'
WRITE(96,*)'SUBTITLE=NOTHING'
WRITE(96,*)'ECHO=NONE'
! WRITE(96,*)'MASS=YES'
! WRITE(96,*)'VOLUME=YES'
WRITE(96,*)'LINE=1000000,*'
WRITE(96,*)'LOADCASE 1'
WRITE(96,*)'          STRESS=POST'
WRITE(96,*)'          STRAIN=POST'
WRITE(96,*)'          DISPLACEMENT=POST'
WRITE(96,*)'          FORCE=ALL'
WRITE(96,*)'          LOAD=102'
WRITE(96,*)'          SPC=104'
WRITE(96,*)'$'

!Bulk Data (Grid Points,element definitions, etc.)
WRITE(96,*)'BEGIN BULK'
WRITE(96,*)'$'
WRITE(96,*)'$   GRID POINTS'
WRITE(96,*)'$'

K=1
WRITE(96,63)'GRDSET',356
DO 23 J=1,Y_NODES
  DO 22 I=1,X_NODES
    WRITE(96,51)'GRID   ',K,(I-1)*ELEM_SIZE,(J-1)*ELEM_SIZE,0.0,0
    K=K+1
22   CONTINUE
23   CONTINUE

WRITE(96,*)'$'
WRITE(96,*)'$   ELEMENT DEFINITIONS'
WRITE(96,*)'$'

OPEN(94,FILE=LAYERS%IDX(1)//'.ILD')
READ(94)
READ(94)
READ(94)

DO 25 J=1,Y_ELEM*X_ELEM
  READ(94,58)ELEM_DATA
  WRITE(96,58)ELEM_DATA
25   CONTINUE
CLOSE(94)

WRITE(96,*)'$'
WRITE(96,*)'$   PROPERTY DEFINITIONS'
WRITE(96,*)'$'

DO 33 I=1,LAYERS%NUM_LAYER
  OPEN(100+I,FILE=LAYERS%IDX(I)//'.ILD')
  READ(100+I)
  READ(100+I)
  READ(100+I)
33   CONTINUE

PLATE_TOPO=0

DO 29 I=1,Y_ELEM*X_ELEM

```

```

IF(LAYERS%SYMMETRIC.EQ.1)THEN
  WRITE(96,53)'PCOMP  ',I,LAYERS%FAILURE,'SYM'
ELSE
  WRITE(96,53)'PCOMP  ',I,LAYERS%FAILURE
ENDIF
K=1
PCP%M=0
PCP%TA=0
PCP%TB=0
DO 28 J=1,LAYERS%NUM_LAYER
  READ(100+J,59)THK_NUM,MAT1,PATH1,THK1,THETA1,MAT2,PATH2,THK2,THETA2
  PLATE_TOPO(I)=PLATE_TOPO(I)+2*THK_NUM
  IF(THK_NUM.EQ.1)THEN
    PCP(K)%M=MAT1
    PCP(K)%TA=THK1
    PCP(K)%TB=THETA1
    K=K+1
  ELSEIF(THK_NUM.EQ.2)THEN
    PCP(K)%M=MAT1
    PCP(K)%TA=THK1
    PCP(K)%TB=THETA1
    K=K+1
    PCP(K)%M=MAT2
    PCP(K)%TA=THK2
    PCP(K)%TB=THETA2
    K=K+1
  ENDIF
28  CONTINUE
DO 35 J=1,K-1,2
  IF(PCP(J)%M.NE.0.AND.PCP(J+1)%M.NE.0)THEN
    WRITE(96,60)'
+',PCP(J)%M,PCP(J)%TA,PCP(J)%TB,'YES',PCP(J+1)%M,PCP(J+1)%TA,PCP(J+1)%TB,'YES'
    ELSEIF(PCP(J)%M.NE.0.AND.PCP(J+1)%M.EQ.0)THEN
    WRITE(96,60)'  '+',PCP(J)%M,PCP(J)%TA,PCP(J)%TB,'YES'
  ENDIF
35  CONTINUE
29  CONTINUE

OPEN(130,FILE='TOPO.DAT')
!Generates a thickness plot of before data
WRITE(130,*)'TITLE = "Single Path Data"'
WRITE(130,*)'VARIABLES = "X", "Y", "Thickness"'
WRITE(130,*)'ZONE I=',X_ELEM+1,' J=',Y_ELEM+1,' F=POINT'
WRITE(130,*)

DO 24 I=1,Y_ELEM+1
  DO 27 J=1,X_ELEM+1
    IF(J.LT.X_ELEM+1.AND.I.LT.Y_ELEM+1)THEN
      WRITE(130,*)(J-1)*ELEM_SIZE,(I-1)*ELEM_SIZE,PLATE_TOPO(I*Y_ELEM-X_ELEM+J)
    ELSE
      WRITE(130,*)(J-1)*ELEM_SIZE,(I-1)*ELEM_SIZE,0
    ENDIF
  ENDIF
27  CONTINUE
24  CONTINUE
CLOSE(130)

DO 34 I=1,LAYERS%NUM_LAYER
  CLOSE(100+I)
34  CONTINUE

WRITE(96,*)'$'
WRITE(96,*)'$ MATERIAL DEFINITIONS'
WRITE(96,*)'$

WRITE(96,54)'MAT8
',1,LAYERS%E1_COMP,LAYERS%E2_COMP,LAYERS%NU12_COMP,LAYERS%G12_COMP,1.0
WRITE(96,68)' +
',LAYERS%THERMX,LAYERS%THERMY,LAYERS%XT,LAYERS%XC,LAYERS%YT,LAYERS%YC,LAYERS%SHEAR
WRITE(96,69,ADVANCE='NO')' + ',LAYERS%TSAIWU
IF(LAYERS%FAILURE.EQ.'STRAIN')THEN

```

```

        WRITE(96,*)1.0
    ELSE
        WRITE(96,*)
    ENDIF
! Boundary Conditions
    WRITE(96,*)'$'
    WRITE(96,*)'$ ENFORCED DISPLACEMENT'
    WRITE(96,*)'$'

    J=(X_NODES*Y_NODES)-X_ELEM
    DO 36 I=1,Y_NODES
        R_EDGE(I)=I*(X_NODES)
36    CONTINUE

    IF(LAYERS%CASENUM.EQ.0)THEN
        WRITE(96,55)'SPCD      ',102,R_EDGE(1),1,LAYERS%X_DISP,R_EDGE(2),1,LAYERS%X_DISP
        DO 37 I=3,Y_NODES-2,2
            WRITE(96,56)'      +
',R_EDGE(I),1,LAYERS%X_DISP,R_EDGE(I+1),1,LAYERS%X_DISP
37    CONTINUE
        IF(Y_NODES-I.EQ.1)THEN
            WRITE(96,56)'      +
',R_EDGE(I),1,LAYERS%X_DISP,R_EDGE(I+1),1,LAYERS%X_DISP
        ELSEIF(Y_NODES-I.EQ.0)THEN
            WRITE(96,56)'      +      ',R_EDGE(I),1,LAYERS%X_DISP
        ENDIF
    ELSEIF(LAYERS%CASENUM.EQ.1)THEN
        WRITE(96,55)'SPCD      ',102,R_EDGE(1),1,LAYERS%X_DISP,R_EDGE(2),1,LAYERS%X_DISP
        DO 38 I=3,Y_NODES-2,2
            WRITE(96,56)'      +
',R_EDGE(I),1,LAYERS%X_DISP,R_EDGE(I+1),1,LAYERS%X_DISP
38    CONTINUE
        IF(Y_NODES-I.EQ.1)THEN
            WRITE(96,56)'      +
',R_EDGE(I),1,LAYERS%X_DISP,R_EDGE(I+1),1,LAYERS%X_DISP
        ELSEIF(Y_NODES-I.EQ.0)THEN
            WRITE(96,56)'      +      ',R_EDGE(I),1,LAYERS%X_DISP
        ENDIF

        WRITE(96,55)'SPCD      ',102,J,2,LAYERS%Y_DISP,J+1,2,LAYERS%Y_DISP
        DO 26 I=J+2,X_NODES*Y_NODES-1,2
            WRITE(96,56)'      +      ',I,2,LAYERS%Y_DISP,I+1,2,LAYERS%Y_DISP
26    CONTINUE
        WRITE(96,56)'      +      ',I,2,DISP
    ELSEIF(LAYERS%CASENUM.EQ.2)THEN
        WRITE(96,55)'SPCD      ',102,J,2,LAYERS%Y_DISP,J+1,2,LAYERS%Y_DISP
        DO 39 I=J+2,X_NODES*Y_NODES-1,2
            WRITE(96,56)'      +      ',I,2,LAYERS%Y_DISP,I+1,2,LAYERS%Y_DISP
39    CONTINUE
        WRITE(96,56)'      +      ',I,2,DISP
    ENDIF

    WRITE(96,*)'$'
    WRITE(96,*)'$ BOUNDARY CONDITIONS'
    WRITE(96,*)'$'
! Two fixed points to insure there is no rigid body motion or rotation
    WRITE(96,*)'$ Constrains node at (0,0) in both directions'
    WRITE(96,57)'SPC1      ',104,12,1
    IF(LAYERS%CASENUM.EQ.0)THEN
        WRITE(96,*)'$ Constrains node at (a/2,0) in both directions'
        WRITE(96,57)'SPC1      ',104,1,X_NODES
    ELSEIF(LAYERS%CASENUM.EQ.1)THEN
        WRITE(96,*)'$ Constrains node at (a/2,0) in both directions'
        WRITE(96,57)'SPC1      ',104,1,X_NODES
        WRITE(96,*)'$ Constrains node at (0,b/2) in both directions'
        WRITE(96,57)'SPC1      ',104,2,J
    ELSEIF(LAYERS%CASENUM.EQ.2)THEN
        WRITE(96,*)'$ Constrains node at (0,b/2) in both directions'
        WRITE(96,57)'SPC1      ',104,2,J
    ENDIF

```

```

! Constraints for y=0 and y=b/2 (top and bottom)
IF(LAYERS%CASENUM.EQ.0)THEN
  WRITE(96,62)'SPC1  ',104,2,2,' THRU ',X_NODES
ELSEIF(LAYERS%CASENUM.EQ.1)THEN
  WRITE(96,62)'SPC1  ',104,2,2,' THRU ',X_NODES
  WRITE(96,62)'SPC1  ',104,2,J+1,' THRU ',X_NODES*Y_NODES
ELSEIF(LAYERS%CASENUM.EQ.2)THEN
  WRITE(96,62)'SPC1  ',104,2,2,' THRU ',X_NODES
  WRITE(96,62)'SPC1  ',104,2,J+1,' THRU ',X_NODES*Y_NODES
ENDIF

! Constraints for x=0 and x=a/2 (left and right)
IF(LAYERS%CASENUM.EQ.0)THEN
  WRITE(96,57)'SPC1
',104,1,R_EDGE(1)+1,R_EDGE(2)+1,R_EDGE(3)+1,R_EDGE(4)+1,R_EDGE(5)+1,R_EDGE(6)+1
  J=6
  DO WHILE(J.LE.Y_ELEM)
    WRITE(96,57,ADVANCE='NO')'  +  ',R_EDGE(J)+1
    J=J+1
    K=1
    DO WHILE(J.LE.Y_ELEM.AND.K.LE.7)
      WRITE(96,61,ADVANCE='NO')R_EDGE(J)+1
      K=K+1
      J=J+1
    ENDDO
    WRITE(96,*)
  ENDDO

  WRITE(96,57)'SPC1
',104,1,R_EDGE(2),R_EDGE(3),R_EDGE(4),R_EDGE(5),R_EDGE(6),R_EDGE(7)
  J=8
  DO WHILE(J.LE.Y_NODES)
    WRITE(96,57,ADVANCE='NO')'  +  ',R_EDGE(J)
    J=J+1
    K=1
    DO WHILE(J.LE.Y_NODES.AND.K.LE.7)
      WRITE(96,61,ADVANCE='NO')R_EDGE(J)
      K=K+1
      J=J+1
    ENDDO
    WRITE(96,*)
  ENDDO
ELSEIF(LAYERS%CASENUM.EQ.1)THEN
  WRITE(96,57)'SPC1
',104,1,R_EDGE(1)+1,R_EDGE(2)+1,R_EDGE(3)+1,R_EDGE(4)+1,R_EDGE(5)+1,R_EDGE(6)+1
  J=7
  DO WHILE(J.LE.Y_ELEM)
    WRITE(96,57,ADVANCE='NO')'  +  ',R_EDGE(J)+1
    J=J+1
    K=1
    DO WHILE(J.LE.Y_ELEM.AND.K.LE.7)
      WRITE(96,61,ADVANCE='NO')R_EDGE(J)+1
      K=K+1
      J=J+1
    ENDDO
    WRITE(96,*)
  ENDDO

  WRITE(96,57)'SPC1
',104,1,R_EDGE(2),R_EDGE(3),R_EDGE(4),R_EDGE(5),R_EDGE(6),R_EDGE(7)
  J=8
  DO WHILE(J.LE.Y_NODES)
    WRITE(96,57,ADVANCE='NO')'  +  ',R_EDGE(J)
    J=J+1
    K=1
    DO WHILE(J.LE.Y_NODES.AND.K.LE.7)
      WRITE(96,61,ADVANCE='NO')R_EDGE(J)
      K=K+1
      J=J+1
    ENDDO
    WRITE(96,*)
  ENDDO

```

```

        ENDDO
    ELSEIF (LAYERS%CASENUM.EQ.2) THEN
        WRITE(96,57)'SPC1
        ,104,1,R_EDGE(1)+1,R_EDGE(2)+1,R_EDGE(3)+1,R_EDGE(4)+1,R_EDGE(5)+1,R_EDGE(6)+1
        J=6
        DO WHILE (J.LE.Y_ELEM)
            WRITE(96,57,ADVANCE='NO')'    +    ',R_EDGE(J)+1
            J=J+1
            K=1
            DO WHILE (J.LE.Y_ELEM.AND.K.LE.7)
                WRITE(96,61,ADVANCE='NO')R_EDGE(J)+1
                K=K+1
                J=J+1
            ENDDO
            WRITE(96,*)
        ENDDO
    ENDIF

    WRITE(96,*)'$'
    WRITE(96,*)'ENDDATA'

    CLOSE(96)
    RETURN
    END

```



## **Vita**

Patrick Tyler Langley was born January 30<sup>th</sup>, 1974 to Larry and Deborah Langley at Buncombe County Hospital in Asheville, North Carolina. His childhood was spent growing up in Boone, NC where he attended Watauga High School. After graduating in 1992, he attended North Carolina State University. At North Carolina State University, he studied Materials Science and Engineering, graduating May of 1997 Magna Cum Laude with a minor in physics. He then, entered Virginia Tech in the Engineering Science and Mechanics department in pursuit of a Master's Degree. Upon graduation, he will be seeking an officer's commission in the United States Navy, with the intent of becoming a Nuclear Engineering Officer with the United States Navy submarine fleet. Beyond that, the stars are the limit.

Tyler Langley  
June 7<sup>th</sup>, 1999